Working Draft

Information Technology -

Fibre Channel - Methodologies for Signal Quality Specification - 2 MSQS-2

Draft Technical Report

Secretariat International Committee for Information Technology Standardization (INCITS)

This is a draft technical report of Accredited Standards Committee INCITS. As such, this is not a completed technical report. The T11.2 Technical Committee may modify this document as a result of comments received during public review and its approval as a technical report.

ABSTRACT

This technical report compiles and provides additional information beyond that supplied in FC-MSQS. The technical report further clarifies jitter and signal quality specification clauses of relevant physical interfaces. The technical report focuses on FC-PI-6 signal characteristics and test methods. It specifies budget methods for equalized links and specifies and describes methods of measurement for links using a reference receiver.

Contacts	**Chairman**	**Technical Editor**
	Dean Wallace	Richard Johnson
	QLogic Corporation	Finisar Corporation
	26650 Aliso Viejo Parkway	1389 Moffett Park Drive
	Aliso Viejo, CA 92656	Sunnyvale, CA 94089-1134
Voice	949 389-6480	408 548-1000
Fax	949 389-6126	Fax: 408 541-6138
email	dean.wallace@qlogic.com	richard.johnson@finisar.com

Other Points of Contact:

	T11.2 Chair:	**T11.2 Vice-Chair:**	**INCITS Secretariat, ITI:**
	Tom Palkert	Dean Wallace	
	Luxtera Corporation	QLogic Corporation	
	2320 Camino Vida Roble	26650 Aliso Viejo Parkway	1250 Eye Street, NW Suite 200
	Carlsbad, CA 92011	Aliso Viejo, CA 92656	Washington, DC 20005
Voice:	952 200-8542	949 389-6480	202-737-8888
Fax:	760 448-3530	949 389-6126	202-638-4922
Email:	tpalkert@luxtera.com	dean.wallace@qlogic.com	incits@itic.org

T11.2 Reflector (for minutes, agendas, etc.)

Internet addresses for subscription to the T11.2 reflector:	Subscribe: t11_2-request@mail.t11.org?subject=subscribe Unsubscribe: t11_2-request@mail.t11.org?subject=unsub-scribe Report Problem Address: t11_2-admins@listserve.com
Internet address for distribution via T11.2 reflector:	t11_2@mail.t11.org
Web Sites	http://www.incits.org/t11 or http:// www.t11.org
Document Distribution Global Engineering 15 Inverness Way East Englewood, CO 80112-5704	Voice: 303-792-2181 or: 800-854-7179 FAX: 303-792-2192

PATENT STATEMENT

Contents

List of figures

1 References

1.1 General

The documents named in this clause contain provisions that, through reference in this text, constitute provisions of this document. At the time of publication, the editions indicated were valid. All standards and technical reports are subject to revision, and parties to agreements based on this technical report are encouraged to investigate the possibility of applying the most recent editions of the following list of documents. Members of IEC and ISO maintain registers of currently valid international standards.

Some references may not be specifically cited in the text but contain information generally related to the subject matter of FC-MSQS.

The URLs cited in this clause were valid at the time of publication.

For more information on the current status of SFF documents, contact the SFF committee at 408-867-6630 (phone), or 408-867-2115 (fax). To obtain copies of these documents, contact the SFF committee at 14426 Black Walnut Court, Saratoga, CA 95070 or from the SFF web site: www.sffcommittee.com.

To obtain Bellcore Documents (GR series documents) contact:
  Telcordia Customer Service
  8 Corporate Place, Room 3A184
  Piscataway, N.J. 08854-4156
  1-800-521-CORE (USA and Canada)
  908-699-5800 (all others)

To obtain ANSI documents contact:
  American National Standard Institute(ANSI)
  American National Standard Institute
  Customer Service
  11 West 42nd Street
  New York, NY 10036
  (212) 642-4900

T11 documents may be obtained from http://www.T11.org.
T10 documents may be obtained from http://www.T10.org.
INCITS documents may be obtained at http://www.incits.org.
IEEE standards may be obtained at http://standards.ieee.org/catalog/olis/index.html.
IEEE 802.3 documents may be obtained at http://www.ieee802.org/3/.
EIA/TIA documents may be obtained at http://www.tiaonline.org/standards/

1.2 Normative references

1.2.1 Approved references

Approved references are those that have been approved by a standards organization.

Approved ANSI standards;
Approved and draft regional and international standards (ISO, IEC, CEN/CENELEC and ITU); and
Approved foreign standards (including BSI, JIS and DIN).
Approved ANSI technical reports
Approved IEEE standards

[1] ANSI/INCITS 450, FC-PI-5, Fibre Channel Physical Interfaces - 5.

[2]   ANSI/INCITS TR-46-2011, FC-MSQS, Fibre Channel - Methodologies for Signal Quality Specification.

[3]   ANSI/INCITS TR-35-2004, FC-MJSQ, Fibre Channel - Methodologies for Jitter and Signal Quality Specification.

[4]   IEEE 802.3-2011, IEEE Standard for Information technology - Telecommunications and information exchange between systems - Local and metropolitan area networks - Specific requirements - Part 3: Carrier sense multiple access with collision detection (CSMA/CD) access method and physical layer specifications.

1.2.2 References under development

At the time of publication, the following referenced standards were still under development. For information on the current status of the documents, or regarding availability, contact the relevant standards body or other organization as indicated.

[5]   ANSI/INCITS Project 2221-D, FC-PI-6, Fibre Channel Physical Interfaces - 6.

[6]   Optical Internetworking Forum CEI-28G-VSR Very Short Reach Interface, OIF2010.404.08.

1.3 Informative references

[7]   SFF-8431 - Specifications for enhanced small form factor pluggable module SFP+.

[8]   G.P. Agrawal, P.J. Anthony, and T.M. Shen, *Journal of Lightwave Technology*, vol. 6, p 620 (1988).

[9]   N. Benvenuto and G. Cherubini, Algorithms for communication systems and their applications, Wiley, ISBN 0-470-84389-6.

[10] S. Bottacchi, Multi-gigabit transmission over multimode optical fibre, Wiley, ISBN 0-471-89175-4.

[11] Gair D. Brown, "Bandwidth and Rise Time Calculations for Digital Multimode Fiber-Optic Data Links", Journal of Lightwave Technology, vol. 10, no. 5, May 1992, pp. 672-678.

[12] D.G. Cunningham and W.G. Lane, Gigabit Ethernet Networking, MacMillan, ISBN 1-7870-062-0, Chapter 9, the Gigabit Ethernet Optical Link Model.

[13] D. Derickson and M. Müller, "Digital Communications Test and Measurement: High-Speed Physical Layer Characterization," Prentice Hall, ISBM 0-13-220910-1, Chapter 9.

[14] D.W. Dolfi, "Proposal to Modify the ISI Penalty calculation in the current GbE Spreadsheet Model", http://www.ieee802.org/3/10G_study/public/email_attach/new_isi.pdf

[15] K. Ogawa, "Analysis of Mode Partition Noise in laser transmission systems," IEEE J. Quantum Electronics, vol. QE-18, no. 5, May 1982, pp. 849-855.

[16] K. Petermann, Laser diode modulation and noise, Kluwer, ISBN 90-277-2672-8, Chapter 7, noise characteristics of solitary laser diodes.

[17] N. L. Swenson, P. Voois, T. Lindsay, and S. Zeng, "Standards compliance testing of optical transmitters using a software-based equalizing reference receiver", paper NWC3, Optical Fiber Communication Conference and Exposition and The National Fiber Optic Engineers Conference on CD-ROM (Optical Society of America, Washington, DC), Feb. 2007

[18] Link model for 10 gigabit Ethernet found at: http://www.ieee802.org/3/ae/public/adhoc/serial_pmd/documents/10GEPBud3_1_16a.xls

2 Compliance test methodology for 32GFC

2.1 Test method general overview

The interoperability points are generally defined for Fibre Channel systems as being immediately after the mated connector. For the delta points this is not an easy measurement point, particularly at high frequencies, as test probes cannot be applied to these points without affecting the signals being measured, and de-embedding the effects of test fixtures is difficult. For delta point measurements reference test points are defined with a set of defined test boards for measurement consistency. The delta point specifications in FC-PI-6 are to be interpreted as being at the SMA outputs and inputs of the reference compliance boards.

In order to provide test results that are reproducible and easily measured, this document defines two test boards that have SMA interfaces for easy connection to test equipment. One is designed for insertion into a host, and one for inserting modules. The reference test boards' objectives are:

•Satisfy the need for interoperability at the electrical level.

•Allow for independent validation of host and module.

•The PCB traces are targeted at 100 Ω differential impedance with nominal 7% differential coupling.

Testing compliance to specifications in a high-speed system is delicate and requires thorough consideration. Using common test boards that allow predictable, repeatable, and consistent results among vendors will help to ensure consistency and true compliance in the testing.

The reference test boards provide a set of overlapping measurements for module and host validation to ensure system interoperability.

2.2 Test point definitions

2.2.1 Host test points

Host system transmitter and receiver compliance are defined by tests in which a Host Compliance Board is inserted as shown in figure 2.1 in place of the module. The test points are B and C.

Host compliance points are defined as the following:

•B: host output at the output of the Host Compliance Board. Delta T output and host return loss specifications shall be met at this point.

•C: host input at the input of the Host Compliance Board. Delta R host return loss specifications shall be met at this point. Stressed Eye Calibration shall be at *C″* for ensuring compliance at *C*. See 2.2.4.

Figure 2.1 - Host compliance board

2.2.2 Module test points

Module transmitter and receiver compliance are defined by tests in which the module is inserted into the Module Compliance Board as shown in figure 2.2. For improved measurement accuracy the reference test card responses may be calibrated out of the measurements and replaced with functions that represent the ideal responses defined in subclause 2.3 for the reference test cards.
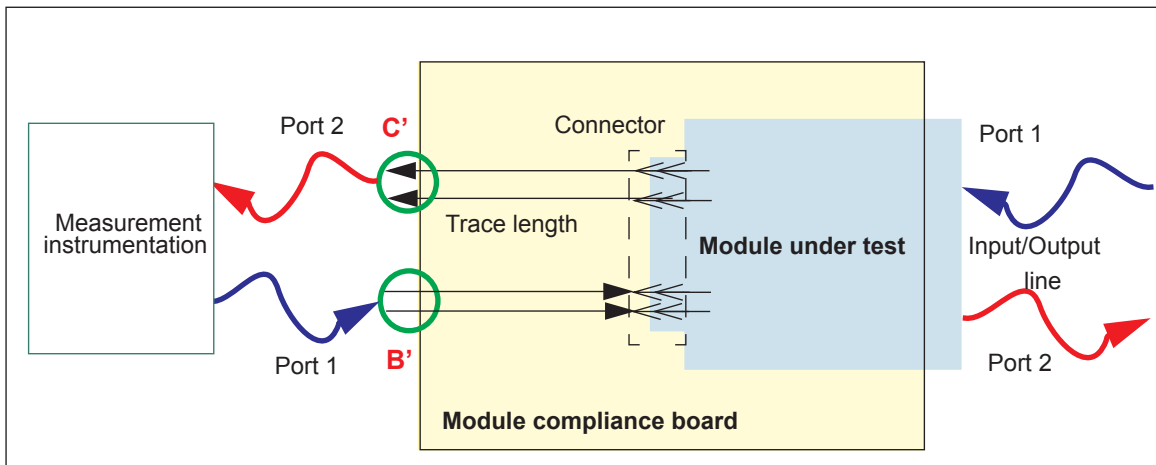
Figure 2.2 -   Module compliance board

Module test points are defined as the following:

- •B': Module transmitter input at the input of the Module Compliance Board. Delta T module return loss specifications shall be met at this point.

- •C': SFP+ module receiver output at the output of the Module Compliance Board. Delta R output and module return loss specifications shall be met at this point.

2.2.3 Module input calibration points

The module transmitter input tolerance signal is calibrated through the Module Compliance Board at the output of the Host Compliance Board as shown in figure 2.3. The opposite data path is excited with an asynchronous test source with PRBS31 or scrambled IDLE for 32GFC. The module input calibration point is at B" with specifications for input signals at Delta T being calibrated at B". Note that point B" has additional trace loss beyond the module pins.
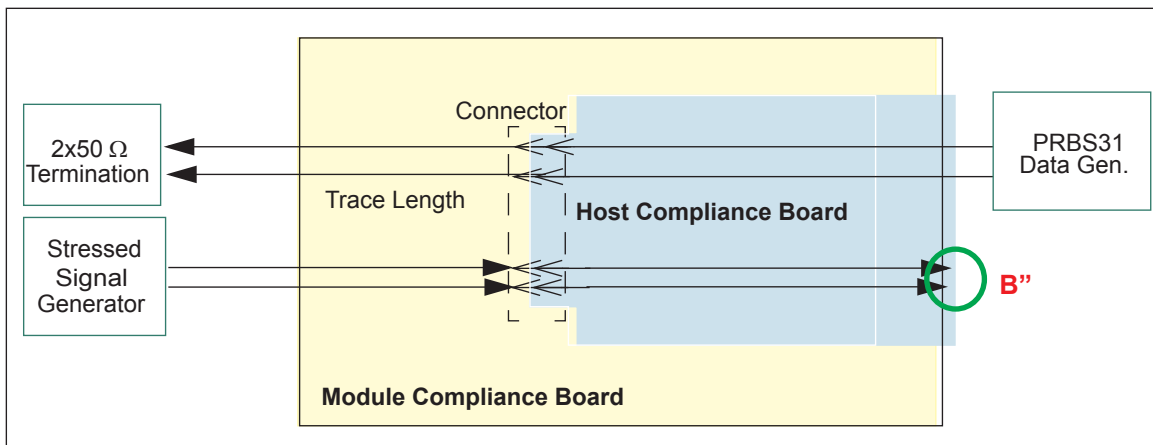
Figure 2.3 - Module input calibration point B"

2.2.4 Host input calibration point

The host receiver input tolerance signal is calibrated through the Host Compliance Board at the output of the Module Compliance Board as shown in figure 2.4. The host input calibration point is at C" with specifications for input signals at Delta R being calibrated at C". Note that the point C" has additional trace loss beyond the edge connector pins.
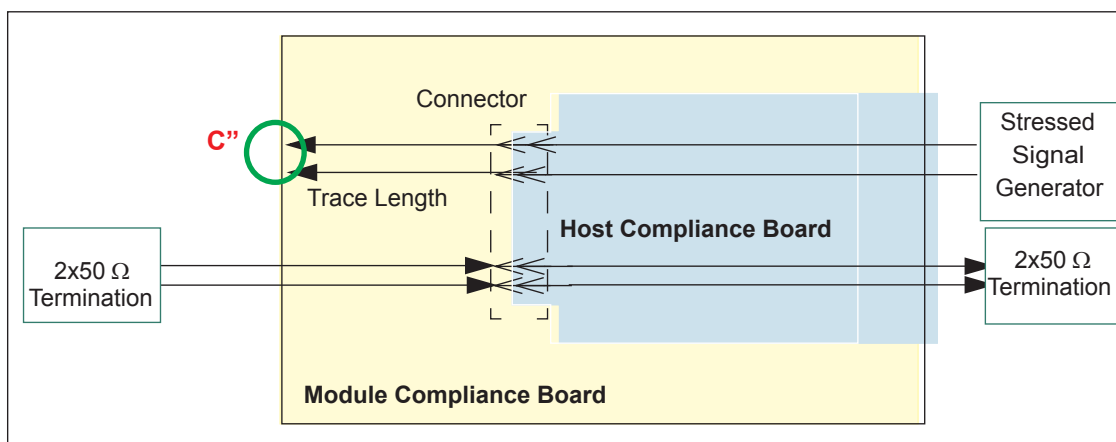
Figure 2.4 - Host input calibration point C"

2.3 Compliance boards for 32GFC

Compliance test boards are made of manufacturable length of PCB trace with specific properties for construction of the Host Compliance Board, and the Module Compliance Board. Compliance boards are intended to ease building practical test boards with non-zero loss. The 32GFC FC-PI-6 specifications incorporate the effect of non-zero loss reference test boards which improve the return loss and slightly

slow down edges. The boards described here are identical to those described in the SFF-8431 SFP+ specification [7].

2.3.1 Host Compliance Board and Module Compliance Board reference through response

The reference differential through response of the Host Compliance Board PCB excluding the SFP+ connector is given by.

$$SDD21(dB) = 2.0\left(0.001 - 0.096 \cdot \sqrt{f} - 0.046 \cdot f \right) \tag{2.1}$$

The reference differential through response of the Module Compliance Board PCB excluding the SFP+ connector is given by:

$$SDD21(dB) = 1.25\left(0.001 - 0.096 \cdot \sqrt{f} - 0.046 \cdot f \right) \tag{2.2}$$

In Equation 2.1 and Equation 2.2, f is the frequency in gigahertz, for 50 MHz < f < 28 GHz. SDD21 is defined from the SMA connectors to the SFP+ connector, excluding the mating pads. From 0.05 GHz to 11.1 GHz the discrepancy between the measured through response and the reference through response SDD21(dB) shall be within ±15% of the reference through response in dB or ±0.1 dB, whichever is larger. For frequencies above 11.1 GHz and up to 28 GHz, the discrepancy between the measured through response and the reference through response SDD21(dB) shall be within ±25% of the reference through response in dB.

The reference through response SDD21 for the host compliance board and for the module compliance board is shown in figure 2.5.
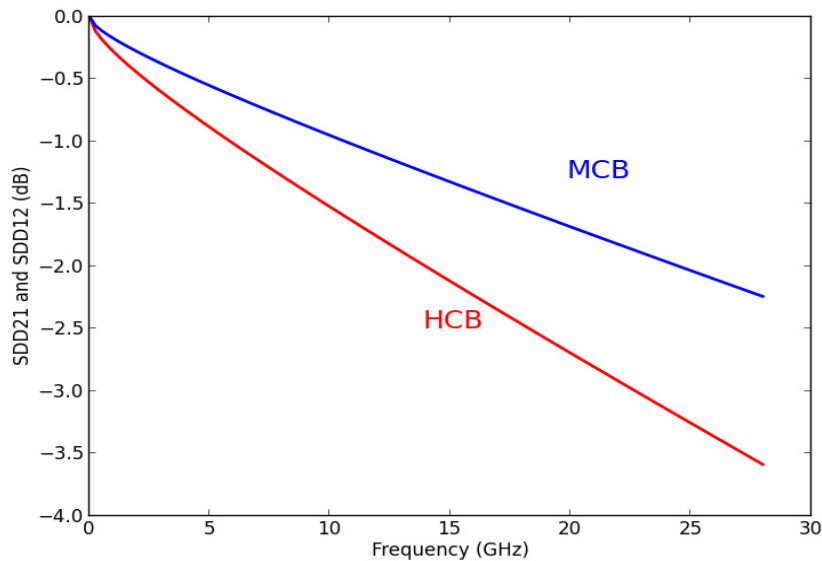
Figure 2.5 - Host and module compliance board reference through response

2.3.2 Specification of mated Host and Module Compliance Boards

Based on measurements of the 32GFC Module Compliance Board (MCB) mated with the 32GFC Host Compliance Board (HCB) the following specifications have been derived for the mated pair. Compliance to these limits help ensure the module and host specifications can be met.
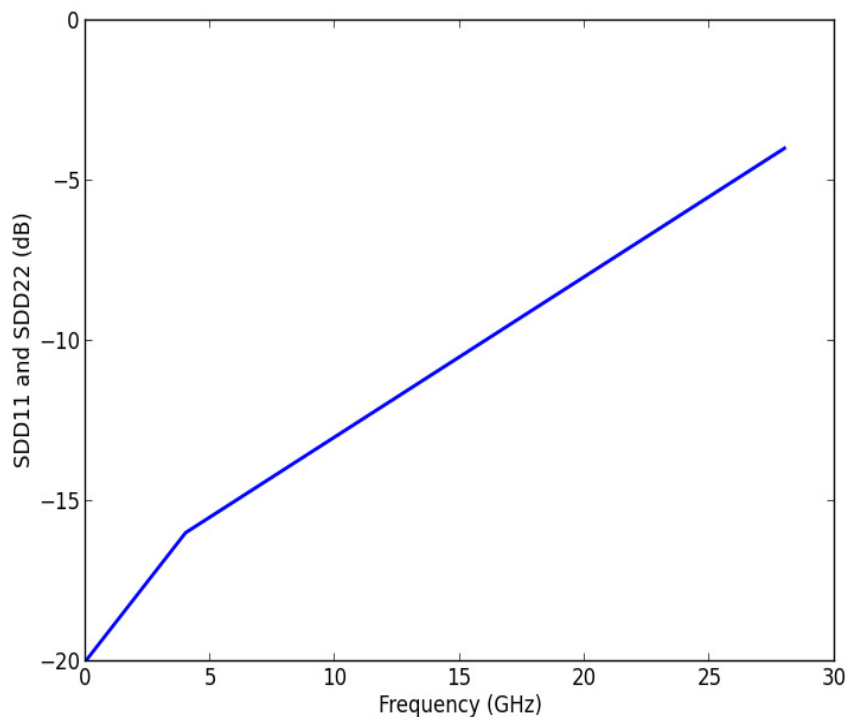
Figure 2.6 - Mated MCB-HCB differential through response

Mated differential response SDD11 and SDD22 for the 32GFC mated Module Compliance Board with the Host Compliance Board are given by:

$$SDDxx(dB) \; \text{min} \; = \; \begin{cases} -20.0 + f & \text{for} \quad 0.05 \le f \le 4 \text{ GHz} \\ -18.0 + 0.5 \cdot f & \text{for} \quad 4 \le f \le 28 \text{ GHz} \end{cases} \qquad (2.3)$$

SDD11 and SDD22 respectively looking in to the Module Compliance Board and the Host Compliance Board are illustrated in Figure 2.6.

Mated response SDD21 and SDD12 of the 32GFC Module Compliance Board mated with the Host Compliance Board are given by:

$$SDDxx(dB) \; \text{max} \; = \; -0.08 \cdot \sqrt{f} - 0.2 \cdot f \quad \text{for} \quad 0.05 \le f \le 28 \text{ GHz} \qquad (2.4)$$

$$SDDxx(dB) \; \text{min} \; = \; \begin{cases} -0.12 - 0.475 \cdot \sqrt{f} - 0.221 \cdot f & \text{for} \quad 0.05 \le f \le 14 \text{ GHz} \\ 4.25 - 0.66 \cdot f & \text{for} \quad 14 \le f \le 28 \text{ GHz} \end{cases} \qquad (2.5)$$

SDD21 and SDD12 for the 32GFC mated Module Compliance Board with the Host Compliance Board are illustrated in Figure 2.7.

Differential to common mode conversion loss SCD21 and SCD12 of the 32GFC mated Module and Host
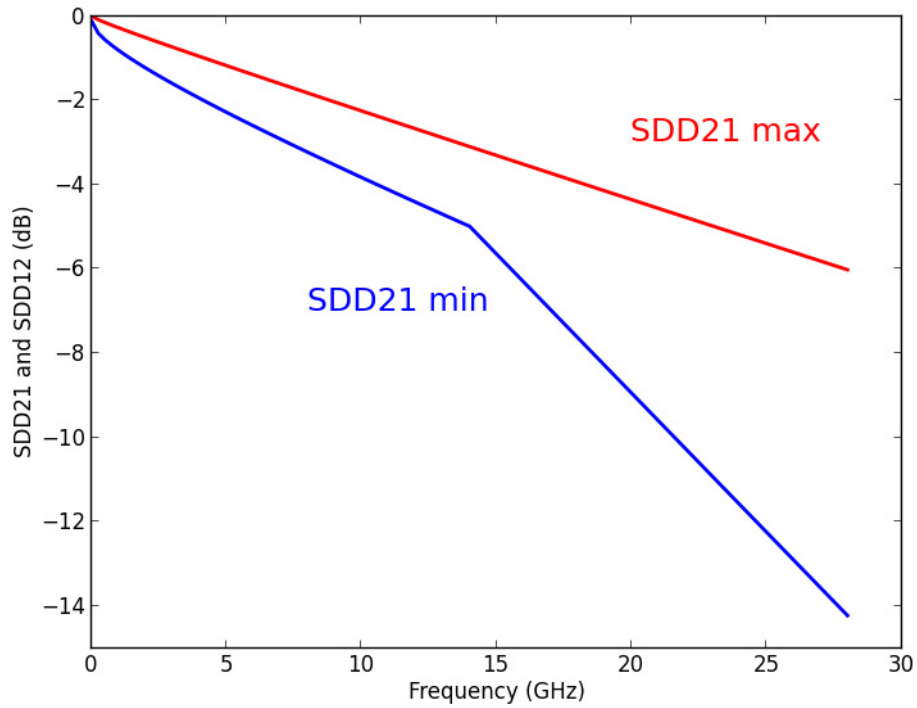
Figure 2.7 - Mated MCB-HCB differential through response

Compliance Board are given by:

$$SCDxx(dB) = \begin{cases} -35 + 1.07 \cdot f & \text{for} \quad 0.05 \le f \le 14 \text{ GHz} \\ -20 & \text{for} \quad 14 \le f \le 28 \text{ GHz} \end{cases} \quad (2.6)$$

SCD21 and SCD12 are illustrated in Figure 2.8.

The Integrated Crosstalk Noise (ICN) shall be less than 1.8 mV rms (assuming 900 mV amplitude and 9.5 ps rise time).
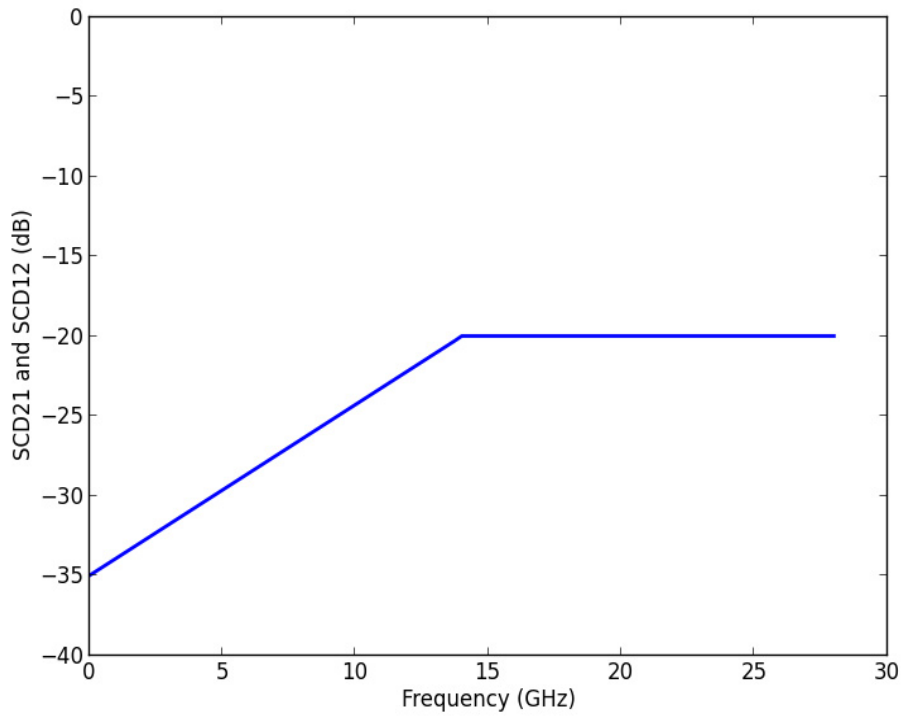
Figure 2.8 - 32GFC Mated MCB-HCB differential to common mode response

01
02
03
04
05
06
07
08
09
10
11
12
13
14
15
16
17
18
19
20
21
22
23
24
25
26
27
28
29
30
31
32
33
34
35
36
37
38
39
40
41
42
43
44
45
46
47
48
49
50
51
52
53
54
55
56

01
02
03
04
05
06
07
08
09
10
11
12
13
14
15
16
17
18
19
20
21
22
23
24
25
26
27
28
29
30
31
32
33
34
35
36
37
38
39
40
41
42
43
44
45
46
47
48
49
50
51
52
53
54
55
56

3 32GFC compliance tests

3.1 Introduction

This clause defines terms, measurement techniques, and conditions for testing jitter and wave shapes. This clause deals with issues specific to Fibre Channel 32GFC and is not intended to supplant standard test procedures referenced in FC-PI-6 [5].

The test block diagrams in this clause should be viewed as functional or logical diagrams, rather than the exact test hardware implementation or platform for the test. For a same logical or functional diagram, there can be several hardware implementations.

All measurements assume non-invasive perfect test equipment unless stated otherwise. All measurements

Table 3.1 - Tests defined in this clause and corresponding test patterns

Test	Subclause	32GFC test pattern
Electrical compliance tests		
Eye width EWx	3.3.1	PRBS9
Eye height EHx	3.3.1	PRBS9
Vertical eye closure	3.3.1 step 9	PRBS9
Electrical stressed receiver test	3.3.2	PRBS31
Crosstalk calibration	3.3.3	PRBS31
Common mode noise rms	3.3.4	
Optical compliance tests		
Transmitter and Dispersion Penalty (TDP)	3.4.1	PRBS31
VECPq	3.4.2	PRBS9
RIN_xOMA	3.4.3	0xFF00
Unstressed optical receiver sensitivity	3.4.4	PRBS31
Stressed optical receiver sensitivity	3.4.5	PRBS31
Optical receiver jitter tracking	3.4.6	PRBS31

made with oscilloscopes should be made with an instrument capable of 40 GHz response, unless stated otherwise

PRBS9 and PRBS31 test patterns are defined in subclause 9.3 of MSQS [2].

Some electrical compliance signals may have closed eye diagrams. Therefore a reference receiver with an equalizer is used to measure eye characteristics. Techniques for configuring such a reference receiver have been developed by the Optical Internetworking Forum in their CEI-28G-VSR physical link layer specification [6]. Fibre Channel gratefully acknowledges the OIF contribution. The electrical compliance methods listed in this clause have been adapted from draft copies of the VSR specification.

The compliance test configurations are detailed in 6.2. Electrical compliance test methods are introduced in 6.3. Optical compliance test methods are reviewed in 6.4.
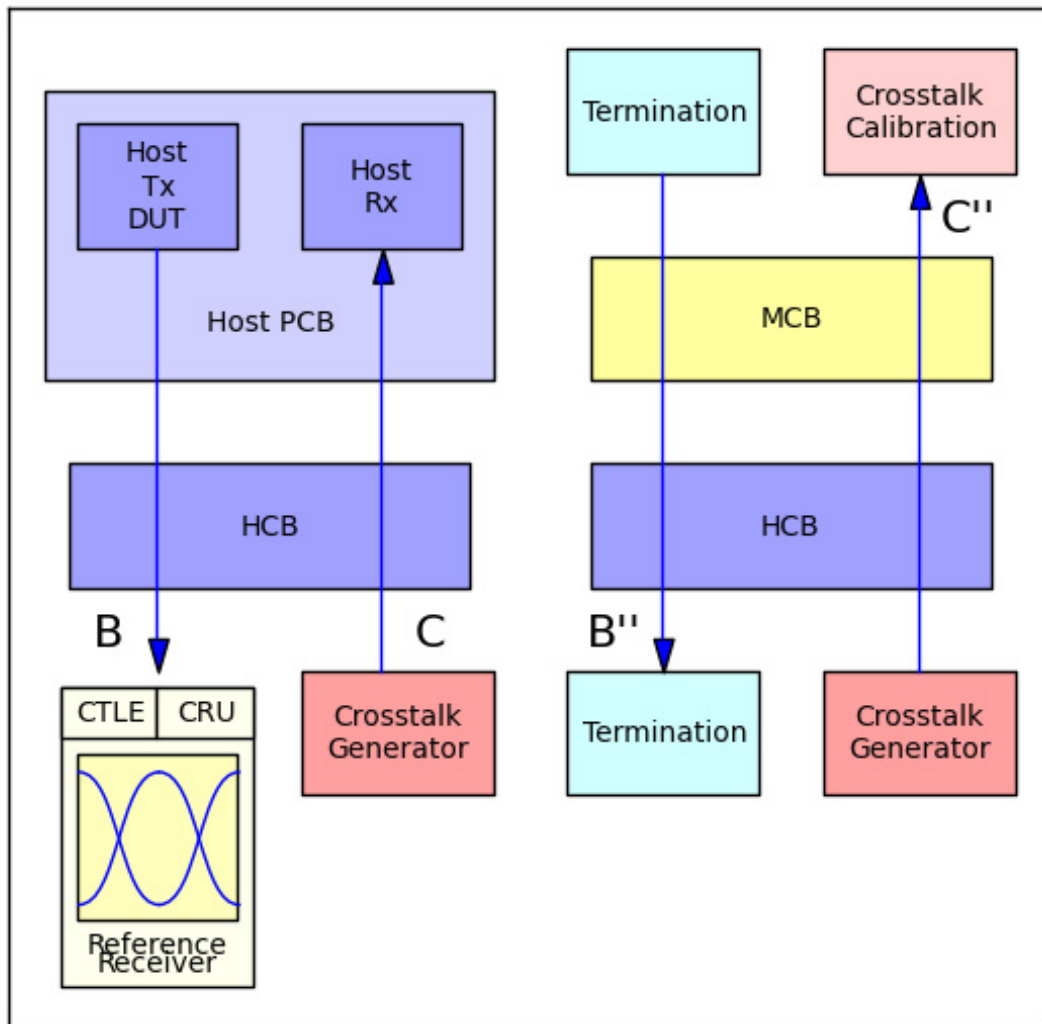
Figure 3.1 - Host output compliance test configuration (left) and crosstalk calibration (right)

3.2 Compliance test configurations

3.2.1 Host output test configuration

The host output eye width EWx and eye height EHx are measured at compliance test point B (as defined in Figure 2.1) using a host compliance board as specified in Clause 5. Eye width and eye height are measured using the method of subclause 3.3.1. The test configuration is shown in Figure 3.1. The signal at compliance test point B may be a closed eye. Therefore a reference receiver with a continuous time linear equalizer (CTLE) is used to measure eye width and eye height, as described in subclause Figure 3.2.8.

DC blocking capacitors are placed at compliance test points B and C between the test equipment and the host ASIC.

The host receive path must be active during this measurement using a crosstalk generator producing a PRBS31 test pattern or valid Fibre Channel signal, or during calibration PRBS9. The output of the crosstalk generator is calibrated using the measurement configuration shown on the right in Figure 3.1.
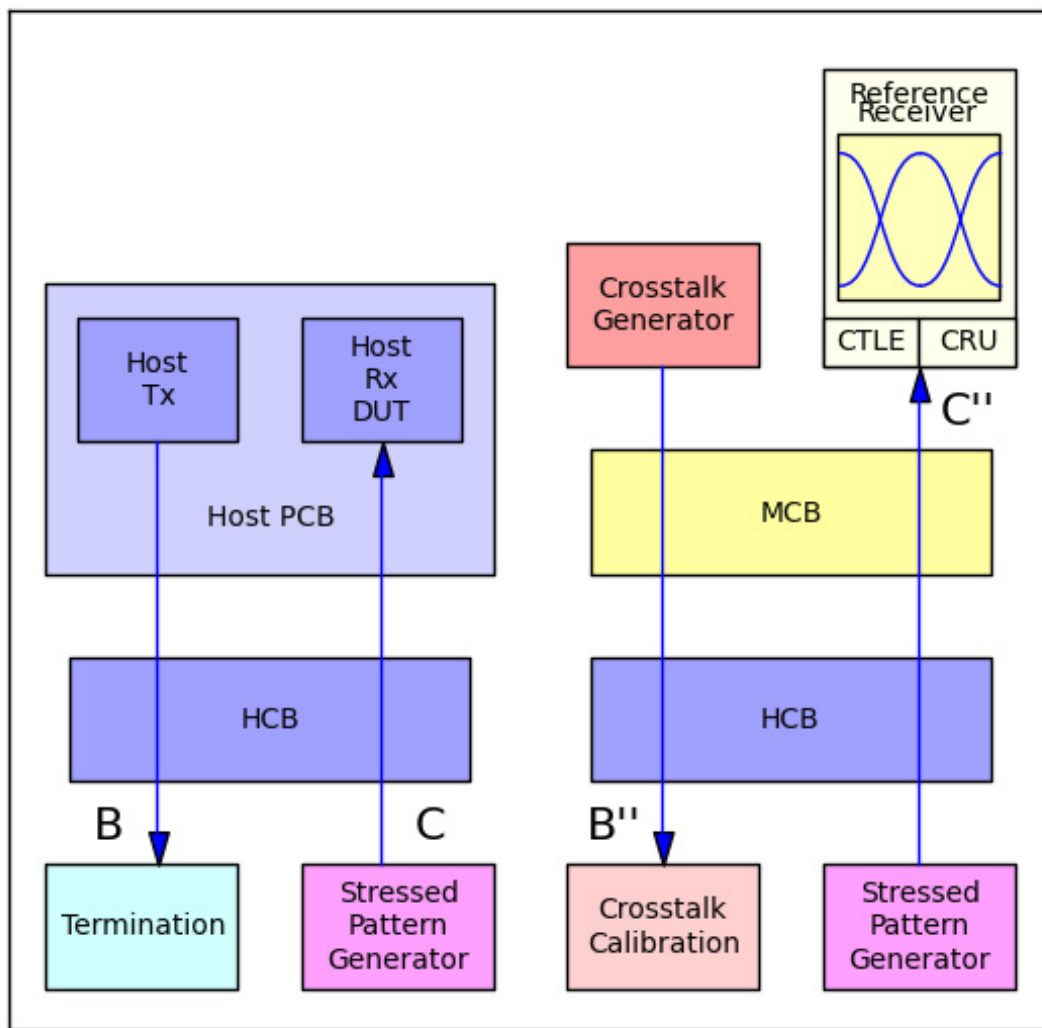
Figure 3.2 - Host input compliance test configuration (left) and calibration (right)

The measured signal after the reference receiver shall meet the requirements of FC-PI-6 [5].

3.2.2 Host input test configuration

The ability of the host input to tolerate jitter at a particular eye width and eye height as specified in FC-PI-6 [5] is tested using a stressed receiver test. The stressed signal is applied at compliance test point C (as defined in Figure 2.1) using a host compliance board as specified in Clause 5. The test configuration is shown on the left of Figure 3.2. The stressed pattern generator is detailed in subclause 3.2.9. The host input stressed receiver test method is detailed in subclause 3.3.2. During calibration the stressed pattern generator sends PRBS9 test patterns; during test it sends PRBS31 test patterns. This assumes that the host ASIC has PRBS31 bit error detection capability.
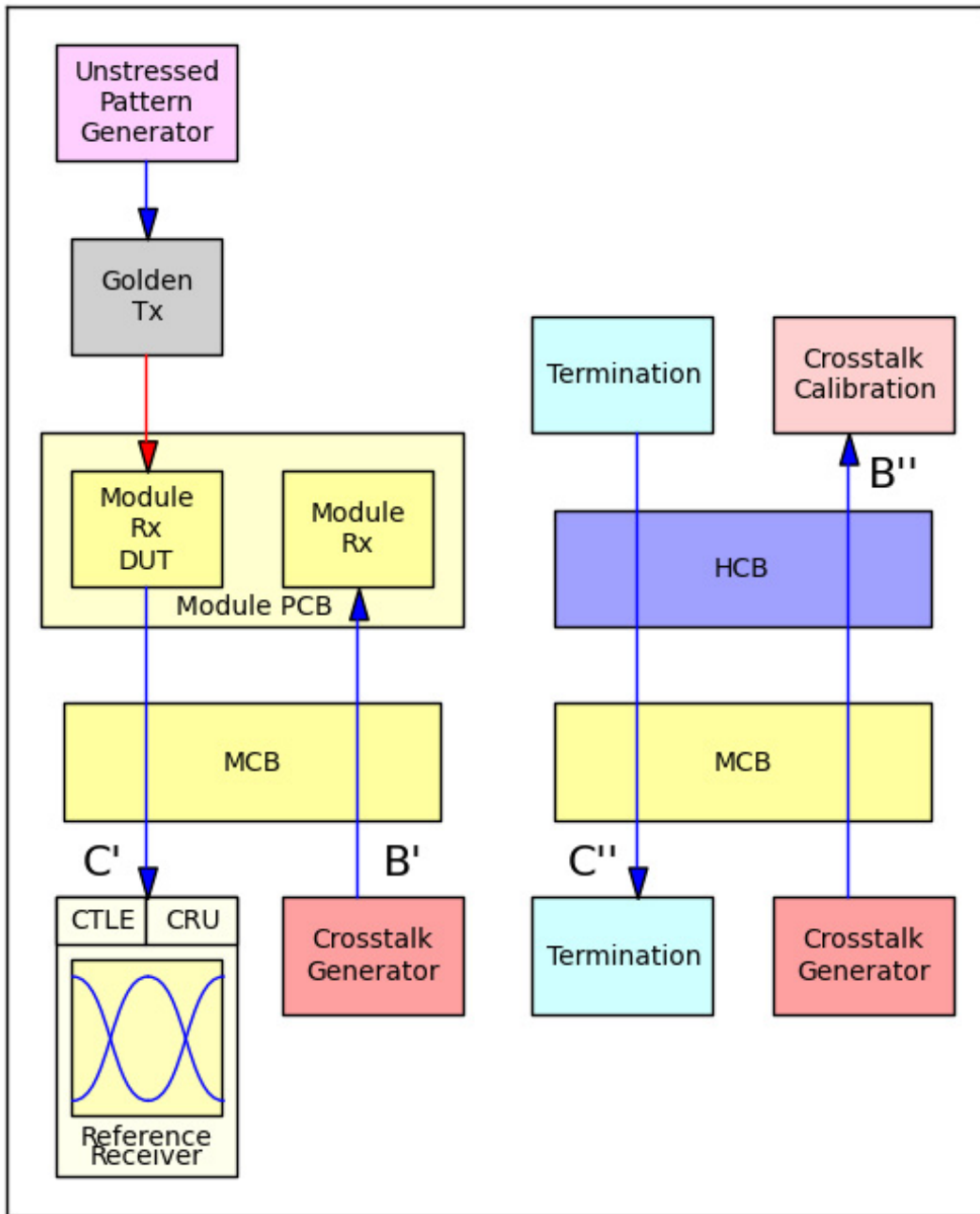
Figure 3.3 - Module electrical output compliance (left) and calibration (right)

3.2.3 Module electrical output test configuration

The eye width and eye height of the electrical output from the module's optical receiver is measured at compliance test point C' (as defined in Figure 2.2) using a module compliance board as specified in Clause 5, and the eye width and eye height test analysis method of subclause 3.3.1. The test configuration is shown in Figure 3.3. Although the signal at compliance test point C' is an open eye, the reference receiver

of subclause 3.2.8 is also used to equalize the module output signal without the use of transmit equalization.

The module optical transmit path must be active during this measurement, using a crosstalk generator producing a PRBS31 test pattern or valid Fibre Channel signal during test, PRBS9 during calibration. The output of the crosstalk generator is calibrated using the measurement configuration shown on the right in Figure 3.3.

The measured signal after the reference receiver shall meet the requirements of FC-PI-6 [5].
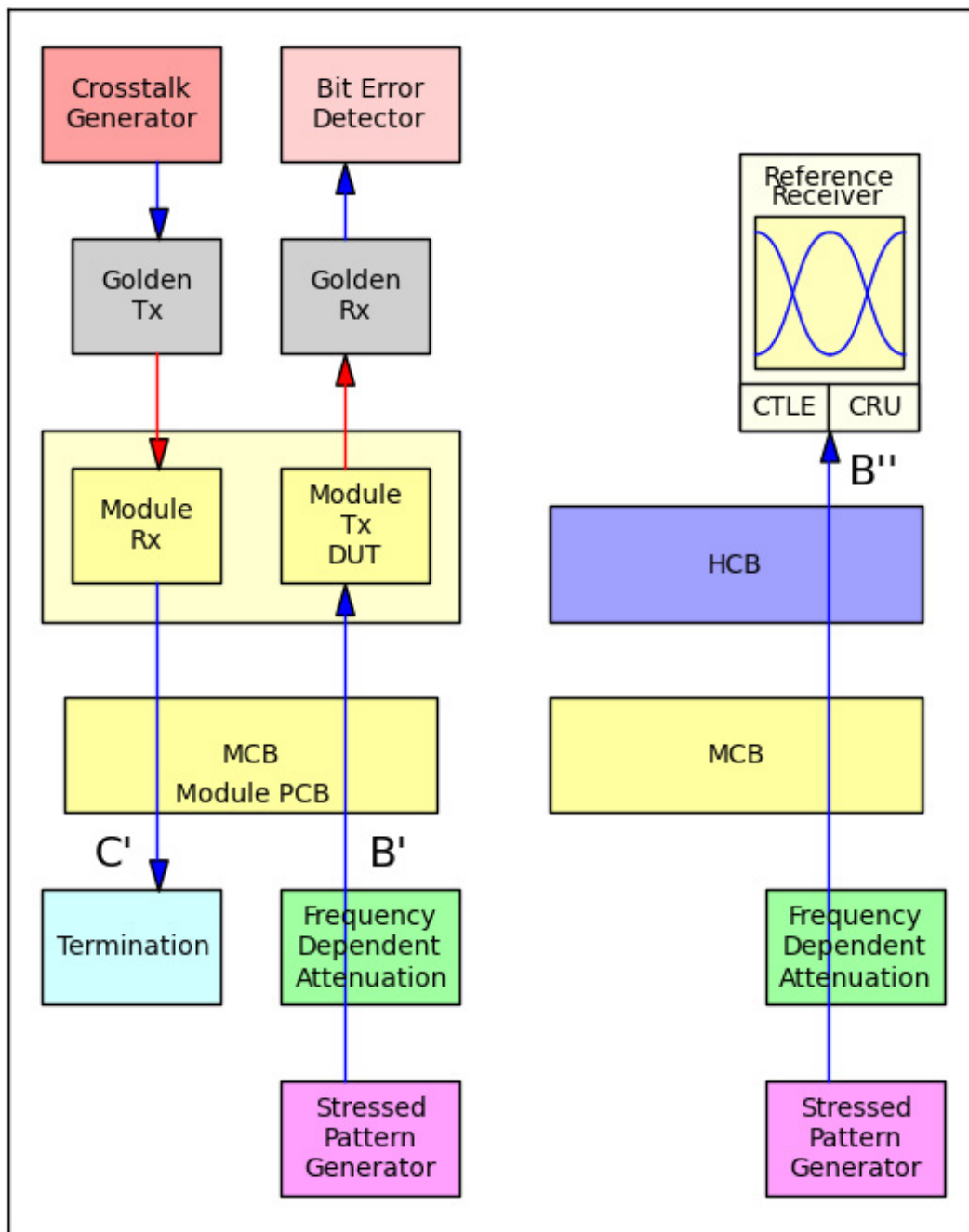
Figure 3.4 - Module electrical input stress test configuration (left) and calibration (right)

3.2.4 Module electrical input stressed receiver test configuration

The ability of the electrical input to the module's optical transmitter to tolerate jitter at a particular eye width and eye height as specified in FC-PI-6 [5] is tested using a stressed receiver test. The stressed signal is applied at compliance test point B' per Figure 2.2 using a module compliance board as specified in Clause 5. During test the stressed pattern generator issues PRBS31 test patterns; during calibration it issues PRBS9 test patterns. The test configuration is shown on the left of Figure 6.4. The stressed pattern generator is detailed in subclause 3.2.9. The module electrical input stressed receiver test method is detailed in subclause 3.3.2. A frequency dependent attenuator (subclause 3.2.10) simulates the host PCB trace loss.
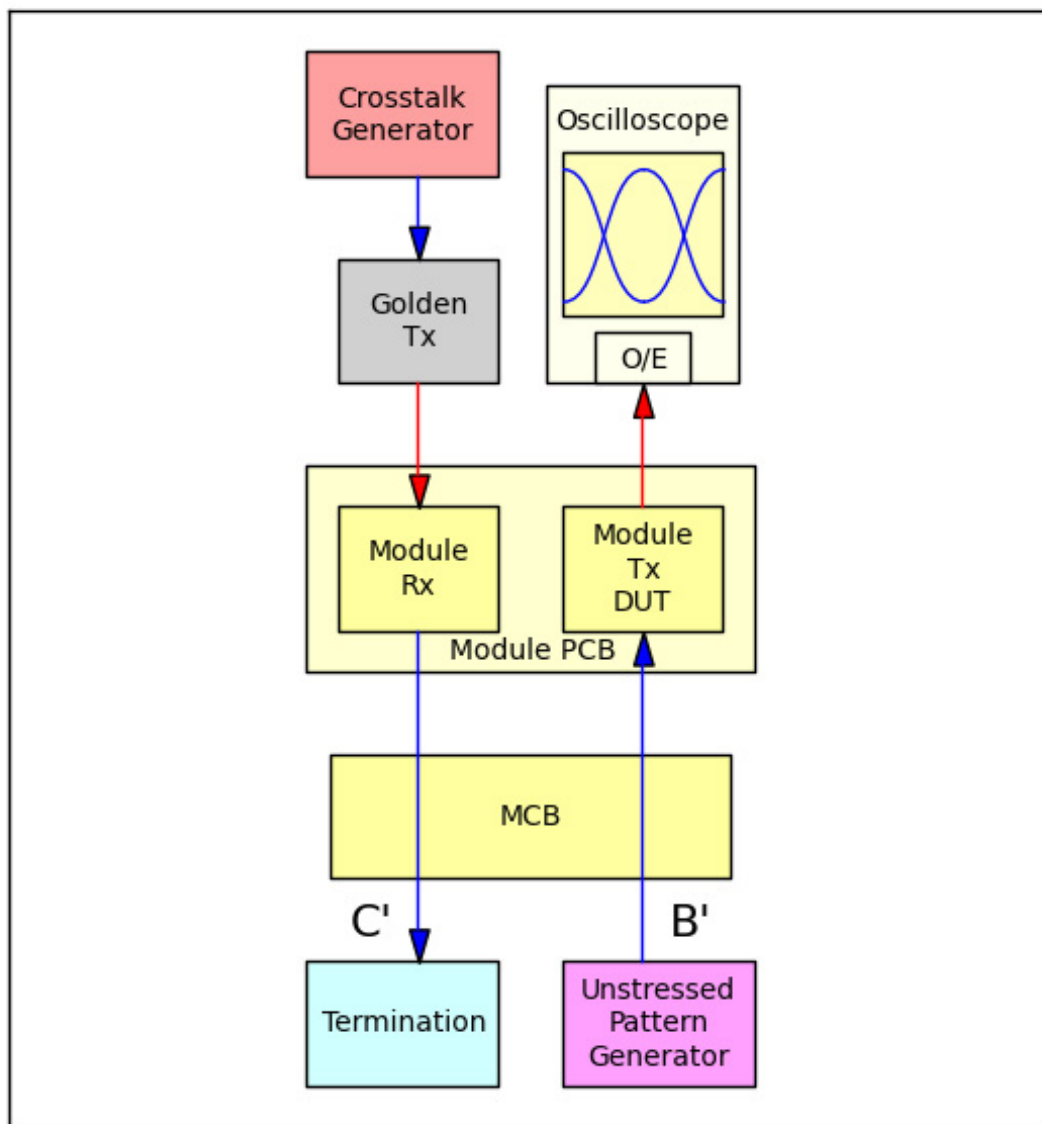
Figure 3.5 - Module optical output compliance test configuration

3.2.5 Module optical output test configuration

Module optical transmitter compliance tests include RIN_xOMA (subclause 3.4.3), Transmitter and Dispersion Penalty (TDP, subclause 3.4.1) for singlemode links, and VECPq (subclause 3.4.2) for multimode links. A typical test configuration for VECPq is shown in 3.5.
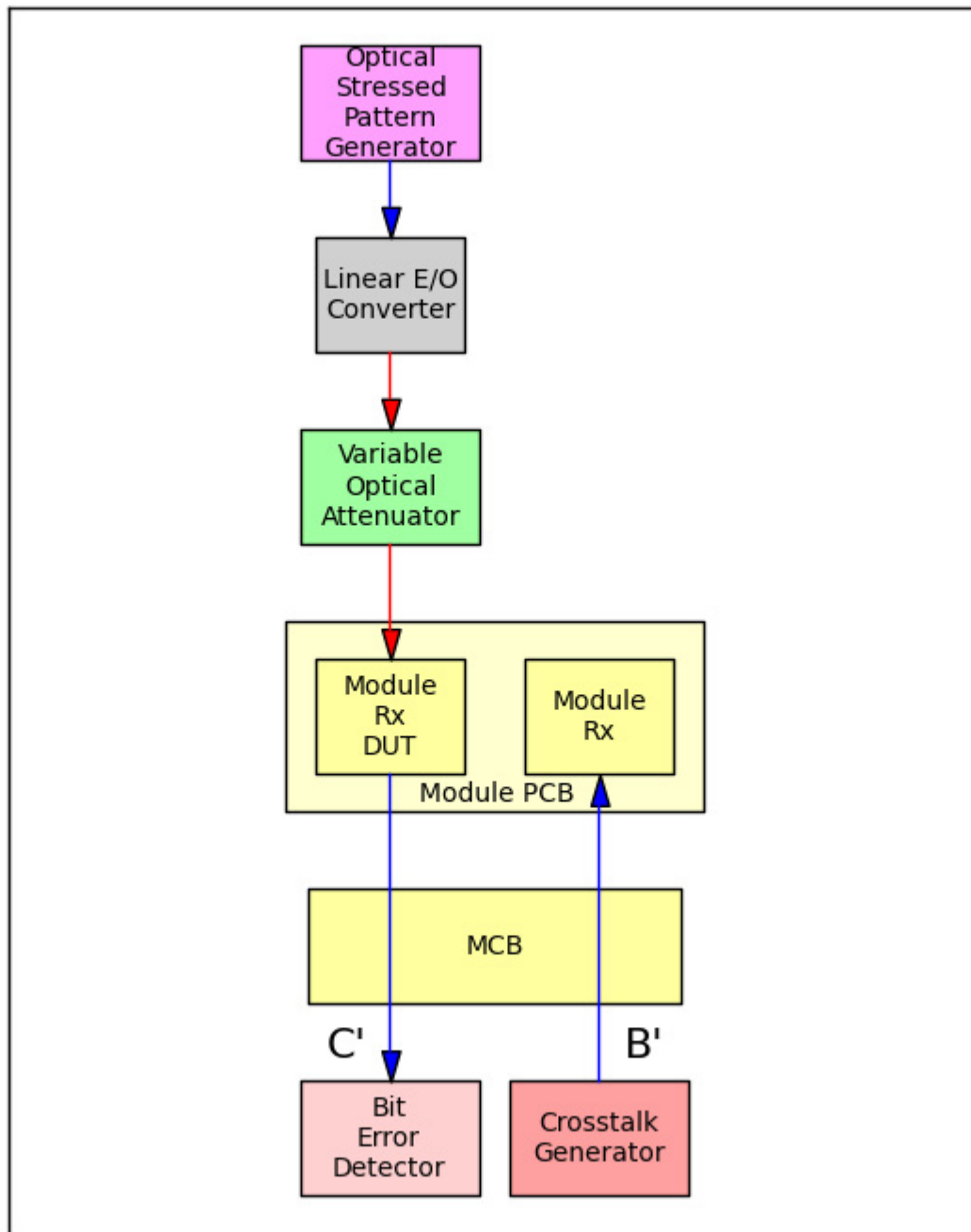
Figure 3.6 - Module optical input stressed receiver sensitivity test configuration

3.2.6 Module optical input stressed receiver test configuration

One compliance test for the module optical receiver for multimode links is the stressed receiver sensitivity (subclause 3.4.5), using the test configuration shown in Figure 3.6, and with the optical stressed pattern generator of Figure 3.10.
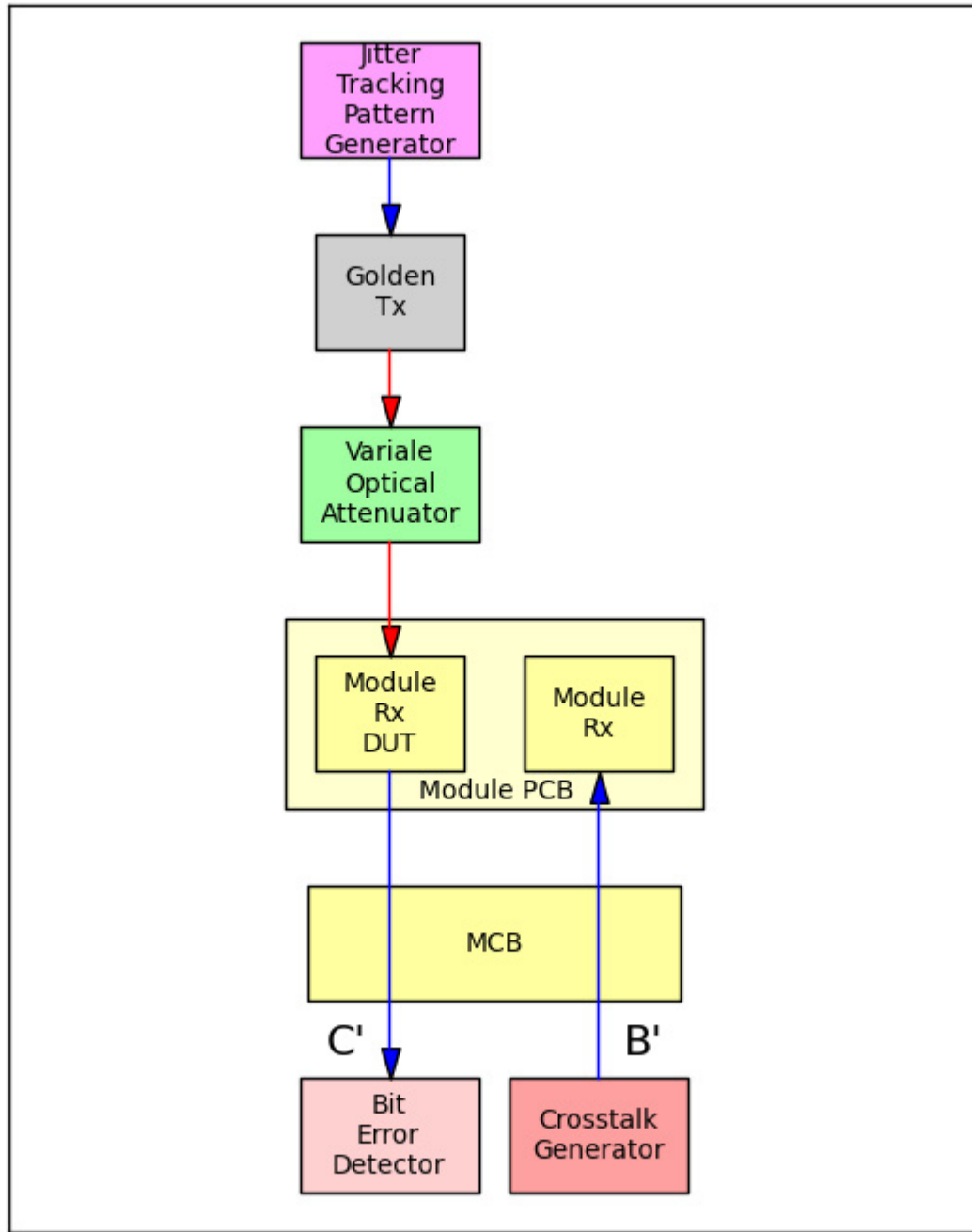
Figure 3.7 - Module optical input jitter tracking test configuration

3.2.7 Module optical input jitter tracking test configuration

Another compliance test for module optical receivers is jitter tracking (subclause 3.4.6), using the test configuration shown in Figure 3.7, with the jitter tracking pattern generator of Figure 3.10.

01
02
03
04
05
06
07
08
09
10
11
12
13
14
15
16
17
18
19
20
21
22
23
24
25
26
27
28
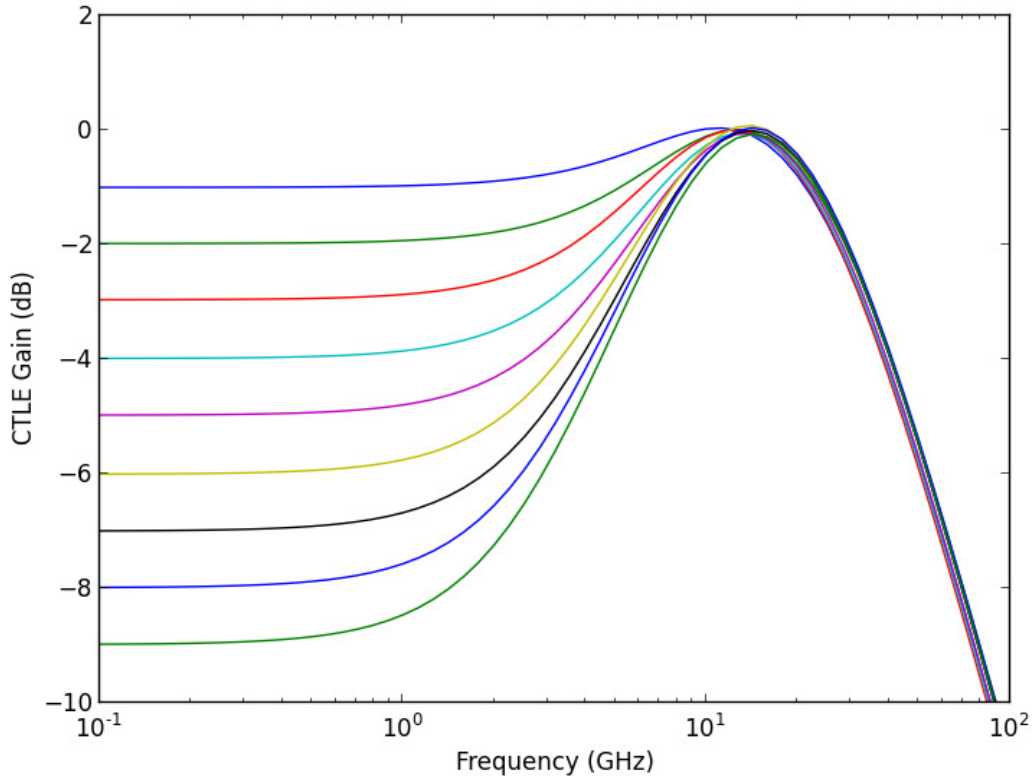
Figure 3.8 - Host output reference receiver equalizer (CTLE) transfer function for gains of 1-9 dB

3.2.8 Reference receiver

3.2.8.1 Reference clock recovery unit (CRU)
The scope is triggered with a clock from a reference clock recovery unit (CRU) with a second order transfer function with a 3 dB tracking bandwidth of fb/2578 and a maximum peaking of 0.1 dB in the jitter transfer response. fb is the baud rate, which for 32GFC is 28.05 Gbd. In the case of a real time scope, the reference CRF can be implemented in software.

3.2.8.2 Reference continuous time linear equalizer (CTLE)
The waveform is observed through a fourth-order Bessel-Thomson response with a bandwidth of 40 GHz concatenated with a Continuous Time Linear Equalizer (CTLE). The filters may be implemented in software. However, the signal is not averaged. The CTLE shall be implemented based on Equation 6.1 in which G is the gail and Z1,P1, and P2 are the CTLE zero and poles coefficients.

$$H(s) = \frac{G \cdot P1 \cdot P2}{Z1} \cdot \frac{S + Z1}{(S + P1) \cdot (S + P2)} \tag{3.1}$$

in which *S=j2πf*.

Figure 6.8 illustrates the frequency response of the reference equalizer used for host output testing with values for Z1, P1, and P2 listed in Table 6.2. Figure 6.x [*Ed: does not exist*] illustrates the frequency response of the reference equalizer used for module output testing with values for Z1, P1, and P2 listed in

Table 6.x [*Ed: does not exist*]. Note that the peaking is centered at 14 GHz. The peaking value equals the difference between the low frequency gain (1 MHz) and the high frequency gain at Nyquist in dB.

Table 3.2 - Reference receiver equalizer coefficients

Peaking (dB)	G	P1/2π (GHz)	P2/2π (GHz)	Z1/2π (GHz)
1	0.890	18.6	14.1	8.3
2	0.795	18.6	14.1	7.1
3	0.710	15.6	14.1	5.7
4	0.631	15.6	14.1	5.0
5	0.563	15.6	14.1	4.4
6	0.500	15.6	14.1	3.8
7	0.446	15.6	14.1	3.4
8	0.396	15.6	14.1	3.0
9	0.355	15.6	14.1	2.7
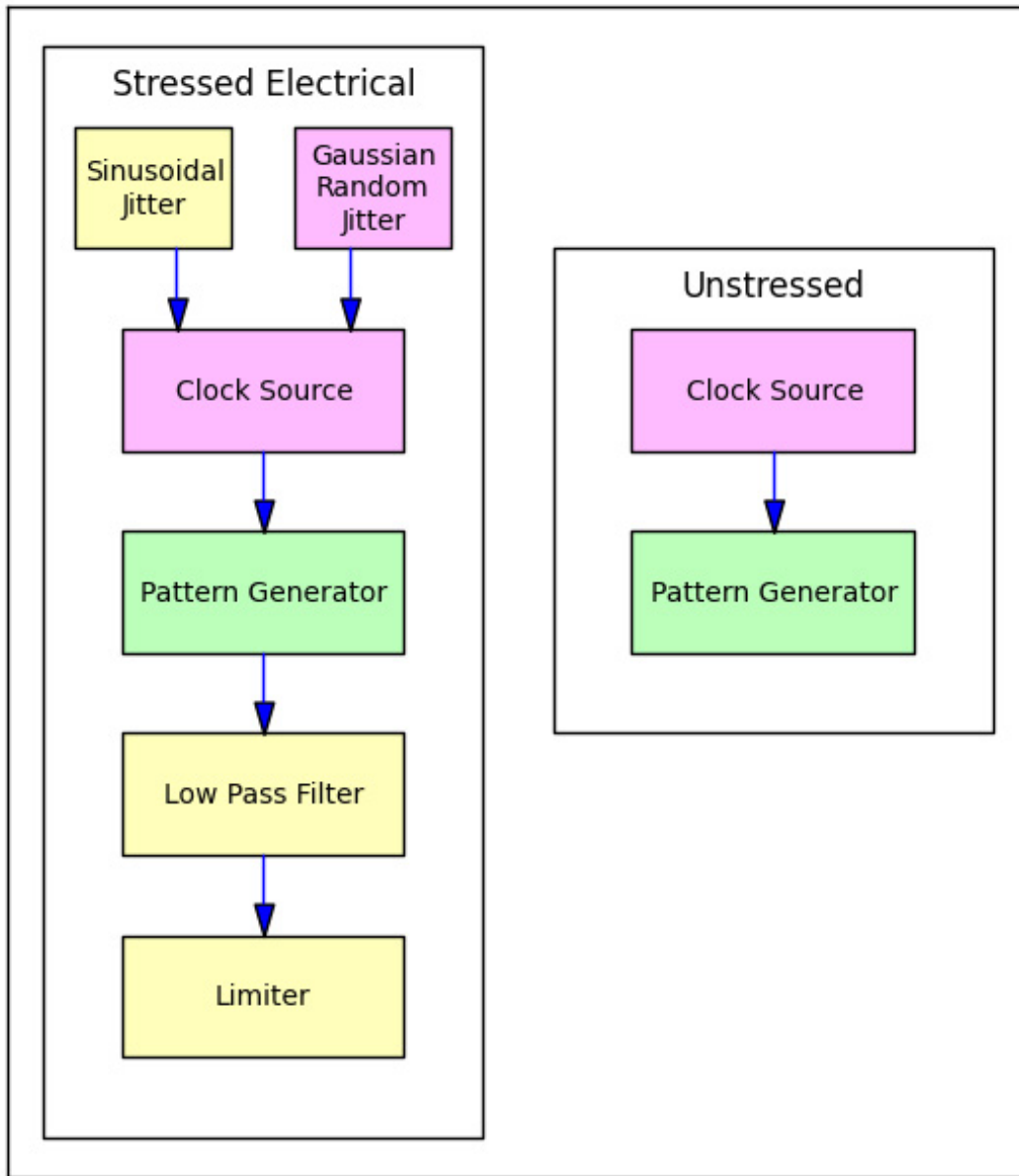
Figure 3.9 - Stressed (left) and unstressed (right) pattern generators

3.2.9 Stressed and unstressed pattern generator

The stressed pattern generator required for electrical input stress tests (Figure 3.2 and Figure 3.4) is detailed on the left in Figure 3.9. This is the most intricate pattern generator configuration. The simplest is the unstressed PRBS9 pattern generator, as used in Figure 3.3 and Figure 3.5 and diagramed on the right in Figure 3.9.

The optical receiver stressed pattern generator (Figure 3.6) is a subset of the stressed pattern generator, and is shown on the left in Figure 3.10. The optical jitter tracking pattern generator is shown on the right in
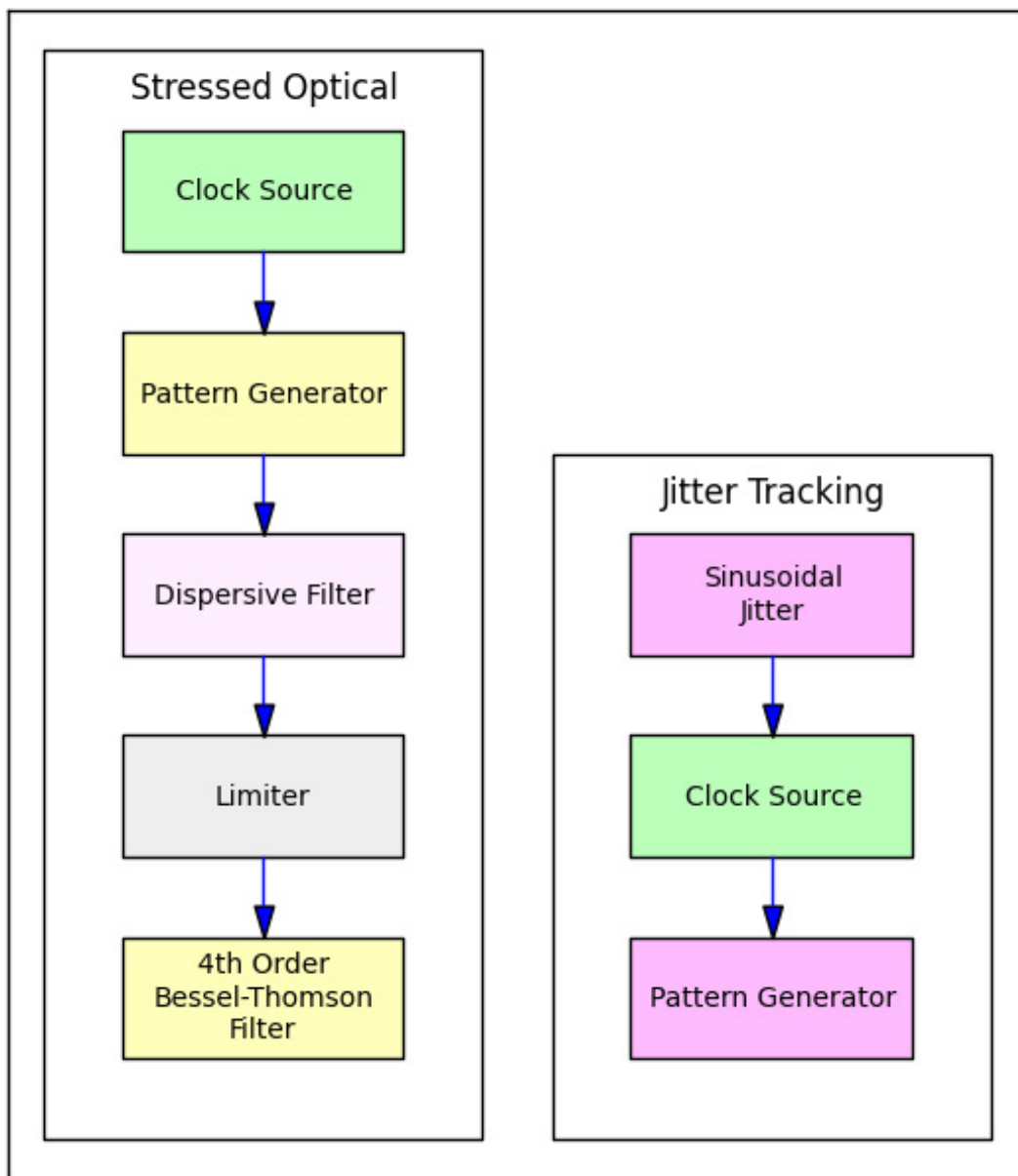
Figure 3.10 - Optical stressed receiver pattern generator (left) and optical jitter tracking pattern generator (right)

Figure 3.10.

01
02
03
04
05
06
07
08
09
10
11
12
13
14
15
16
17
18
19
20
21
22
23
24
25
26
27
28
29
30
31
32
33
34
35
36
37
38
39
40
41
42
43
44
45
46
47
48
49
50
51
52
53
54
55
56

3.2.10 Frequency dependent attenuation

[*Ed.: needs content!*]

Figure 3.11 - Compliance test point B and C jitter and eye height measurement

3.3 Electrical compliance test methods

3.3.1 Eye width EWx and eye height EHx

EWx and EHx represent the eye width (EW) and eye height (EH) defined to the 10^{-x} BER point, in which x corresponds to the BER requirement listed in FC-PI-6 [5]. For x ≤ 6, the eye width and eye height can be directly calculated using steps listed below. For x>6, the eye width and eye height are extrapolated using the methods described in steps 6 and 8.

The test method for measuring either the host or module electrical output eye width and eye height is as follows:

1) Set the host or module to PRBS9 test pattern. This allows a pattern lock when using a sub-sampling scope to measure the received equalized eye.
2) Capture the receive signal at compliance test points B or C with a scope triggered with a clock from a reference clock recovery unit (CRU) as described in subclause3.2.8. For compliance point B, the scope shall be AC coupled.
3) Sample the signal with a minimum sampling rate of 3 (equally spaced) samples per unit interval. Collect sufficient samples equivalent to 4 million unit intervals in order to construct normalized cumulative distribution function (normalized CDF) of the post processed captured signals to a probability of 10^{-6} (without extrapolation) as described below.
4) Apply the reference receiver as defined in subclause 3.2.8 to equalize the captured signal in step 3. For module electrical compliance test, the CTLE peaking in the reference receiver shall be set at either 1 dB or 2 dB. Any CTLE setting which meets both the EHx and EWx requirements defined in FC-PI-6 [5] is acceptable. For host compliance test, the CTLE peaking in the reference receiver shall be set at one of 8 settings from 3 dB to 10 dB in 1 dB steps. Any CTLE setting which meets both the EHx and EWx requirements defined in FC-PI-6 [5] is acceptable. The range of 3-10 dB is

5) Use the differential equalized signal from step 4 to construct CDFs of the jitter at zero crossing, for both left edge (CDFL) and right edge (CDFR) of the eye, as a distance from the center of the eye. Calculate the eye width EW6 as the difference in time between the CDFR and CDFL with a value of 10^{-6}. CDFL and CDFR are calculated as the cumulative sum of histograms of the zero crossing samples at the left and right edges of the eye normalized by the total number of sampled unit intervals (e.g., sampled unit intervals are 4 million per step 2 recommendation). For a pattern with 50% transition density (TD) the maximum value for the CDFL and CDFR will be 0.5. CDFL and CDFR are equivalent to bathtub curves in which the bit error ratio (BER) is plotted versus sampling time.

6) Apply Dual-Dirac and tail fitting separately to CDFL and CDFR to estimate random jitter. Calculate the best linear fit in Q-scale over the range of probabilities of 10^{-4} to 10^{-6} of the CDFL and CDFR to yield RJL and RJR respectively. RJL is the rms value of the jitter estimated from CDFL; RJR is the rms value of the jitter estimated from CDFR. Eye width EWx at the 10^{-x} probability is extrapolated as given in Equation 3.2, with the mapping of bit error ratio 10^{-x} to Q as given in Equation 3.3, using norminv which is available from Excel, Matlab, or Octave.

$$EWx \ = \ EW6 - [Q(x) - Q(6)] \cdot (RJL + RJR) \qquad (3.2)$$

$$Q(x) \ = \ -norminv\left(\frac{10^{-x}}{TD}, 0, 1\right) \qquad (3.3)$$

7) Use the differential equalized signal from step 4 to construct the CDFs of the signal amplitude in the middle 5% of the eye, for both logic one (CDF1) and logic zero (CDF0), as a distance from the center of the eye. Calculate the eye height EH6 as the difference in amplitude between CDF1 and CDF0 with a value of 10^{-6}. CDF0 and CDF1 are calculated as the cumulative sum of histograms of the amplitude samples at the to and bottom of hte eye normalized by the total number of sampled unit intervals (e.g., sampled unit intervals are 4 million per step 2 recommendation). For a pattern with a well balanced number of ones and zeros the maximum value for CDF0 and CDF1 will be 0.5. The middle of the eye is define UI/2 away from the mean zero corssing points of the equalized signal from step 4.

8) Apply Dual Dirac and tail fitting separately to CDF1 and CDF0 to estimate noise at the middle of the eye. Calculate the best linear fit in Q-scale over the range of probabilities 10^{-4} to 10^{-6} of the CDF1 and CDF0 to yield RN1 and RN0 respectively. RN1 is the rms value of the noise estimated from CDF1; RN0 is the rms value of the noise estimated from CDF0. Eye height EHx is extrapolated as

$$EHx \ = \ EH6 - [Q(x) - Q(6)] \cdot (RN0 + RN1) \qquad (3.4)$$

9) At compliance test point C calculate vertical eye closure (VEC) as 20*log(AV/EH7), in which AV is the eye amplitude of the equalized waveform. Eye amplitude is defined as the mean value of logic one minus the mean value of logic zero in the central 5% of the eye.

10) Passing is defined as a single equalizer setting that meets both EHx and EWx specifications listed in FC-PI-6 [5].

3.3.2 Electrical input stressed receiver test

The test configuration for host input stressed receive compliance is detailed in subclause.3.2.2. The test configuration for module electrical input stressed receive compliance is detailed in subclause 3.2.4.

The host and module electrical input shall tolerate a peak-to-peak sinusoidal jitter with frequency and amplitude define by FC-PI-6 [5].

The reference receiver of subclause 3.2.8 is used to calibrate the stressed receiver test signal at C" for the host and at B" for the module using a PRBS9 test pattern. During test the test pattern for stressed receive test shall be PRBS31; during calibration the test pattern is PRBS9.

To assure accurate test signal calibration, the jitter magnitude of the individual components should be calibrated successively in order of increasing magnitude. All of the stress sources should be enabled during the calibration process, with the higher magnitude sources set to 0 jitter magnitude during the calibration measurement of the lower magnitude components. The high deviation (> 1 UI) sinusoidal jitter component specified by the sinusoidal jitter mask can be measured either directly by a reference receiver clock recovery unit with phase error measurement capability, or directly on a oscilloscope when using a divide by four clock test pattern (00001111). If a sampling oscilloscope is used for the latter method, it must be triggered from a clean (unjittered) clock sourced from the stressed pattern generator, rather than the reference receiver CRU in order to measure the lower frequency SJ components.

The receiver under test shall meet the BER specified in FC-PI-6 [5].

3.3.3 Crosstalk signal calibration

The crosstalk source is asynchronous to the main pattern generator. The amplitude and risetime of the crosstalk source are given in FC-PI-6 [5]. During test the crosstalk pattern is PRBS31 or valid Fibre Channel signal; during calibration the test pattern is PRBS9.

3.3.4 Common mode noise rms

Common mode noise specification is to be measured using the following test procedure.

The data pattern is normal traffic or a common test pattern. Connect both waveform polarities through a suitable test fixture to a 50 ohm communication analysis oscilloscope system. Waveforms are not triggered (free-run mode). Scope shall have a minimum bandwidth (including probes) of 1.8 times the signaling rate. No filtering except AC coupling with a high-pass 3dB low frequency not greater than 10MHz.

The two inputs are summed for common mode analysis. Set the horizontal scale for full width to span one UI. Set up a vertical histogram with full display width. Measure the rms value of the histogram. Common mode rms value (Ncm) is half the rms value of the histogram.

Apply Equation 3.5 to account for instrumentation noise.

$$Ncm = \sqrt{measured_{Ncm}^{2} - instrumentation_{noise}^{2}} \qquad (3.5)$$

3.4 Optical compliance test methods

3.4.1 Transmitter and Dispersion Penalty (TDP) for 3200-SM variants

Transmitter and dispersion penalty (TDP) is measured per IEEE 802.3 subclause 52.9.10 [4], amended such that receiver sensitivity is measured per 6.4.4 corresponding to a BER limit of 10^{-6}.

3.4.2 VECPq

VECPq is defined in subclause 2.2.3.5, and its method of measurement and calculation is given by clause 6 of MSQS [2]. For 3200-SN variants, the reference Q, denoted as Q_0, is calculated by Equation 3.3 for a reference BER of 10^{-6}.

3.4.3 Relative intensity noise RIN_xOMA

Relative intensity noise RIN_xOMA is measured per subclause 2.2.4.4 of MSQS [2], but with the return loss (single dominant reflection) as defined by FC-PI-6 [5].

3.4.4 Unstressed receiver sensitivity

The unstressed receiver sensitivity should be measured per subclause 2.3.1.2 of MSQS [2], but for a reference BER of 10^{-6}.

3.4.5 Stressed receiver sensitivity

The stressed receiver sensitivity should be measured per subclause 2.3.1.1 of MSQS [2], but for a reference BER of 10^{-6}.

3.4.6 Optical receiver jitter tracking

This procedure measures the ability of a receiver to track low frequency jitter without the occurrence of errors.

Figure 3.7 illustrates the measurement configuration for the receiver jitter tracking test. A pattern generator output is impaired by frequency modulation of the generating clock source. The pattern generator is connected to the receiver under test via a variable attenuator.

Two sets of jitter frequency and amplitude combinations are specified for each variant to which this procedure applies. These values are applied as the conditions of the two separate receiver jitter tracking tests. The variable attenuator is configured to set the amplitude at the receiver, in OMA for optical signals and VMA for electrical signals, to the jitter tolerance test amplitude specified for the variant. For each test, a BER of better than 10^{-6} shall be achieved.

Various implementations may be used, provided that the resulting jitter matches that specification. Phase or frequency modulation may be applied to induce the sinusoidal jitter, and the modulation may be applied to the clock source or to the data stream itself.

4 Extending the Link Budget Spreadsheet Model

4.1 Scope and overview

The 10 gigabit Ethernet link model has proven to be a powerful tool to facilitate optical Physical Layer specifications for laser-based links using both single-mode (SMF) and multimode (MMF) fiber [18]. It was reviewed in Clause 4 of MSQS [2]. Consider for example the 1600-M5E-SN-I physical link specification for multimode fiber links (Table 11 in FC-PI-5 [1]). A link budget analysis (Fibre Channel document T11/12-043v0) predicts a worst case eye diagram as shown in the left diagram of Figure 4.1. The eye closing is indicated by the dashed blue lines. For the 16GFC specification the inner eye just touches the desired eye mask, the red hexagonal region.
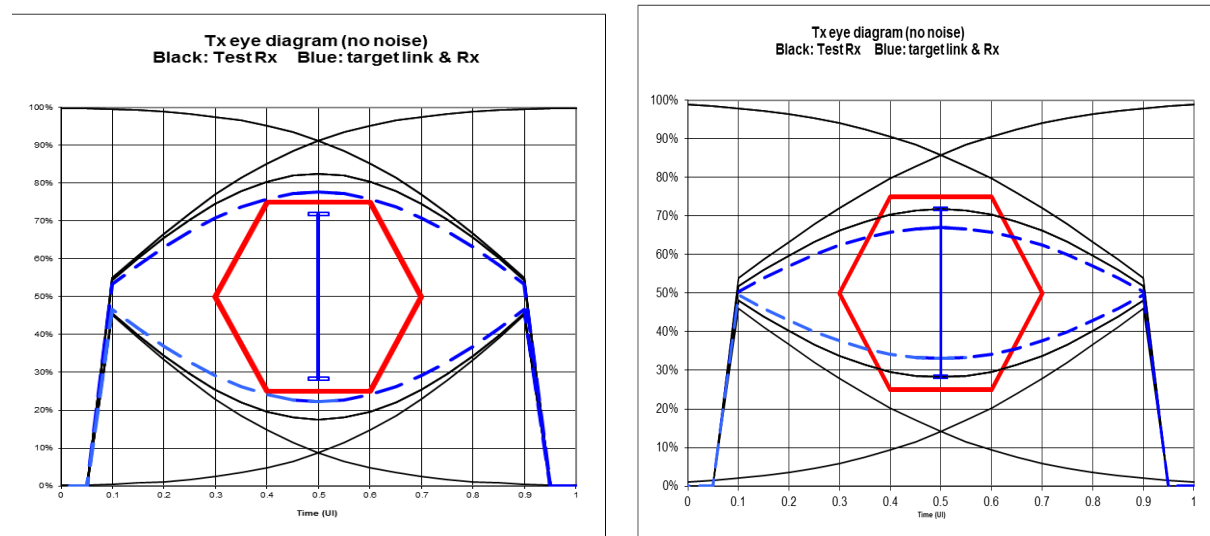
Figure 4.1 - Typical eye diagrams for 16GFC (left) and 32GFC (right) MMF variants

A partial list of parameters defining the 1600-M5E-SN-I variant is given in Table 4.1, labeled as the "16GFC" variant. Next to that is a candidate "32GFC" variant for consideration for possible inclusion in FC-PI-6 [5]. Because of technical limitations, not all parameters of the candidate 32GFC variant can scale by a factor of 2 compared with the 16GFC variant. As a consequence, the composite optical link response is anticipated to be slower for the 32GFC in proportion to the signaling symbol period. The corresponding eye diagram shown in the right diagram of Figure 4.1 is more fully closed, resulting in unacceptable link performance for Fibre Channel applications. The candidate 32GFC analysis is contained in Fibre Channel document T11/12-044v0.

Two possible techniques under consideration for improving 32GFC link performance include equalization in the receiver and forward error correction (FEC). The scope of the present clause is to extend the link model to include equalization and FEC to facilitate comparisons of alternative link architectures. In the process, key concepts in the original 10 gigabit Ethernet link model will be more fully elucidated. The linear fiber link model is reviewed in 4.2, in the absence of equalization or forward error correction mitigations. A simple 3-tap feed-forward equalizer (FFE) is modeled in 4.3, initially neglecting noise impacts. A sample eye diagram for the 32GFC link using a 3-tap FFE is shown in Figure 4.2. Basic noise analytical methods are discussed in 4.4, followed by a detailed analysis of laser relative intensity noise (RIN). Noise impact on optimum equalizer tap weights is reviewed in 4.5. Mode partition noise (MPN) is discussed in 4.6. Forward error correction (FEC) is studied in .

Table 4.1 - Partial listing of critical link design parameters for a 16GFC and a 32GFC variant.

Link Element	Parameter	16GFC	32GFC
Host	Signaling Rate	14.025 GBd	28.05 GBd
Transmitter	10%-90% rise time	51 ps	32 ps
	$RIN_{12}OMA$	-128 dB/Hz	-131 dB/Hz
	Min wavelength	840 nm	840 nm
	Spectral width	0.59 nm	0.50 nm
Fiber Link	Length	100 m	100 m
	Modal bandwidth	2000 MHz-km	4500 MHz-km
Receiver	Bandwidth	11 GHz	16.8 GHz
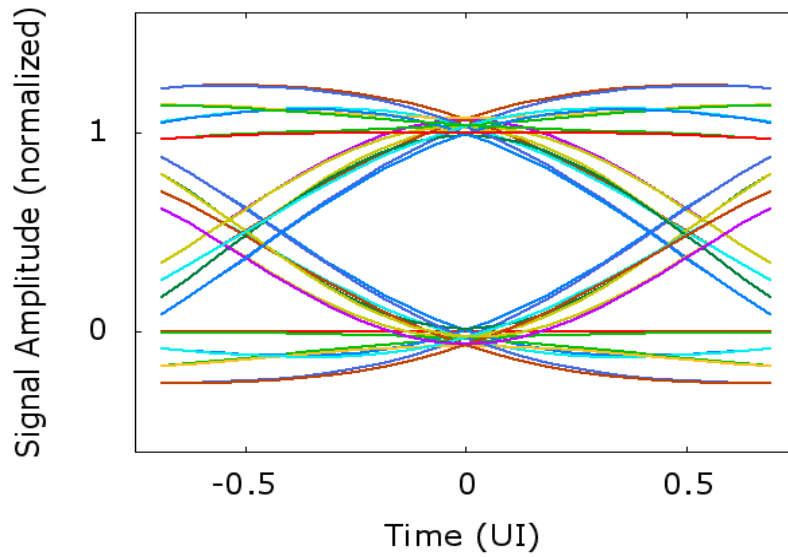
Figure 4.2 - 32GFC link eye diagram with 3-tap feed forward equalizer (FFE).

4.2 Composite optical link response

4.2.1 Dominant power penalty is P_{isi}

To understand better the eye closure shown for the 32GFC candidate in Figure 4.1, consider the following breakdown of link budget power penalties, as shown in Figure 4.3 and as reported by the link model. We find that the dominant contribution is P_{isi}, the power penalty due to inter-symbol interference as discussed in subclause 4.4.2, as given by Equation 4.7 of MSQS [2], and as reported by Dolfi [14]. A detailed derivation of MSQS Equation 4.7 will be given in this subclause.
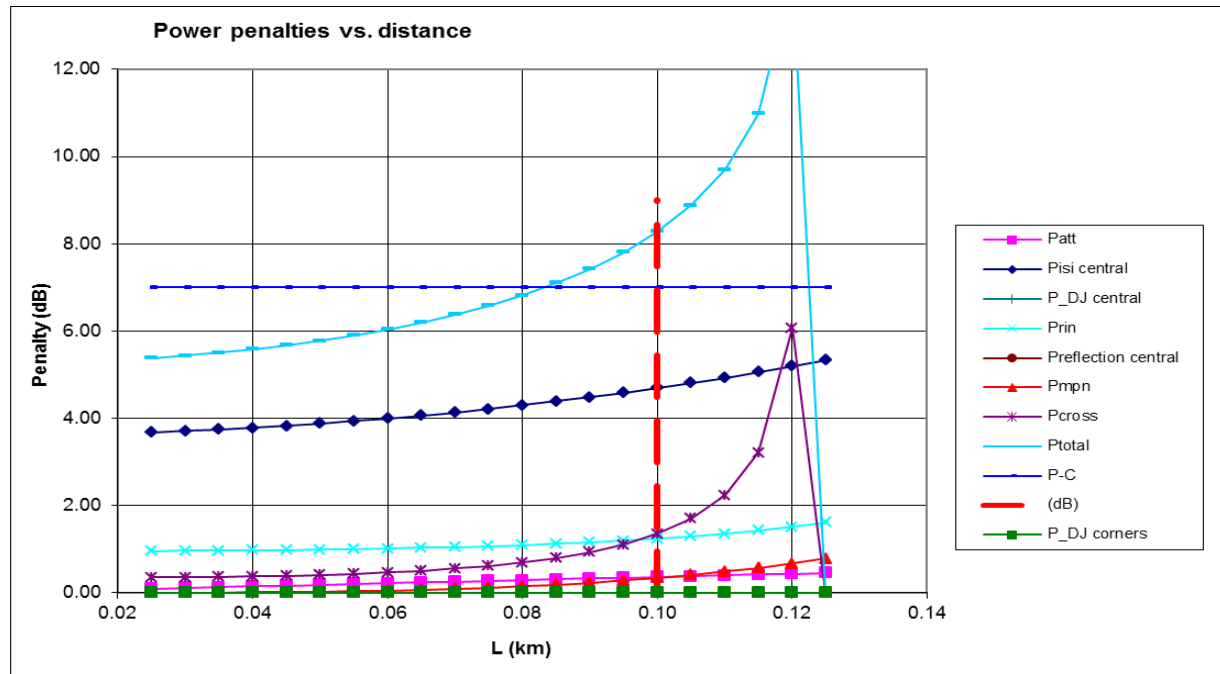
Figure 4.3 - Breakdown of link power penalites for the 32GFC candidate specification

4.2.2 Derivation of the unit pulse response

We start with a block diagram of the linear optical link response model as shown in Figure 4.4. The model starts with an input binary signal stream $\{x_n\}$. The first block is NRZ pulse generator $p(t)$ which outputs a series of pulses in response to $\{x_n\}$. The nominal pulse interval is T, the inverse of the nominal signaling rate B. However, at selected steps in the analysis as noted we will consider degradation due to pulse width shrinkage. The blocks $I_t(t)$, $I_{cd}(t)$, $I_{md}(t)$, $I_f(t)$, and $I_r(t)$ represent Gaussian impulse responses corresponding to the transmitter, fiber chromatic dispersion, fiber modal dispersion, fiber link, and receiver respectively. The fiber chromatic dispersion and modal response combine to define a fiber channel response

$$I_f(t) \equiv I_{cd}(t) \otimes I_{md}(t) \quad . \tag{4.1}$$

The individual response blocks convolve to define a composite unit pulse response $h(t)$. The unit pulse response convolves with the input bit stream $\{x_n\}$ to define the signal $y(t)$ delivered to the final block, the

slicer. The slicer determines whether the output signal should be a *0* or a *1*.
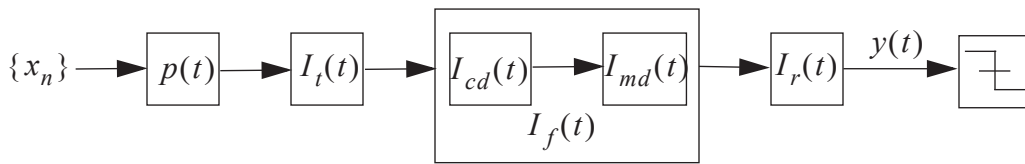
Figure 4.4 - Link model block diagram.

Next let us summarize in Table 4.2 the symbols to be used in this clause.

Table 4.2 - Symbol definitions.

Symbol	Definition	Location
a	equalizer tap weight ratio	Equation 4.31
a_i, $a(\lambda)$	normalized power content for multimode laser	4.6
B	nominal symbol rate	4.2.2
D	linear dispersion	Equation 4.85
$error$	error associated linear equalizer tap weights	Equation 4.28
$eye(t)$	generalized eye shape function for MPN analysis	4.6.3
f	frequency	4.4.3.1
$G(f)$	tap sampling spectrum	Equation 4.52
$g(t)$	tap sampling impulse response	Equation 4.24
$gain$	gain needed to normalizer modulation amplitude with equalizer	Equation 4.30
H	5x3 matrix useful for calculating MMSE tap weights	Equation
$h(t)$	unit pulse response in absence of equalization	Equation 4.6
$\widehat{h}(t)$	unit tap response with linear equalizer	Equation 4.23
h_{-1}, h_0, h_1	unit pulse response in absence of equalization at decsion times -T,0,T	4.3.2
$\widehat{h}_{-2}$, $\widehat{h}_{-1}$, $\widehat{h}_0$, $\widehat{h}_1$, $\widehat{h}_2$	unit pulse response with equalization at decision times -2T,-T,0,T,2T	Equation 4.39
$I_c(t)$	impulse response for composite optical link	Equation 4.7
$l_c(f)$	frequency response of composite optical link	Equation 4.28

Table 4.2 - Symbol definitions.

Symbol	Definition	Location
$I_t(t), I_r(t), I_{tap}(t)$ $I_{cd}(t), I_{md}(t), I_f(t)$	impulse response of transmitter (t), receiver (r), tap, chromatic dispersion (cd), modal dispersion (md), and fiber (combined cd and md)	Figure 4.4, Figure 4.21
ISI	eye opening of most closed eye, linear units, scaled to modulation amplitude	4.2.3
J	cost function for minimum mean square error (MMSE) calculation of optimum equalizer tap weights	Equation 4.28
k_{oma}	Ogawa k-factor for mode partition noise analysis	Equation 4.100
k_{rin}	factor for calculating laser RIN when composite impulse response is Gaussian	Equation 4.47
n_r, n_{rin}, n_{total}	standard deviation of receiver noise (r), laser RIN, and total noise (combination of r and rin)	4.4.2, Equation 4.58
NEF	noise enhancement factor	Equation 4.55
$p(t)$	ideal rect pulse profile	Equation 4.3
$\wp(\delta y)$	probability distribution for noise δy	Equation 4.38
P_{alloc}	effective system power budget	Equation 4.73
P_{isi}	power penalty to compensate for inter-symbol interference	Equation 4.19
P_{mpn}	power penalty to compensate for mode partition noise	Equation 4.109, Equation 4.114
P_{rin}	power penalty to compensate for laser relative intensity noise (RIN)	Equation 4.62
PWS	pulse width shrinkage	4.2.2, Figure 4.8
Q	signal-to-noise ratio, dimensionless	4.4.2
Q_0	signal-to-noise ratio corresponding to 10^{-12} BER	4.4.2
$RIN(f)$	laser relative intensity noise, a function of frequency	Equation 4.44
$S(\lambda)$	dispersion slope	Equation 4.86
$S(t)$	slope of eye diagram at optimum decision time	Equation 4.110
s	signal strength	4.4.1
s_{min}	minimum signal strength needed to achieve 10^{-12} BER under worst case conditions	Equation 4.57

Table 4.2 - Symbol definitions.

Symbol	Definition	Location
t	time	
T	nominal symbol period, inverse of B	4.2.2
$t_{0.1}, t_{0.9}$	time for edge response to reach 10% and 90% of final quiescent value	Figure 4.6
T_c	rise time (10%-90%) for composite optical link	Equation 4.8, Equation 4.25, Equation 4.48, Equation 4.54
$T_t, T_{cd}, T_{md}, T_f, T_r, T_{tap}$	rise time (10%-90%) for transmitter (t), chromatic dispersion (cd), modal dispersion (md), fiber (f), receiver (r), and equalizer tap	4.2.2
u, v	scaling times for version 1 and version 2 impulse response functional forms	Table 4.3
v	phase velocity of light propagating through fiber link	Equation 4.79
v_g	group velocity of light propagating through fiber link	Equation 4.80
$W(f)$	noise spectral density	Equation 4.42
x_n	incident signal bit sequence of 0's and 1's	4.2.2, Figure 4.4
$y(t)$	receive signal presented to slicer for determination of output sequence of 0's and 1's, in absence of equalization	4.2.2, Figure 4.4
$\widehat{y}(t)$	receive signal presented to slice, with equalization	Equation 4.22
β	propagation constant for light traveling through fiber	Equation 4.78
β	dimensionless parameter in mode partition noise analysis	Equation 4.105
$\delta(t)$	Dirac delta function	
$\delta y(t)$	noise contribution to signal presented to the slicer	4.4.2
λ	wavelength of light in vacuum	
λ_c	center wavelength of multimode laser	4.6.2
$\rho(t)$	noise auto-correlation function	Equation 4.35
σ_{mpn}	noise-to-signal ratio for mode partition noise	Equation 4.108, Equation 4.113
σ_{rin}	noise-to-signal ratio for laser RIN	Equation 4.49

Table 4.2 - Symbol definitions.

Symbol	Definition	Location
$\tau_{-1}, \tau_0, \tau_1$	linear equalizer tap weights	4.3.1, Figure 4.12
$\tau(\lambda)$	transit time per unit length of fiber	Equation 4.82
ω	angular frequency	Equation 4.77

In the absence of any bandwidth limitations, the ideal signal y(t) presented to the slicer would be

$$y(t) \; = \; \sum x_n \cdot \delta(t - nT) \otimes p(t) \qquad (4.2)$$

in which $\delta(t)$ is the Dirac delta function and *p(t)* is the rect function defined by

$$p(t) \equiv \begin{cases} 1 & -\dfrac{T}{2} < t < \dfrac{T}{2} \\ 0 & otherwise \end{cases} \qquad (4.3)$$

Convolution is defined by the following integral:

$$f(t) \otimes g(t) \equiv \int_{-\infty}^{\infty} f(t') \cdot g(t - t')dt' \qquad (4.4)$$

However because of finite fiber link bandwidth limitations, the signal *y(t)* presented to the slicer is degraded as defined by

$$y(t) \; = \; \sum_n x_n \cdot \delta(t - nT) \otimes h(t) \qquad (4.5)$$

in which the unit pulse response *h(t)* is given by the following convolution operation:

$$h(t) \; = \; p(t) \otimes I_c(t) \qquad (4.6)$$

We define a composite impulse response *I_c(t)* by

$$I_c(t) \equiv I_t(t) \otimes I_{cd}(t) \otimes I_{md}(t) \otimes I_r(t) \qquad (4.7)$$

The degraded unit pulse response spreads into adjacent symbol periods, as shown in Figure 4.5. This is intersymbol interference (ISI).

In Figure 4.4, each of the blocks labeled with an *I(t)* is assumed to have a Gaussian impulse response. The composite fiber link response is given by the convolution of these various blocks; the convolution of a collection of Gaussians is a Gaussian. Each Gaussian is characterized by a rise time, defined as the time interval from the 10% to the 90% levels. The composite rise time T_c is given by the square root of the sum of the squares of the constituent rise times; see Equation 4.8. Several useful equations derived from this
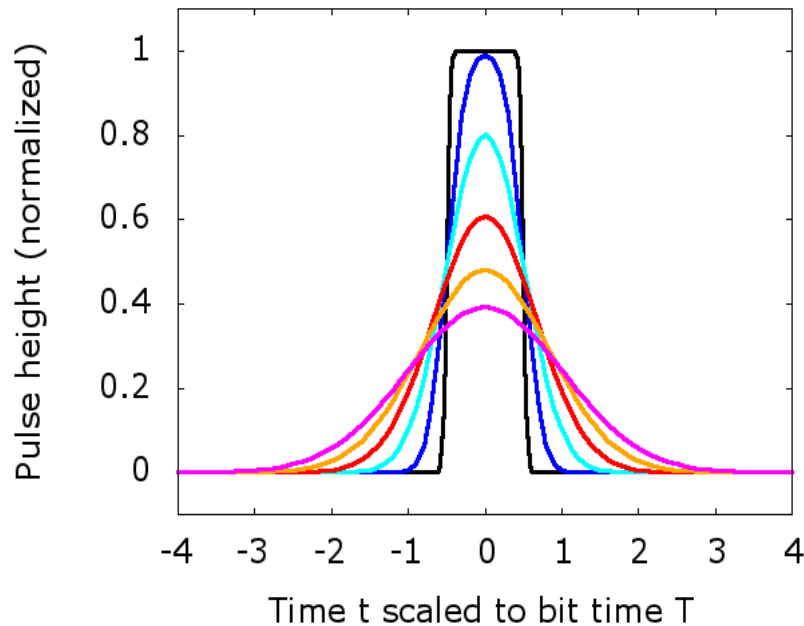
Figure 4.5 - Typical unit pulse profiles for various values of the composite link rise time T_c

Gaussian impulse response assumption are listed in Table 4.3.

Caution: the composite fiber link response time T_c as used in this clause will have multiple definitions depending upon the context of the discussion. In the present context (Figure 4.4) it has the definition

$$T_c^2 \equiv T_t^2 + T_{cd}^2 + T_{md}^2 + T_r^2 \tag{4.8}$$

Two alternative functional developments are sketched in Table 4.3, starting from almost identical impulse response Gaussians, differing only by a factor of 2 in the exponent, but leading to very different functional forms. For clarity, two different scaling times are listed: u and v., which we will shortly define in terms of the composite rise time T_c.

The functions in Table 4.3 adopt the terminology of probability analysis (*pdf* = probability distribution function, *cdf* = cummulative distribution function), even though the present discussion concerns temporal response rather than probability analysis. Nevertheless the functions available from probability analysis apply equally well to the temporal response analysis.The impulse response function $I(t) = pdf(t)$ is normalized to unity.

$$\int_{-\infty}^{\infty} pdf(t)dt = 1 \tag{4.9}$$

A key intermediate step in obtaining the unit pulse response is to calculate the edge response *cdf(t)*, i.e., the convolution of the composite impulse response with a unit step function, with results as shown in Figure 4.6.

$$cdf(t) = pdf(t) \otimes step(t) = \int_{-\infty}^{t} p(df(t'))dt' \tag{4.10}$$

.

Table 4.3 - Gaussian impulse response expressions

Measure	Version 1	Version 2
Composite impulse response	$pdf_1(t) = (\pi)^{-\frac{1}{2}} \cdot u^{-1} \cdot \exp\left(\frac{-t^2}{u^2}\right)$	$pdf_2(t) = (2\pi)^{-\frac{1}{2}} \cdot v^{-1} \cdot \exp\left(\frac{-t^2}{2v^2}\right)$
	$pdf(t) = \dfrac{A}{T_c} \cdot \exp\left(\dfrac{-B \cdot t^2}{T_c^{\,2}}\right)$ $A = \dfrac{2erfinv(0.8)}{\sqrt{\pi}} = \sqrt{\dfrac{2}{\pi}} \cdot norminv(0.9) = 1.0225$ $B = [2erfinv(0.8)]^2 = 2[norminv(0.9)]^2 = 3.2847$		
Edge response (Excel)	$cdf_1(t) = \frac{1}{2} \cdot \left[1 + erf\left(\frac{t}{u}\right)\right]$	$cdf_2(t) = normdist\left(\frac{t}{v}\right)$
Edge response (Matlab)	$cdf_1(t) = \frac{1}{2} \cdot \left[1 + erf\left(\frac{t}{u}\right)\right]$	$cdf_2(t) = normcdf\left(\frac{t}{v}\right)$
Inverse edge response (Excel)	Excel offers no inverse function	$t = v \cdot norminv(cdf)$
Inverse edge response (Matlab)	$t = u \cdot erfinv(2 \cdot cdf - 1)$	$t = v \cdot norminv(cdf, 0, 1)$
Time scale	$\dfrac{T_c}{u} = 2erfinv(0.8) = 1.812$	$\dfrac{T_c}{v} = 2norminv(0.9) = 2.563$
Composite frequency response	$I(f) = \exp(-\pi^2 \cdot u^2 \cdot f^2)$	$I(f) = \exp(-2\pi^2 \cdot v^2 \cdot f^2)$
	$I(f) = \exp\left[\dfrac{-\pi^2 \cdot T_c^{\,2} \cdot f^2}{4erfinv^2(0.8)}\right] = \exp(-3.005 T_c^{\,2} \cdot f^2)$		
3 dB bandwidth	$f_{3dB} = \dfrac{C}{T_c}$ $C = \dfrac{2\sqrt{\ln 2}}{\pi} erfinv(0.8) = 0.48030$		

in which

$$step(t) = \begin{cases} 0 & \text{for} \quad t < 0 \\ 1 & \text{for} \quad t > 0 \end{cases} \tag{4.11}$$

The convolved edge response grows from 0 to 1. Let us define $t_{0.1}$ as the time at which the edge response
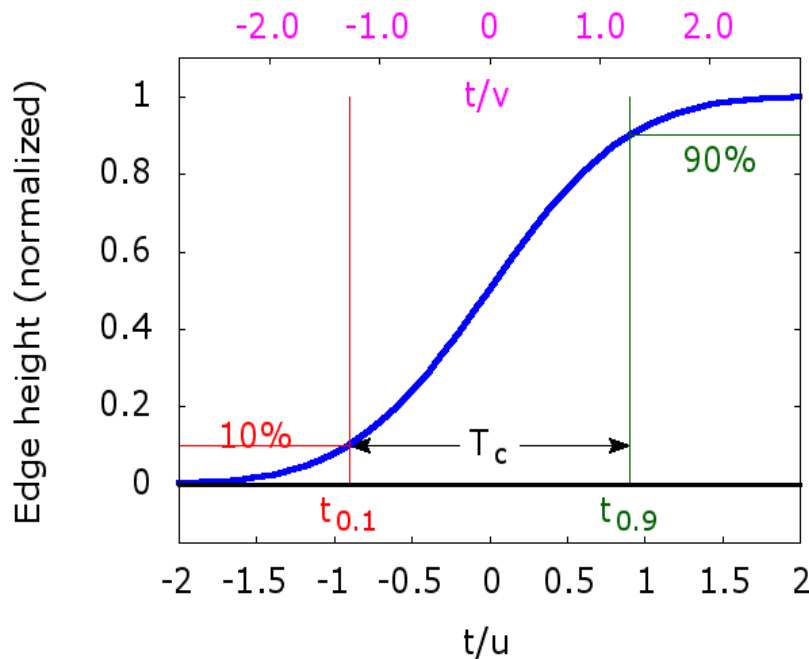
Figure 4.6 - Composite fiber link edge response.

reaches 10% of its final quiescent level. We similarly define $t_{0.9}$ as the time at which the edge response reaches 90% of its final quiescent level. The composite rise time T_c is defined as the interval from $t_{0.1}$ to $t_{0.9}$. The primary time scaling parameter is the composite fiber link rise time T_c; we need to calculate the scaling times u or v in terms of T_c. This is done by inverting the edge response, i.e., by calculating the time $t_{0.1}$ at which the edge response ("*cdf*" in Table 4.3) reaches 10% of the final quiescent level, i.e., a value of 0.1:

$$0.1 = \frac{1}{2} \cdot \left[1 + erf\left(\frac{t_{0.1}}{u}\right) \right] \tag{4.12}$$

with inverse

$$\frac{t_{0.1}}{u} = erfinv(-0.8) = -0.90619 \tag{4.13}$$

Similar expressions apply for $t_{0.9}$. From the above we have

$$\frac{T_c}{u} = \frac{t_{0.9} - t_{0.1}}{u} = 2\,erfinv(0.8) = 1.81238 \tag{4.14}$$

Similar arguments can be applied for the Version 2 function sequence in Table 4.3:

$$\frac{T_c}{v} = \frac{t_{0.9} - t_{0.1}}{v} = 2\,norminv(0.9) = 2.5631 \tag{4.15}$$

The reason for giving such detail is that the inverse error function is not commonly available, whereas the inverse normalized cdf is more readily available. Therefore unit pulse derivations given in the literature (such as Botacchi [10]) start with a Version 2 sequence, then switch to an error function expression by a square root of 2 time scale change. This is the source of the square root of 2 factor in the denominator in

01 Equation 4.7 of MSQS [2].

03 Once we have the edge response, deriving the unit pulse response for pulse period T is straightforward.

$$h(t) \ = \ \frac{1}{2}\left\{ erf\left[\frac{1.812}{T_c} \cdot \left(t + \frac{T}{2}\right)\right] - erf\left[\frac{1.812}{T_c} \cdot \left(t - \frac{T}{2}\right)\right]\right\} \qquad , \qquad (4.16)$$

09 or using the Version 2 function sequence in Table 2.3 we have

$$h(t) \ = \ normdist\left[2.563 \cdot \frac{\left(t + \frac{T}{2}\right)}{T_c}\right] - normdist\left[2.563 \cdot \frac{\left(t - \frac{T}{2}\right)}{T_c}\right] \qquad (4.17)$$

18 Typical solutions for the unit pulse response h(t) are shown in Figure 4.5. Black, blue, cyan, red, yellow, 19 and magenta correspond to T_c/T = 0.1, 0.5, 1.0, 1.5, 2.0, 2.5.

21 Because of the symmetry of the Gaussian impulse response, the unit pulse profile exhibits symmetry about 22 $t = 0$: $h(-t) = h(t)$. We have particular interest in the values of the unit pulse at decision times $t = nT$ for inte- 23 ger n. Consider Figure 4.7 in which $h_0 = h(0)$, $h_1 = h(T)$, and $h_2 = h(2T)$ are plotted as functions of the com- 24 posite rise time T_c. For the values of T_c of interest in this report, $Tc \leq 1.8$, we find that the unit pulse 25 response has negligible value for $n > 1$.

27 When calculating the power penalty due to intersymbol interference, the penalty is exacerbate when the 28 pulse centered at $t = 0$ has pulse width shrinkage (PWS) applied to it. Typical unit pulse profiles with and 29 without pulse width shrinkage are shown in Figure 4.8. The black and dark blue curves correspond to $T_c =$ 30 $0.1T$, the cyan and red curves correspond to $T_c = 1.5T$. The black and cyan curves correspond to *PWS = 0*
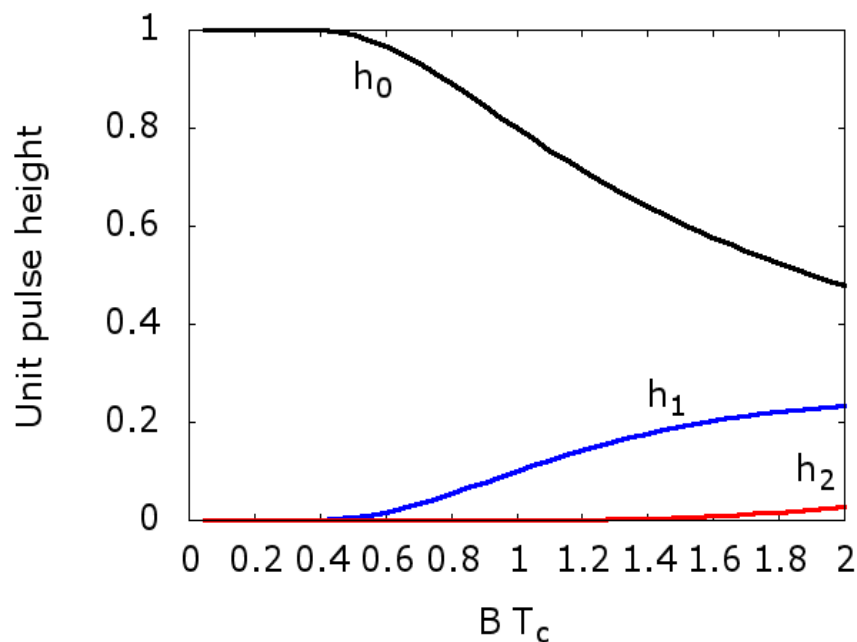
Figure 4.7 - Height of the unit pulse profile h(t) at decision times t = nT for n = 0, 1, and 2.
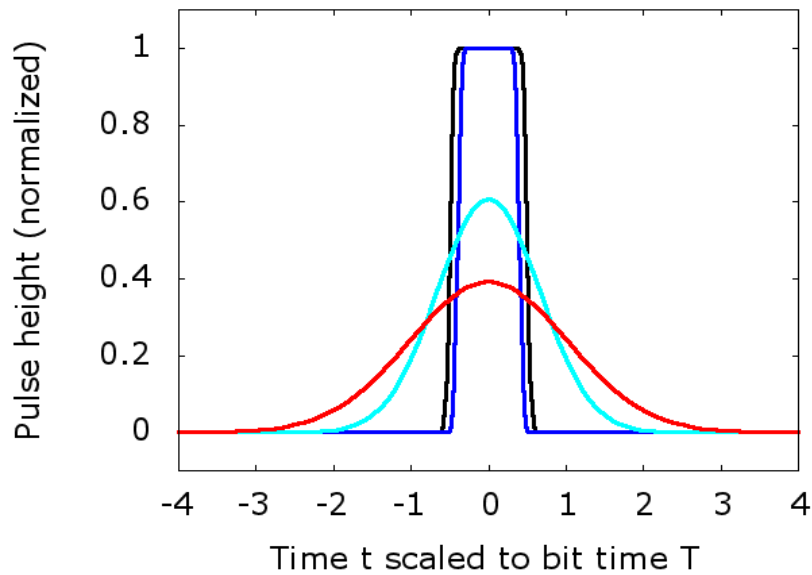
Figure 4.8 - Examples of pulse width shrinkage.

UI, the dark blue and red curves correspond to *PWS = 0.2 UI*. Equation 2.14 for *h(t)* is easily extended to incorporate PWS by replacing *T* with *T(1-PWS)*.
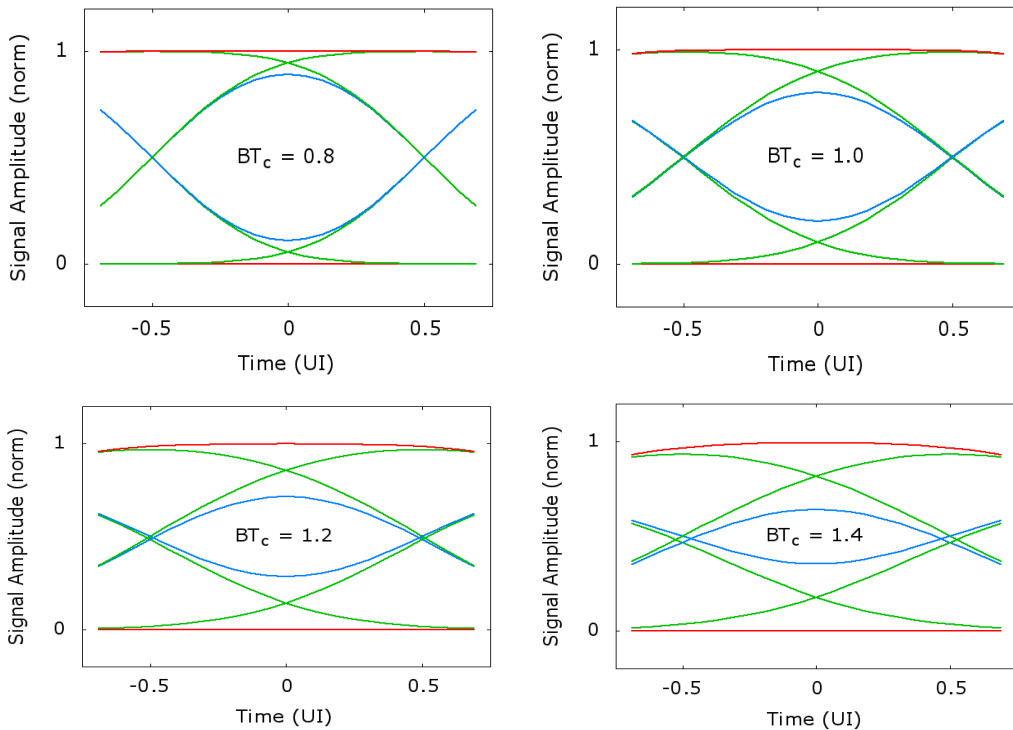
Figure 4.9 - Typical unequalized link eye diagrams

4.2.3 Vertical eye closure

Given the unit pulse response *h(t)* of Equation 4.16, it is straightforward to calculate the composite optical

link response to an arbitrary bit sequence.

Table 4.4 - Comparison of rise times and consequent eye openings for the 16GFC and 32GFC specifications from Table 2.1.

Measure	16GFC	32GFC
Transmitter rise time	51.2 ps	31.9 ps
Fiber chromatic dispersion rise time	16.3 ps	13.9 ps
Fiber modal dispersion rise time	24.0 ps	10.7 ps
Receiver rise time	29.9 ps	19.5 ps
Composite fiber link rise time	66.0 ps	41.3 ps
Pulse width shrinkage	0.12 UI	0.12 UI
T_c / T(1-PWS)	1.052	1.316
Eye opening, linear (normalized)	0.553	0.339
P_{isi}	2.57 dB	4.70 dB

One of the more instructive analyses that can be applied to an arbitrary bit sequence is to plot its eye diagram, as shown for example in Figure 4.9. Of particular interest is the innermost eye, shown as a dashed blue line in Figure 4.1.

For the optical link in the absence of equalization, the innermost eye occurs in response to a single isolated 1 embedded in a series of 0's, and conversely in response to a single isolated 0 embedded in a series of 1's. From Equation 4.16, for a single isolated 1 evaluated at the center of the eye (the decision time *t=0*), the upper eye lid is at level *erf(0.906T/T$_c$)*, and the lower eye lid is at level *1-erf(0.906T/T$_c$)*. Thus in linear units the eye opening, which we will call *ISI*, is

$$ISI \;=\; 2erf\left(0.906\frac{T}{T_c}\right) - 1 \qquad (4.18)$$

The ISI power penalty is given by
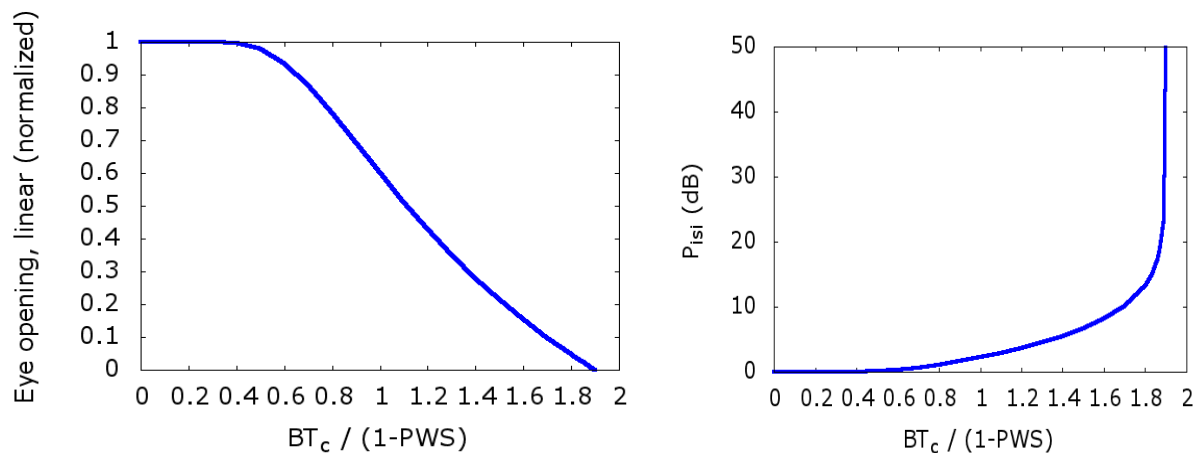
Figure 4.10 - Linear eye opening (left) and P$_{isi}$ (right) for link without equalization

$$P_{isi} = -10 \cdot \log_{10}(ISI) \tag{4.19}$$

Incorporating the *PWS* contribution, we can write the equation for *ISI* as

$$ISI = 2erf\left[\frac{0.906\,T(1-PWS)}{T_c}\right] - 1 \tag{4.20}$$

The eye completely closes when

$$\frac{0.906\,T(1-PWS)}{T_c} = erfinv(0.5) \tag{4.21}$$

which evaluates to be $T_c=1.9T(1-PWS)$. A plot of P_{isi} vs. $T_c/[T(1-PWS)]$ is given in Figure 4.10, showing linear eye closure on the left, and the corresponding P_{isi} power penalty in dB on the right.

Let us consider the 16GFC and 32GFC link specifications listed in Table 4.1. Assuming for the 16GFC case a 100 meters of OM3 fiber, and for the 32GFC case a 100 meters of OM4 fiber, we can calculate the composite fiber link rise times and corresponding eye opening as shown in Table 2.4.

Let us arbitrarily set the limit of allowed eye closure for Fibre Channel applications at 50%. Therefore the candidate 32GFC link configuration, which exceeds this 50% eye closure, will require some additional method to keep the eye open, such as the linear equalizer considered in 4.3.

4.2.4 TWDP unit pulse profile

It would be desirable to have some experimental measure of unit pulse response *h(t)* to compare with the
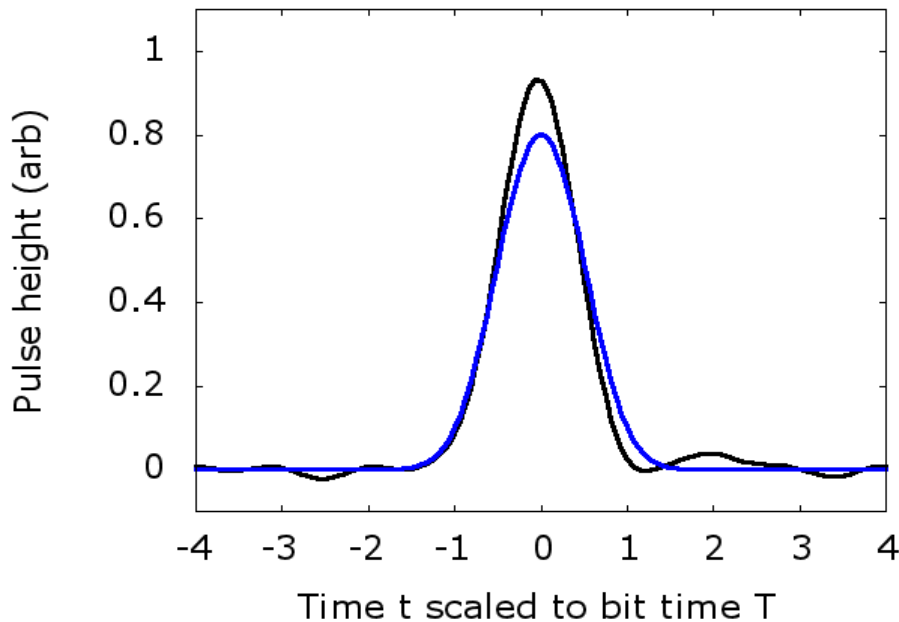
Figure 4.11 - TWDP fit compared with a Gaussian composite response with Tc = T.

highly idealized Gaussian model prediction. The TWDP waveform capture and analysis, discussed in Clause 5 of MSQS [2], offers a partial solution in terms of a measured transmitter waveform and an idealized 4th order Bessel-Thomson reference receiver. One of the first steps in the TWDP analysis is to calculate an affine linear approximation of the transmitter response. See Swenson *et al.* [17] for details on the affine approximation. Normally the affine approximation is used to simulate a slow square wave response, enabling optical modulation amplitude (OMA) to be calculated. However, with a modest change in the Matlab script, it is easy to simulate a unit pulse response. Figure 4.11 compares a TWDP analysis of a 16GFC VCSEL transmitter with a Gaussian model unit pulse response $h(t)$ for $T_c=T$.

This concludes our discussion of intersymbol interference for a fiber link in the absence of equalization in the receiver.

4.3 Linear equalizer

4.3.1 3-tap feed forward equalizer (FFE) block diagram

An equalizer in the receiver can mitigate against excessive intersymbol interference. To illustrate the concepts, we will analyze a very simple form of linear equalizer, a 3-tap feed forward equalizer (FFE) with T time interval between taps. See Figure 4.12 for a block diagram. The time delay elements are indicated by the top pair of squares. This equalizer has three taps with tap weights τ_{-1}, τ_0, and τ_{+1}. Each tap has associated with it a finite bandwidth such that each tap has a Gaussian impulse response $I_{tap}(t)$.

In this subclause we assume a noiseless optical link; noise analysis is introduced in the next subclause. In 4.3.2 we calculate the unit pulse response in the presence of a 3-tap equalizer. In 4.3.3 we review alternative tap setting "policies." In 4.3.4 we exhibit typical eye diagrams induced by the equalizer, and calculate eye closure introduced by pulse width shrinkage.
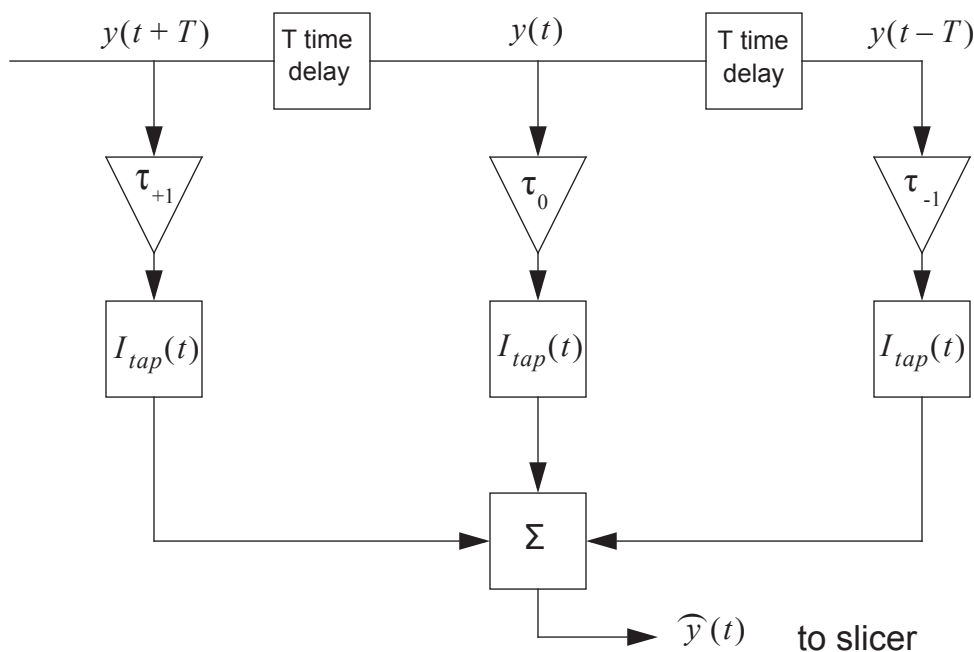
Figure 4.12 - Block diagram of a 3-tap feed forward equalizer (FFE).

4.3.2 Unit pulse response with equalization

In the presence of an equalizer the signal delivered to the slicer $\widehat{y}(t)$ is

$$\widehat{y}(t) \;=\; \sum_{n} x_n \cdot \delta(t - nT) \otimes \widehat{h}(t) \tag{4.22}$$

We denote the equalized unit pulse response as $\widehat{h}(t)$ which is given by

$$\widehat{h}(t) \;=\; h(t) \otimes I_{tap}(t) \otimes g(t) \tag{4.23}$$

in which *h(t)* is the unequalized unit pulse response given by Equation 4.6.The three tap sampling function *g(t)* is

$$g(t) \;=\; \tau_{-1} \cdot \delta(t - T) + \tau_0 \cdot \delta(t) + \tau_1 \cdot \delta(t + T) \tag{4.24}$$

In which *δ(t)* is the Dirac delta function.

We define a new composite response by convolving the Gaussian tap impulse response with the fiber link elements to define a new composite response, such that the response time T_c is given by

$$T_c^{\;2} \;=\; T_t^{\;2} + T_{cd}^{\;2} + T_{md}^{\;2} + T_r^{\;2} + T_{tap}^{\;2} \tag{4.25}$$

Under the influence of this 3-tap equalizer, the signal $\widehat{y}(t)$ delivered to the slicer is defined by a modified unit pulse response, given by the matrix equation

$$\widehat{h}(t) \;=\; \tau_{-1} \cdot h(t - T) + \tau_0 \cdot h(t) + \tau_1 \cdot h(t + T) \quad . \tag{4.26}$$

Of particular interest are the pulse response values at decision times *t = nT* for integer *n*. We assume that *h(nT)* for *n < -1* and *n > 1* are so small that we can safely neglect them, which is generally true for $T_c \leq 1.5T$ as can be verified from Figure 4.5. We will represent the unit pulse values by the triplet *(h_{-1},h_0,h_1)*.

After passing through the equalizer, the unit pulse response becomes $\widehat{h}(t)$. The non-negligible equalized unit pulse values at decision times are given by a quintuplet, as calculated by the following matrix equation.

Let us define the 5x3 matrix as *H*.

$$
\begin{bmatrix} \widehat{h}_{-2} \\ \widehat{h}_{-1} \\ \widehat{h}_{0} \\ \widehat{h}_{1} \\ \widehat{h}_{2} \end{bmatrix} = \begin{bmatrix} h_{-1} & 0 & 0 \\ h_{0} & h_{-1} & 0 \\ h_{1} & h_{0} & h_{-1} \\ 0 & h_{1} & h_{0} \\ 0 & 0 & h_{1} \end{bmatrix} \bullet \begin{bmatrix} \tau_{-1} \\ \tau_{0} \\ \tau_{1} \end{bmatrix}
\tag{4.27}
$$

We have yet to define the tap weights $(\tau_{-1}, \tau_{0}, \tau_{1})$; this is the next topic of discussion.

4.3.3 Tap setting policy

We refer to the algorithm defining optimum tap settings as the equalizer "policy." For a linear equalizer the usual policy for determining optimum tap settings is to minimize the mean square error (MMSE) of the resulting unit pulse response, as detailed shortly. To appreciate the advantages of the MMSE policy and as a tutorial exercise, let us first consider an alternative "naïve" policy.

We have three degrees of freedom, the three tap weights. We can use them to set the equalized unit pulse response at *t = 0* to be 1 and the response at *t = T* and *t = -T* to be zero. This leaves the unit response at *t = 2T* and *t = -2T* unconstrained. The result is that the unit pulse at *t = 2T* and *t = -2T* can become excessive.

A better strategy is to have all 5 unit pulse values approach the ideal value *(0,0,1,0,0)* as closely as possible. This is an under constrained problem: we have 3 tap weights to control 5 parameters. We can only approximate the desired response with a finite number of taps. We choose the tap weights such that the "cost" given in Equation 4.28 is minimized. The unit pulse responses resulting from the naïve policy and the MMSE policy are compared in Figure 4.13.

$$
J = \hat{h}_{-2}^{2} + \hat{h}_{-1}^{2} + (1 - \hat{h}_{0})^{2} + \hat{h}_{1}^{2} + \hat{h}_{2}^{2}
\tag{4.28}
$$

Tap weights that minimize the MMSE cost function *J* are given by

$$
\begin{bmatrix} \tau_{-1} \\ \tau_{0} \\ \tau_{1} \end{bmatrix} = (H^{T} \cdot H)^{-1} \cdot \begin{bmatrix} h_{1} \\ h_{0} \\ h_{-1} \end{bmatrix}
\tag{4.29}
$$

in which H is the 5-row 3-column matrix defined by Equation .
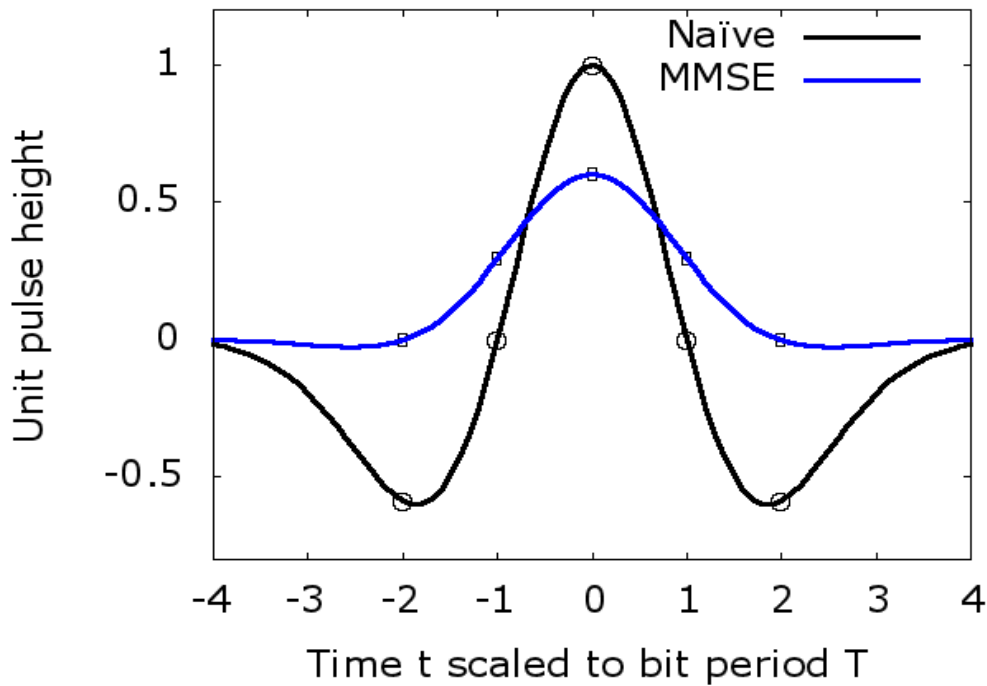
Figure 4.13 - Comparison of 3-tap FFE unit pulse response defined by a "naïve" policy and by a MMSE policy.

A strict application of the MMSE tap setting policy results in a slight reduction in modulation amplitude presented to the slicer. Consider for example the eye diagram shown in Figure 4.14. This is an extreme example (T_c=1.85T) which would not be considered for a Fibre Channel application because of excessive eye
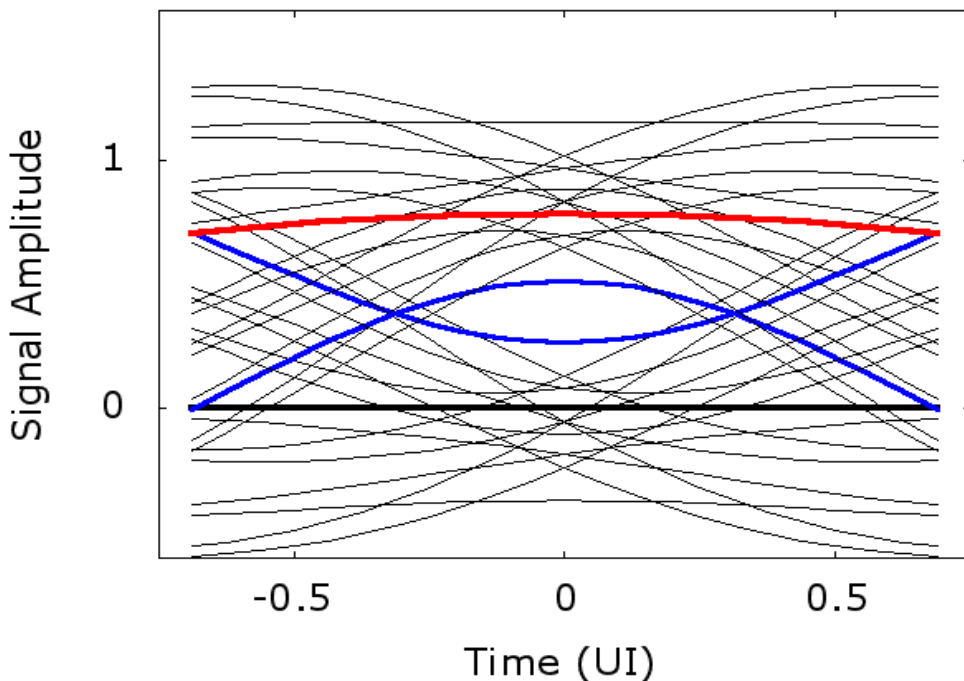
Figure 4.14 - Response to a 11111 bit sequence (the red line) sags below the desired 1 level.

closing, but it demonstrates most clearly the reduction in modulation amplitude. The response to a 11111 bit sequence is indicated by the red line. Ideally we would like this line to be at 1 at $t=0$, but as shown in Figure 4.14 it sits at about 0.7. Thus we define a third tap setting policy in which we use MMSE to define the relative tap weights, but apply sufficient gain to all taps to normalize the modulation amplitude. The gain needed is given by

$$gain = (\hat{h}_{-2} + \hat{h}_{-1} + \hat{h}_0 + \hat{h}_1 + \hat{h}_2)^{-1} \qquad (4.30)$$

This will be the tap-setting policy assumed in the remainder of this report.

Because of symmetry of the composite impulse response, the tap weights τ_{-1} and τ_1 are equal. We will find it convenient to introduce a tap ratio parameter a defined as

$$a \equiv \tau_{-1}/\tau_0 = \tau_1/\tau_0 \qquad . \qquad (4.31)$$

The gain can then be expressed as

$$gain = \frac{1}{(h_0 + 2h_1) \cdot (1 + 2a)} \qquad (4.32)$$

Sample 3-tap FFE eye diagrams, with gain, are shown in Figure 4.15.

We consider the impact of noise on optimum tap weights later in 4.5.

4.3.4 Eye diagrams and P_{isi}

The inner eye for a 3-tap FFE link, the blue lines in Figure 4.14, correspond to a 10101 bit sequence (the
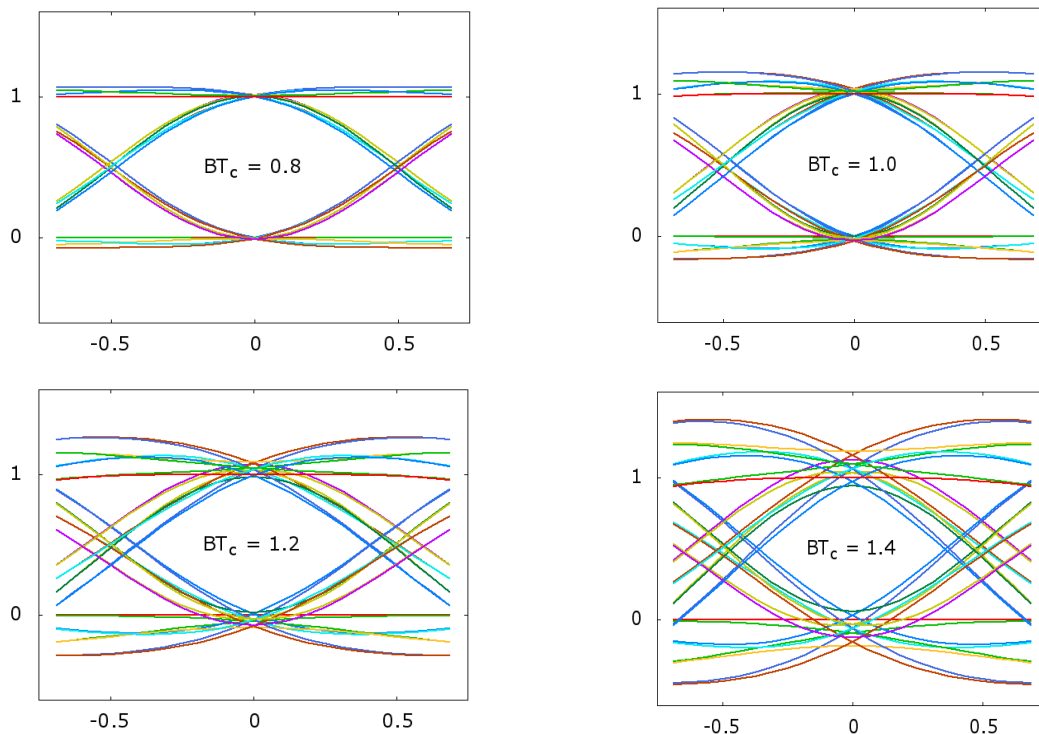
Figure 4.15 - Typical 3-tap FFE eye diagrams.
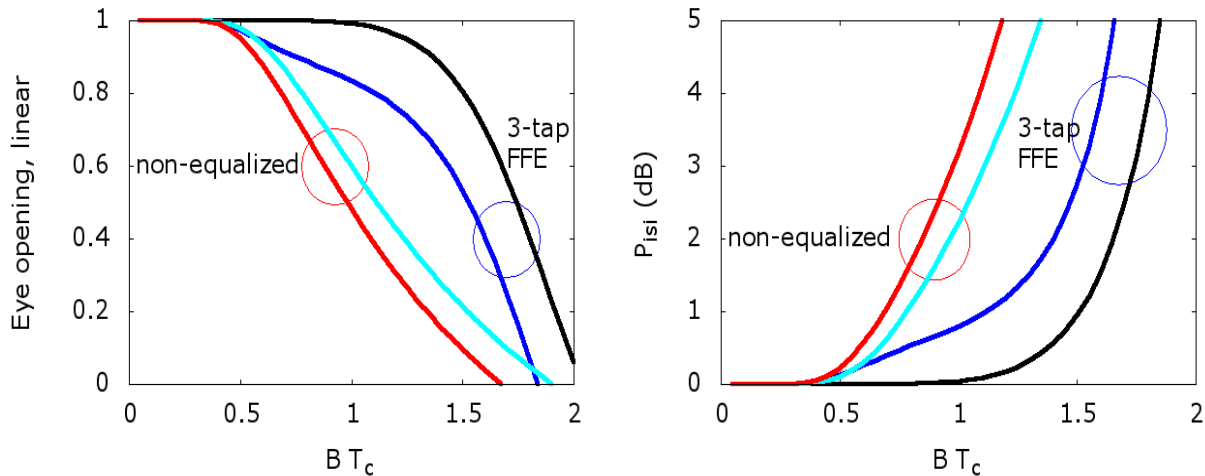
Figure 4.16 - Eye closure comparison of non-equalized and 3-tap FFE link

upper lid) and a 01010 bit sequence (the lower lid). Pulse width shrinkage will exacerbate eye closure; this should be applied to the center bit. Results are shown in Figure 4.16. This figure compares the eye closing performance of an unequalized link (red and cyan lines) and a 3-tap FFE link (dark blue and black lines), for *PWS = 0 UI* (cyan and black lines) and for *PWS = 0.12 UI* (red and dark blue lines). The abscissa is the composite fiber link rise time T_c scaled to the nominal symbol period *T*. A half-closed eye occurs for *Tc* of approximately *T* for an unequalized link. With 3-tap FFE, *Tc > 1.5T* before a half-closed eye is observed.

This concludes our discussion of 3-tap FFE in a noiseless link. We next turn our attention to noise impairment.

4.4 Laser relative intensity noise (RIN)

4.4.1 Block diagram of the noise model

The goal of this subclause is to calculate the power penalty required to compensate for laser relative intensity noise, hereinafter referred to as RIN for brevity. In the process we will introduce measures of noise statistics and alternative definitions of RIN.

We start with a block diagram of the noise model as presented in Figure 4.17. There are multiple noise sources to consider. The dominant noise source is receiver noise n_r. For the present discussion we also consider a small additional noise source n_{rin} due to laser RIN. Because laser RIN adds to the noise burden, the signal strength must be increased correspondingly to maintain the desired bit error rate goal of at most 10^{-12}. This strength increase corresponds to the power penalty for RIN.

In 4.4.2 we introduce statistical measures of noise impairment. In 4.4.3 we consider a frequency spectrum description of laser RIN in a fiber optic link. We conclude in 4.4.4 with a calculation of the requisite power
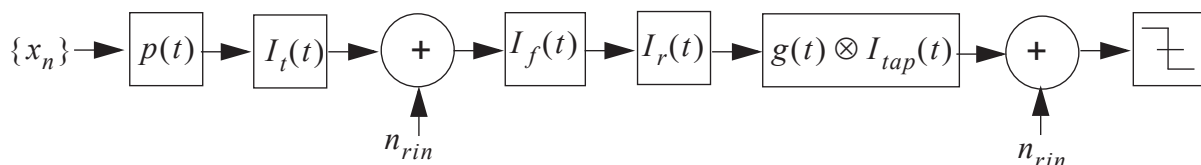
Figure 4.17 - Block diagram of laser relative intensity noise (RIN) impairment model

penalty to compensate for laser RIN.

The magnitudes of most noise terms such as laser RIN grow in proportion to the signal strength. The one exception to this is the receiver noise n_r, which we assume stays constant. As a consequence we will find it useful to define dimensionless signal-to-noise ratios Q and noise-to-signal ratios σ.

Let us review the definition of signal strength. In the process we will introduce mathematical symbols and tools which will serve us well when we study noise. Consider Figure 4.18 which shows typical signals $y(t)$ delivered to the slicer in the receiver, as indicated in Figure 4.4. Of particular interest are signal levels y_{zero} and y_{one} produced in response to slow square wave inputs. As discussed in MSQS [2] subclause 2.2.1, these are fundamental in defining signal amplitude.

Let us introduce the bracket notation $<y(t)>$ which in the present context denotes averaging over time:

$$\langle y(t) \rangle \equiv \lim_{T \to \infty} \int_{t_0}^{t_0 + T} y(t)\,dt \qquad (4.33)$$

When considering random noise processes, as we will in the next subclause, an alternate interpretation of the bracket notation is a statistical ensemble average, assumed to give the same result as averaging over time.

When considering a slow square wave input with equal times for zero and one intervals, $<y(t)>$ is y_{avg}, half-way between y_{zero} and y_{one}. This is the threshold level y_{thresh} for the slicer in the receiver to distinguish between zero levels and one levels. The Gigabit Ethernet link model used the average optical power as its measure of signal strength. Receiver sensitivity and laser RIN were defined with respect to average signal amplitude.
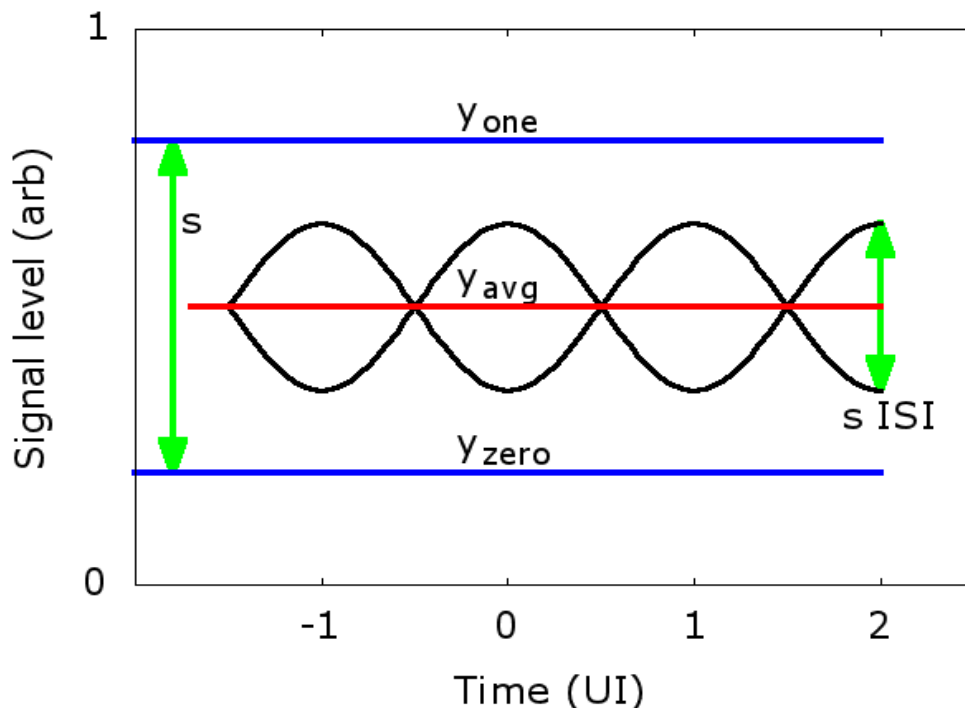
Figure 4.18 - Measures of signal amplitude
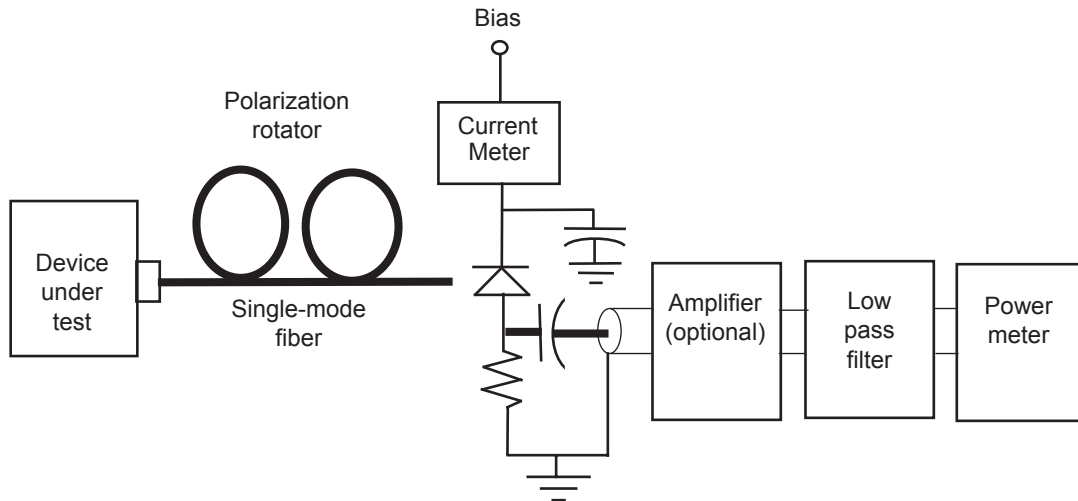
Figure 4.19 - Measurement of laser relative intensity noise (RIN$_{12}$), based on FC-PH
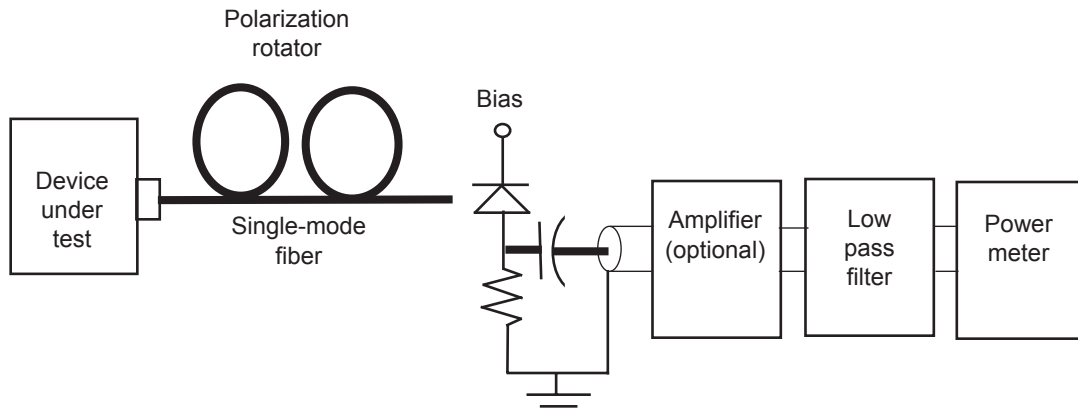
Figure 4.20 - Measurement of laser relative intensity noise (RIN$_{12}$OMA), based on MSQS

However, to have a complete description of link properties, an additional parameter was also required: the extinction ratio. The 10 Gigabit Ethernet committee chose instead of average power to use modulation amplitude as its measure of signal strength. In Figure 4.18 the modulation amplitude is the interval from y_{zero} to y_{one}, denoted by *s* in the present discussion. Transmitter output and receiver sensitivity are defined with respect to the optical modulation amplitude.

For signal-to-noise and noise-to-signal measures, the appropriate signal amplitude is ½*s* rather than *s*. This is best understood by comparing Figure 4.19 (based on FC-PH), showing the measurement configuration for RIN$_{12}$ assuming an average power measure of signal strength, and Figure 4.20 (based on MSQS [2]) showing the measurement configuration for RIN$_{12}$OMA. In Figure 4.19 and Figure 4.20, the measure of signal strength results from an RF power measurement in response to a slow square wave input signal. "Slow" means that ISI degradation will be minimal. In Figure 4.19, signal amplitude is measured by separate DC response circuit corresponding to yavg. In Figure 4.20, signal amplitude is measured using the same power meter as used to measure noise level. The RF power measurement is a function of the square of the signal y(t). Because of the blocking capacitor in Figure 4.20, the reference level for assessing signal power will be <y(t)>, i.e., y_{avg}. Thus the power measurement is proportional to the second moment of the signal, called the signal variance:

$$\langle [y(t) - \langle y(t) \rangle]^2 \rangle \ = \ \langle y^2(t) \rangle - \langle y(t) \rangle^2 \tag{4.34}$$

For a slow square pulse signal the variance will be $(\frac{1}{2}s)^2$ as we can see from Figure 4.18.

4.4.2 Measures of noise statistics

The following material has been adapted from Petermann [16]. We start by considering the signal $y(t)$ presented to the slicer, the element in the receiver responsible for determining 1's and 0's. We assume that this signal contains two additive noise contributions of the form $y(t)+\delta y_r(t)+\delta y_{rin}(t)$, in which $\delta y_r(t)$ is receiver noise and $\delta y_{rin}(t)$ is laser noise. We assume that $\delta y_r(t)$ and $\delta y_{rin}(t)$ have zero mean: $<\delta y_r(t)> = 0$ and $<\delta y_{rin}(t)> = 0$, in which the brackets denote ensemble average. We further assume that the receiver noise $\delta y_r(t)$ and the laser noise $\delta y_{rin}(t)$ are not correlated, i.e., $<\delta y_r(t)\, \delta y_{rin}(t)> = 0$.

An important measure of noise statistics is the auto correlation function $\rho(t)$, defined as

$$\rho(t) \ = \ \langle \delta y(t_0) \cdot \delta y(t_0 + t) \rangle \tag{4.35}$$

Separate auto correlation functions $\rho_r(t)$ and $\rho_{rin}(t)$ can be defined for the receiver noise and for the laser RIN. The noise terms are assumed to exhibit stationarity, meaning that the ensemble average of the auto correlation function is expected to be independent of time t_0 in Equation 4.35. When constituent noise contributors are not correlated, the aggregate noise variance $\rho_{total}(t)$ is given by the sum of the constituent autocorrelations:

$$\rho_{total}(t) \ = \ \rho_r(t) + \rho_{rin}(t) \tag{4.36}$$

In optical link analyses, the second moment of the noise signal is especially important. The second moment is called the variance:

$$\langle [\delta n(t)]^2 \rangle \ = \ \rho(0) \tag{4.37}$$

We will furthermore assume that all noise sources conform to a Gaussian probability distribution $\wp[\delta y(t)]$ with standard deviation n:

$$\wp(\delta y) \ = \ \frac{1}{n\sqrt{2\pi}} \cdot \exp[-(\delta y)^2/2n^2] \tag{4.38}$$

The standard deviation

$$n^2 \ = \ \langle [\delta n(t)]^2 \rangle \ = \ \rho(0) \tag{4.39}$$

is a convenient measure of noise magnitude. With this Gaussian probability assumption, we can calculate the fraction of time for which bit errors are introduced at the slicer. Errors occur when the local noise level exceeds the signal level s. We can calculate the bit error ratio by the tail integral of the Gaussian probability distribution:

$$BER = \int_{s}^{\infty} \wp(\delta y)d(\delta y) \qquad (4.40)$$

which can be expressed as

$$BER(Q) = \frac{1}{2} \cdot erfc(Q/\sqrt{2}) \qquad (4.41)$$

See 5.4 in MSQS [2]. In Equation 4.41 we have introduced the dimensionless signal-to-noise ratio parameter $Q = s/n$. In particular, the limiting BER of 10^{-12} as required for a compliant Fibre Channel link corresponds to a signal-to-noise ratio $Q_0 = 7.03$.

4.4.3 Noise frequency spectrum

4.4.3.1 Noise spectrum in the absence of an equalizer
In Equation 4.35 of 4.4.2 we introduced the auto correlation function $\rho(t)$. The Fourier transform of the auto correlation function, which we identify as the noise spectral density $W(f)$, constitutes an equally important measure of noise impairment.

$$\rho(t) = \int_{-\infty}^{\infty} \exp(2\pi ift) \cdot W(f)df \qquad (4.42)$$

The variance is given by:

$$n^2 = \rho(0) = \int_{-\infty}^{\infty} W(f)df \qquad (4.43)$$

Laser RIN is defined by

$$RIN(f) = 10\log_{10}\left[W(f)/\left(\frac{s}{2}\right)^2\right] \qquad (4.44)$$

For modeling of noise impairment we typically assume that the noise is "white," meaning that the spectral noise density $W(f)$ maintains a constant noise density W_0 from DC to extremely high frequencies. To limit the noise impairment delivered to the slicer, we require the composite fiber link to have finite bandwidth response. Let us calculate the channel frequency response and its impact upon laser RIN variance delivered to the slicer.

Consider a fiber link in the absence of an equalizer:

$$\langle[\delta y_{rin}(t)]^2\rangle = W_0 \cdot \int_{-\infty}^{\infty} |I_c(f)|^2 df = n_{rin}^2 \qquad (4.45)$$

$I_c(f)$ is the frequency spectrum of the composite fiber link impulse response. If the impulse response is Gaussian, then its frequency response is also Gaussian, of the form given in Table 4.3. Equation 4.45 has an analytic solution of the form

$$n_{rin}^2 = \frac{W_0 \cdot k_{rin}}{T_c} \tag{4.46}$$

k_{rin} is defined by

$$k_{rin} = \sqrt{2/\pi} \cdot erfinv(0.8) = 0.723 \tag{4.47}$$

The composite rise time T_c appearing in Equation 4.46 is for the fiber link response downstream of the point at which the laser noise is injected. In the block diagram sketched in Figure 4.21, this excludes transmitter rise time T_t. Thus we define

$$T_c^2 = T_{cd}^2 + T_{md}^2 + T_r^2 \tag{4.48}$$

We find it useful to define a dimensionless noise-to-signal ratio σ_{rin} as

$$\sigma_{rin} \equiv n_{rin} / \left(\frac{s}{2}\right) \tag{4.49}$$

Combining Equation 4.44, Equation 4.46, and Equation 4.49 we obtain

$$\sigma_{rin}^2 = \frac{k_{rin}}{T_c} \cdot 10^{0.1 RIN} \tag{4.50}$$

4.4.3.2 Noise spectrum with an equalizer

With an equalizer present, Equation 4.45 becomes

$$n_{rin}^2 = W_0 \int_{-\infty}^{\infty} |I(f)|^2 \cdot |G(f)|^2 df \tag{4.51}$$

in which $G(f)$ is the frequency spectrum of the 3-tap equalizer impulse response $g(t)$ defined by Equation 4.24.

$$G(f) = \frac{1}{2\pi} \cdot \int_{-\infty}^{\infty} g(t) \cdot \exp(-2\pi i f t) dt = \tau_{-1} \cdot e^{2\pi i f T} + \tau_0 + \tau_1 \cdot e^{-2\pi i f T} \tag{4.52}$$

For Gaussian composite fiber link response, Equation 4.51 has an analytical solution which can be expressed in the form

$$\sigma_{rin}^2 = \frac{k_{rin} \cdot NEF}{T_c} \cdot 10^{0.1 RIN} \tag{4.53}$$
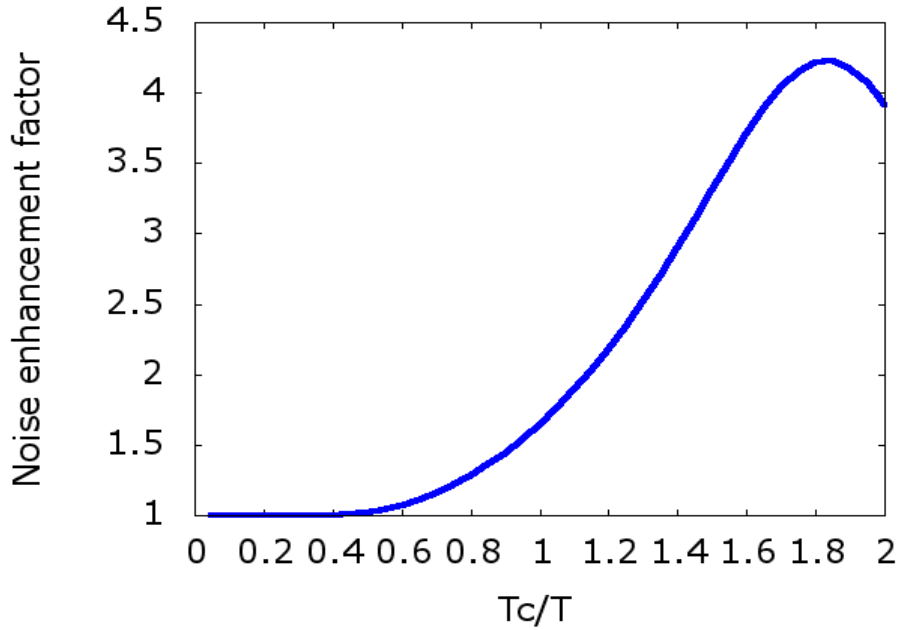
Figure 4.21 - Noise enhancement factor (NEF) vs. composite rise time T_c

in which the composite rise time T_c is given by

$$T_c^{\ 2} = T_{cd}^{\ 2} + T_{md}^{\ 2} + T_r^{\ 2} + T_{tap}^{\ 2} \tag{4.54}$$

and we define a Noise Enhancement Factor (*NEF*) given by

$$NEF = (\tau_0^2 + 2\tau_1^2) + 4\tau_0\tau_1 \exp\left(\frac{-AT^2}{T_c^2}\right) + 2\tau_1^2 \exp\left(\frac{-4AT^2}{T_c^2}\right) \tag{4.55}$$

in which

$$A = 2erfinv^2(0.8) = 1.6424 \tag{4.56}$$

The noise enhancement factor is plotted in Figure 4.21 as a function of T_c/T.

4.4.4 RIN power penalty

To conclude 4.4, we calculate the power penalty P_{rin} needed to compensate for increased noise introduced by laser RIN.

To start, consider only receiver noise in the absence of any laser RIN impairment. We assume a fixed amount of receiver noise n_r. Let us denote by s_{min}, the minimum signal level required to achieve the Fibre Channel goal of 10^{-12} BER or better, even under worst case conditions. Worst case includes ISI-induced eye closing, such as shown by the dashed lines in Figure 4.1. Thus we need an eye opening of at least

$Q_0 n_r$ at the inner eye, with proportionately larger signal at the '*0*' and '*1*' levels. $Q_0 = 7.03$ as discussed in 4.4.2. Let us denote the eye opening of the innermost eye by *ISI* in linear units, normalized to the OMA level. Thus the OMA signal level required is

$$s_{min}/2 = (Q_0/ISI) \cdot n_r \tag{4.57}$$

Next add laser RIN noise n_{rin}. The total noise delivered to the slicer is n_{total}, given by

$$n_{total}^2 = n_r^2 + n_{rin}^2 \tag{4.58}$$

This larger noise level requires a larger signal strength *s* to maintain 10^{-12} BER under worst case conditions, such that

$$s/2 = (Q_0/ISI) \cdot n_{total} \tag{4.59}$$

We need one more relation, from Equation 2.36:

$$n_{rin} = \sigma_{rin} \cdot s/2 \tag{4.60}$$

We define the power penalty P_{rin} as

$$P_{rin} \equiv 10 \cdot \log_{10}\left(\frac{s}{s_{min}}\right) = 10 \cdot \log_{10}\left(\frac{n_{total}}{n_r}\right) \tag{4.61}$$

which can be written as

$$P_{rin} = 10 \cdot \log_{10}\left(\frac{1}{\sqrt{1 - \sigma_{rin}^2 \cdot Q_0^2 / ISI^2}}\right) \tag{4.62}$$

This concludes our study of laser RIN.

4.5 Noise impact on optimum equalizer tap weights

Almost all forms of linear equalizer optimize tap weights in the presence of noise. Two examples include calculating tap weights in response to a special set of training signals, and adaptive equalizers that converge onto an optimum set of tap weights. Noise will shift the optimum tap ratio *a*, as detailed in this subclause. The following derivation follows Chapter 2 of Benvenuto and Cherubini [9].

The optimum tap weights are given by

$$R_{ij} \cdot \begin{bmatrix} \tau_{-1} \\ \tau_0 \\ \tau_1 \end{bmatrix} = p_i \tag{4.63}$$

in which R_{ij} is a Toeplitz matrix given by the autocorrelation

$$R_{ij} \equiv \langle [y(iT) + \delta y(iT)] \cdot [y(jT) + \delta y(jT)] \rangle \tag{4.64}$$

and p_i is the correlation of the actual signal against the ideal signal d_i,

$$p_i \equiv \langle [yiT) + \delta y(iT)] \cdot d_i \rangle \quad \cdot \tag{4.65}$$

We would usually normalize the signal strength s to unity for simplicity. However for clarity in the following derivation we will explicitly display factors of s. The ideal signal d_i is

$$d_i = s \cdot (0, 0, 1, 0, 0)^T \tag{4.66}$$

T denotes transpose.

$$\langle y(iT) \cdot y(jT) \rangle = s^2 H^T \cdot H \tag{4.67}$$

H is the 3x5 matrix introduced in Equation . The signal and noise terms are assumed to be uncorrelated:

$$\langle y(iT) \cdot \delta y(jT) \rangle = 0 \tag{4.68}$$

for all values of i and j.

The noise autocorrelation is assumed to have the form

$$\langle \delta y(iT) \cdot \delta y(jT) \rangle = n_{total}^2 \delta_{ij} \tag{4.69}$$

with n_{total} as given by Equation 4.58 and δ_{ij} is the Kronecker delta function ($\delta_{ij}=1$ when $i=j$, 0 otherwise).

$$\langle y(iT) \cdot d_i \rangle = s^2 H^T \cdot d_i = s^2 \begin{bmatrix} h_1 \\ h_0 \\ h_1 \end{bmatrix} \tag{4.70}$$

in which one factor of s comes from $y(iT)$ and the second factor of s comes from d_i.

We also have

$$\langle \delta y(iT) \cdot d_i \rangle = 0 \tag{4.71}$$

Combining all of this, and making use of the symmetry of our composite impulse response, we have

$$\begin{bmatrix} \tau_1 \\ \tau_0 \\ \tau_1 \end{bmatrix} = \left[H^T \cdot H + \frac{n_{total}^2}{s^2} \cdot \delta_{ij} \right]^{-1} \cdot \begin{bmatrix} h_1 \\ h_0 \\ h_1 \end{bmatrix} \qquad (4.72)$$

Next we want to derive an expression for the signal-to-noise ratio s / n_{total}, using arguments very similar to those leading to Equation 4.59. In the present discussion, we consider not only the power penalty P_{isi} due to ISI, but all penalties including all noise terms. We assume a power budget of P_{alloc} for all power penalties. Then the minimum signal-to-noise ratio that will assume 10^{-12} BER under worst case conditions is

$$s / n_{total} = Q_0 \cdot 10^{0.1 P_{alloc}} \equiv 1 / \sigma_{total} \qquad (4.73)$$

For a 3-tap equalizer, an analytic solution exists for the tap ratio a:

$$a = \frac{h_1}{h_0} \cdot \left(\frac{2h_1^2 - h_0^2 + \sigma_{total}^2}{h_0^2 - h_1^2 + \sigma_{total}^2} \right) \qquad (4.74)$$

As a reminder,
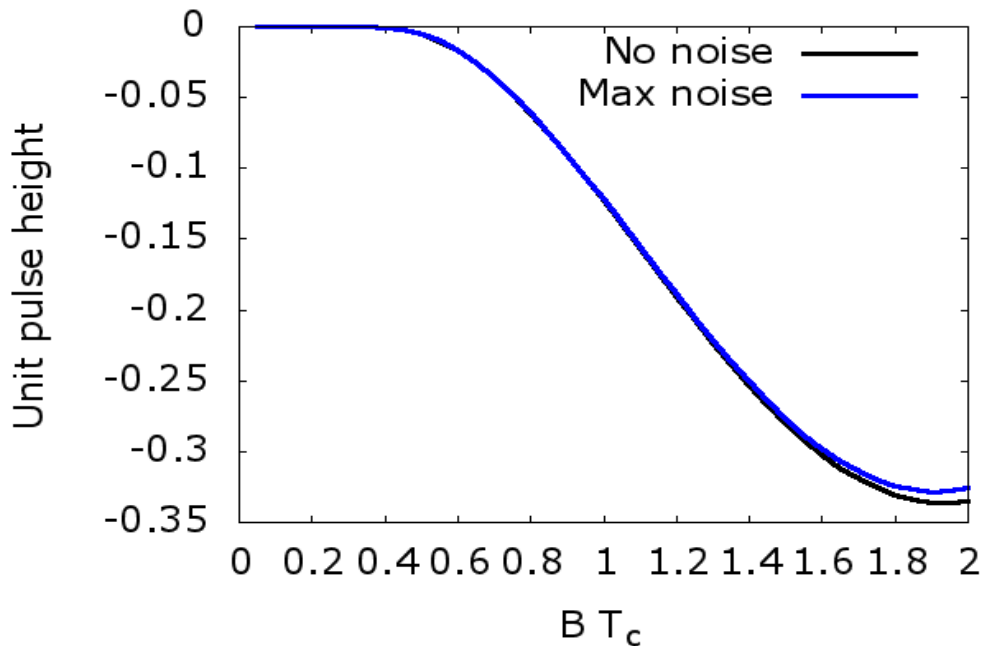
Figure 4.22 - **Plot of tap ratio a as a function of composite rise time T_c**

$$h_0 \equiv h(t = 0) = erf(0.906\,T/T_c) \tag{4.75}$$

and

$$h_1 \equiv h(t = T) = 0.5\,erf(3 \cdot 0.906\,T/T_c) - 0.5\,erf(0.906\,T/T_c) \tag{4.76}$$

A plot of the tap ratio *a* is shown in Figure 4.22.

4.6 Mode partition noise (MPN)

4.6.1 Introduction to MPN concepts

The next noise source to be analyzed is Mode Partition Noise, hereinafter abbreviated as MPN. This occurs whenever the laser in the transmitter emits in multiple spectral lines, e.g. Fabry-Perot or VCSEL lasers. MPN is not present for single wavelength, e.g. DFB, lasers. MPN occurs with both single mode fiber links and multimode fiber links.

To understand the basic concepts of MPN, consider Figure 4.23, which is Figure 6.40 from Cunningham and Lane [12]. This figure shows a spectral scan of a CD laser taken in one minute intervals. The total power summed over all modes remains essentially constant, but the distribution of that power amongst individual modes varies randomly over time.

Each spectral line of the laser has associated with it a unique wavelength. Because of chromatic dispersion in optical fiber, each spectral component propagates along an optical fiber with slightly different propagation times. Thus MPN introduces random timing variations in the signal reaching the receiver.

The shape of the eye in the receiver will map this timing variation into a signal amplitude variation. It is this signal amplitude variation that we refer to as MPN.
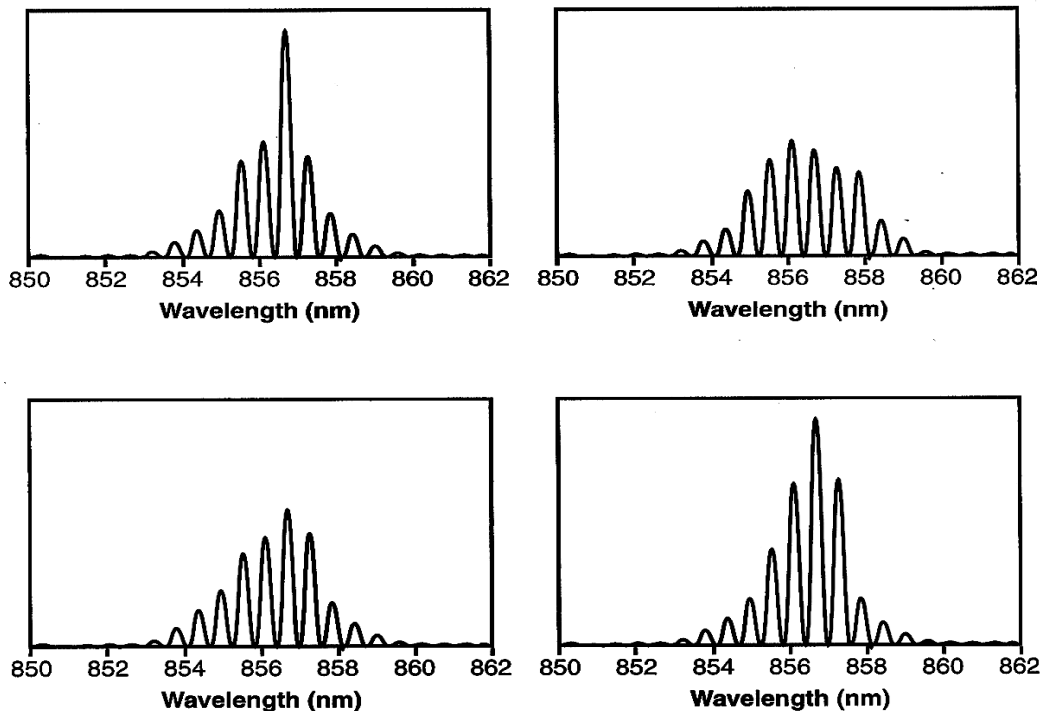
Figure 4.23 - Demonstration of mode partition effect, from Cunningham and Lane.

01 We begin MPN analysis in 4.6.2 with a review of chromatic dispersion. In 4.6.3 we present a generalized
02 version of Ogawa's mode partition analysis, introducing his dimensionless k-factor [15]. Our generalization
03 is to consider an arbitrary eye diagram shape. In 4.6.4 we calculate MPN impairment for an unequalized
04 link. We conclude in 4.6.5 with an analysis of MPN impairment in an equalized link. We demonstrate than
05 an unfortunate consequence of linear equalization is a significantly exacerbated sensitivity to MPN degra-
06 dation.

4.6.2 Chromatic dispersion

Let us start the MPN analysis with a brief review of chromatic dispersion in optical fiber. Consider light propagation in a medium with index of refraction $n(\lambda)$. Let c be the speed of light in vacuum, and λ be the wavelength of light in vacuum. We identify a radian light frequency ω as

$$\omega \equiv \frac{2\pi c}{\lambda} \tag{4.77}$$

and a propagation constant β as

$$\beta \equiv \frac{2\pi n}{\lambda} \tag{4.78}$$

Phase velocity v is defined as

$$v \equiv \frac{\omega}{\beta} = \frac{c}{n} \tag{4.79}$$

Group velocity v_g is defined as

$$v_g \equiv \frac{\partial \omega}{\partial \beta} \tag{4.80}$$

One measure of dispersion is group velocity dispersion (GVD):

$$GVD \equiv \frac{\partial^2 \omega}{\partial \beta^2} \tag{4.81}$$

with dimensions L^2/T (L = length, T = time).

Instead of group velocity, we prefer to use its inverse, the propagation transit time per unit length of fiber. In acoustics this is known as slowness. We give it the symbol $\tau(\lambda)$ (not to be confused with equalizer tap weights):

$$\tau(\lambda) = \frac{1}{v_g} = \frac{\partial \beta}{\partial \omega} = \frac{1}{c}\left(n - \lambda\frac{dn}{d\lambda}\right) \tag{4.82}$$

A second measure of dispersion is group delay dispersion (GDD), defined as

$$GDD = \frac{\partial \tau}{\partial \omega} \tag{4.83}$$

with dimensions T^2/L.

We prefer a third measure of dispersion, derived from a Taylor series expansion of the transit time per unit length about wavelength λ_c, the center wavelength of the transmitter laser:

$$\tau(\lambda) \approx \tau(\lambda_c) + \frac{\partial \tau}{\partial \lambda}(\lambda - \lambda_c) + \frac{1}{2} \cdot \frac{\partial^2 \tau}{\partial \lambda^2}(\lambda - \lambda_c)^2 + \ldots \tag{4.84}$$

We associate linear dispersion $D(\lambda)$ with the first derivative

$$D(\lambda) \equiv \frac{\partial \tau(\lambda)}{\partial \lambda} = -\frac{\lambda}{c} \cdot \frac{\partial^2 n(\lambda)}{\partial \lambda^2} \tag{4.85}$$

with dimensions T/L^2, and a dispersion slope $S(\lambda)$ with the second derivative

$$S(\lambda) \equiv \frac{\partial^2 \tau(\lambda)}{\partial \lambda^2} \tag{4.86}$$

We typically express linear dispersion $D(\lambda)$ in units of ps/km-nm.

For fiber dispersion we often approximate the wavelength dependence of the index of refraction with a functional form

$$n(\lambda) \approx c_0 + c_1 \lambda^2 + \frac{c_2}{\lambda^2} \tag{4.87}$$

The linear dispersion $D(\lambda)$ can then be expressed as

$$D(\lambda) = \frac{S_0 \lambda}{4} \cdot \left(1 - \frac{\lambda_0^4}{\lambda^4}\right) \tag{4.88}$$

The linear dispersion is negative for short wavelengths, positive for long wavelengths, and is zero at wavelength λ_0 with slope S_0.

The propagation time for mode i through fiber length L is

$$t_i = t_0 + DL(\lambda_i - \lambda_c) + \ldots \tag{4.89}$$

in which λ_c is the center wavelength for the transmitter laser and t_0 is the propagation time for the center wavelength.

Let us consider some numbers. Typical dispersion at 850 nm for OM3 and OM4 fiber is -110 ps/nm.km. Assume 100 meters of fiber: this gives -11 ps/nm. Two spectral lines separated by 0.5 nm will incur a differential delay of 5.5 ps. At 28.05 GBd this corresponds to 0.16 UI.

4.6.3 Ogawa k_{oma} factor

The next step in our MPN analysis is to study statistical measures of the mode partition process, especially the auto-correlation function. Unfortunately we have little detailed knowledge of mode partition statistics for any given laser, making this approach essentially intractable. Ogawa [15] has demonstrated how to substitute an intractable statistical analysis with a single dimensionless k_{OMA} parameter in the range $0 \leq k_{oma} \leq 1$. This single parameter encapsulates all of the statistics necessary for a signal amplitude noise analysis. It can be measured in the laboratory to define parameter ranges for broad classes of lasers.

We will present a generalized version of Ogawa's analysis. He considered noise response for an unequalized eye. We consider a general eye of shape $eye(t)$, leaving the precise definition of the normalized function $eye(t)$ to later subclauses.

Consider a laser with N discrete modes which we will identify with index i, $1 \leq i \leq N$. The ith mode has associated with it wavelength λ_i. When traveling through fiber of length L with linear dispersion D, each mode incurs propagation time shift t_i referenced to propagation time for the central wavelength λ_c:

$$t_i = DL(\lambda_i - \lambda_c) \tag{4.90}$$

This maps into a signal amplitude which we will express by a normalized function $eye(t_i)$.

We assume that the sum of powers distributed over all modes remains essentially constant. Let us define the symbol a_i as the power in the ith mode, normalized to the total power.

$$\sum_{i=1}^{N} a_i = 1 \tag{4.91}$$

Thus the signal delivered to the receiver at the optimum decision time $t = 0$ has the form

$$y_{mpn} = \sum_{i=1}^{N} a_i \cdot eye(t_i) \tag{4.92}$$

The MPN noise variance $\langle \delta y_{mpn}^2 \rangle$ is given by

$$\langle \delta y_{mpn}^2 \rangle = \langle y_{mpn}^2 \rangle - \langle y_{mpn} \rangle^2 \tag{4.93}$$

in which the average signal $\langle y_{mpn} \rangle$ is

$$\langle y_{mpn} \rangle = \sum_{i=1}^{N} \langle a_i \rangle eye(t_i) \tag{4.94}$$

We may not know the power distribution a_i at any given instant, but its time average $\langle a_i \rangle$ can be measured by an optical spectrum analyzer. Thus $\langle y_{mpn} \rangle$ is a tractable expression.

The time average of the square of the signal $\langle y_{mpn}^2 \rangle$ is

$$\langle y_{mpn}^2 \rangle = \sum_{i=1}^{N} \sum_{j=1}^{N} \langle a_i \cdot a_j \rangle eye(t_i)eye(t_j) \tag{4.95}$$

This unfortunately is where the analysis breaks down. We don't know the time averaged autocorrelation $\langle a_i a_j \rangle$ and have no easy way of measuring it.

Ogawa replaced the intractable general expression with a tractable worst case expression. He presented an analysis that showed the worst case MPN noise variance occurs when all of the power at any given instant is concentrated into just one mode and not distributed amongst several modes. Thus

$$\langle a_i \cdot a_j \rangle = 0 \tag{4.96}$$

when $i \neq j$. Furthermore, since a_i contains either all of the light or none of it at any given instant, we can write

$$a_i^2 = a_i \tag{4.97}$$

for the worst case condition. Let us define symbol $\langle \delta y_{mpn}^2 \rangle_{max}$ for this worst case condition:

$$\langle \delta y_{mpn}^2 \rangle_{max} = \langle y_{mpn}^2 \rangle_{max} - \langle y_{mpn} \rangle^2 \tag{4.98}$$

in which $\langle y_{mpn} \rangle$ is given by Equation 4.94 and

$$\langle y_{mpn}^2 \rangle_{max} = \sum_{i=1}^{N} \langle a_i \rangle \cdot eye^2(t) \tag{4.99}$$

To link the intractable variance of interest to this extreme but tractable expression, Ogawa introduces a dimensionless k factor, which we express as k_{oma} to emphasize that the signal amplitude measure is based upon modulation amplitude.

$$k_{oma}^2 \equiv \frac{\langle \delta y_{mpn}^2 \rangle}{\langle \delta y_{mpn}^2 \rangle_{max}} \tag{4.100}$$

k_{oma} can range from 0 for no MPN impairment (e.g., with a DFB laser) to 1 for maximum MPN impairment. We might not be able to calculate k_{oma} from first principles, but we can measure it in the laboratory, establishing parameter ranges for broad classes of lasers.

To facilitate deriving analytic expressions for the maximum variance, we replace the discrete sum over individual modes with an integral over wavelength, assuming a Gaussian envelope of the form

$$a(\lambda) = \frac{1}{\Delta\lambda\sqrt{2\pi}} \cdot \exp\left[\frac{-(\lambda - \lambda_c)^2}{2(\Delta\lambda)^2}\right] \tag{4.101}$$

Note that this is normalized such that

$$\int_{-\infty}^{\infty} a(\lambda)d\lambda = 1 \tag{4.102}$$

This concludes our introduction to the Ogawa k_{oma} factor. Next we calculate MPN impairment for two cases of eye diagram shape *eye(t)*.

4.6.4 MPN with no equalization

Consider an unequalized eye. The worst case noise will occur when the eye has the most curvature, to convert timing jitter into signal amplitude jitter. This happens for a 101010... bit pattern; see Figure 4.18. To a good approximation,

$$eye(t) \approx y_{avg} + \frac{1}{2} \cdot ISI \cdot s \cdot \cos(\pi Bt) \tag{4.103}$$

y_{avg} is defined in Figure 4.18, *ISI* is the linear measure of eye opening as introduced in 4.2.3 and 4.3.4, *s* is the modulation amplitude defined in Figure 4.18, and *B* is the nominal symbol rate. Equation 4.94 when approximated by an integral has an analytic solution of the form

$$\langle y_{mpn}\rangle = y_{avg} + \frac{s}{2} \cdot ISI \cdot \exp\left(-\frac{\beta^2}{2}\right) \tag{4.104}$$

introducing a dimensionless parameter β defined by

$$\beta \equiv \pi \cdot B \cdot D \cdot L \cdot \Delta\lambda \tag{4.105}$$

Similarly the integral equation equivalent of Equation 4.99 also has an analytic solution of the form

$$\langle y_{mpn}^2\rangle_{max} = y_{avg}^2 + y_{avg} \cdot ISI \cdot s \cdot \exp\left(-\frac{\beta^2}{2}\right) + \frac{1}{8} \cdot ISI^2 \cdot s^2 \cdot [1 + \exp(-2\beta^2)] \tag{4.106}$$

whence

$$\langle \delta y_{mpn}^2\rangle_{max} = \frac{1}{8} \cdot ISI^2 \cdot s^2 \cdot [1 - \exp(-\beta^2)]^2 \tag{4.107}$$

We define a noise-to-signal ratio σ_{mpn} as

$$\sigma_{mpn} = \frac{ISI \cdot k_{oma}}{\sqrt{2}}[1 - \exp(-\beta^2)] \tag{4.108}$$

01 In analogy to the arguments given in 4.4.4, we calculate the power penalty for MPN as

$$P_{mpn} = 10 \cdot \log_{10}\left(\frac{1}{\sqrt{1 - \sigma_{mpn}^2 \cdot Q_0^2 / ISI^2}}\right) \qquad (4.109)$$

See Agrawal et al. [11], Brown [11], and Cunningham and Lane [12].

Let's evaluate the MPN power penalty for typical link parameters as given in Table 4.5. Thus we see that even at 28.05 GBd, noise power penalty due to MPN impairment is modest. Note that this calculation did not include pulse width shrinkage. The MPN impairment will increase in the presence of pulse width shrinkage.

Next let us consider MPN impairment for a typical equalized eye. Consider the typical link parameters as

Table 4.5 - MPN impairment for typical 32GFC unequalized link

Parameter	Value	Units
B	28.05	GBd
L	100	meters
λ_c	850	nm
D	108	ps/nm*km
$\Delta\lambda$	0.5	nm
β	0.476	dimensionless
k_{oma}	0.3	dimensionless
σ_{mpn}	0.043	dimensionless
Q_0	7.03	dimensionless
P_{mpn}	0.21	dB

given in Table 4.5.

4.6.5 MPN with equalization

In the presence of equalization, the inner eye takes on a diamond shape which significantly increases the signal amplitude noise level in the presence of mode partition. This can be seen from Figure 4.2. Let us approximate the eye in the neighborhood of the optimum decision time $t = 0$ by a linear ramp of the form

$$eye(t) \approx eye(0) + \frac{S}{2} \cdot S \cdot B \cdot t \qquad (4.110)$$

As discussed in 4.4.1, our signal amplitude is ½s. S is the slope of the eye, normalized so that time is in UI and amplitude is scaled to ½s. Because of chromatic dispersion, wavelength deviation from center wavelength λ_c maps into time shift t as expressed for example by Equation 4.89.

$$\langle y_{mpn} \rangle = eye(0) \qquad (4.111)$$
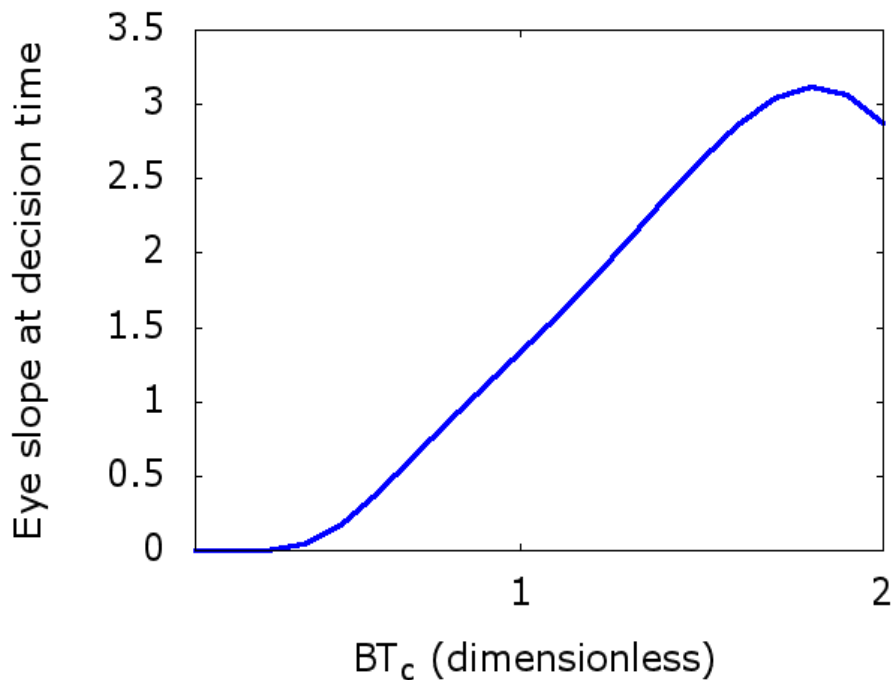
Figure 4.24 - Maximum slope of 3-tap FFE eye at optimum decision time

and

$$\langle y_{mpn}{}^2 \rangle_{max} = eye^2(0) + \left(\frac{s}{2} \cdot S \cdot B \cdot D \cdot L \cdot \Delta\lambda \right)^2 \qquad (4.112)$$

Let us use the parameter β as defined in Equation 4.105 to obtain

$$\sigma_{mpn} = \frac{k_{oma} \cdot S \cdot \beta}{\pi} \qquad (4.113)$$

The power penalty is

$$P_{mpn} = 10 \cdot \log_{10}\left(\frac{1}{\sqrt{1 - \sigma_{mpn}{}^2 \cdot Q_0{}^2}} \right) \qquad (4.114)$$

ISI-induced eye closing is so minimal with an equalizer that the ISI adjustment of Equation 4.109 is not considered here.

Consider Figure 4.25 which shows the growth in MPN noise penalty with growth in the parameter β defined in Equation 4.105. This figure assumes Q_0 = 7.03, k_{oma} = 0.3, and S = 1.9. Note that the penalty for an equalized link is generally higher, with its noise floor limit of 10^{-12} BER occurring sooner, compared with the penalty for an unequalized link The noise floor at 10^{-12} occurs when

$$Q_0 \cdot \sigma_{mpn} = 1 \tag{4.115}$$

For an unequalized link, from Equation 4.108 we find

$$\beta_{limit} = \sqrt{-\log_e\left(1 - \frac{\sqrt{2}}{k_{oma} \cdot Q_0}\right)} \tag{4.116}$$

For an equalized link, from Eq.2.112 we find

$$\beta_{limit} = \frac{\pi}{k_{oma} \cdot Q_0 \cdot S} \tag{4.117}$$

Let's evaluate the MPN power penalty for typical link parameters, as shown in Table 4.6. For a typical equalized link we find a 5-fold increase in MPN impairment compared with an unequalized link. Furthermore, the value of β at which we hit the noise floor at 10^{-12} for an unequalized link is 1.05, whereas the limiting β for an equalized link is 0.78.

Thus we have found in the discussion of laser RIN in 4.4 and of MPN in 4.6 that a linear equalizer, while opening the eye, has the unfortunate behavior of exacerbating noise impairment. We need some means of reducing sensitivity to noise. This is offered by Forward Error Correction (FEC), our next topic.

Table 4.6 - MPN impairment for typical 32GFC equalized link

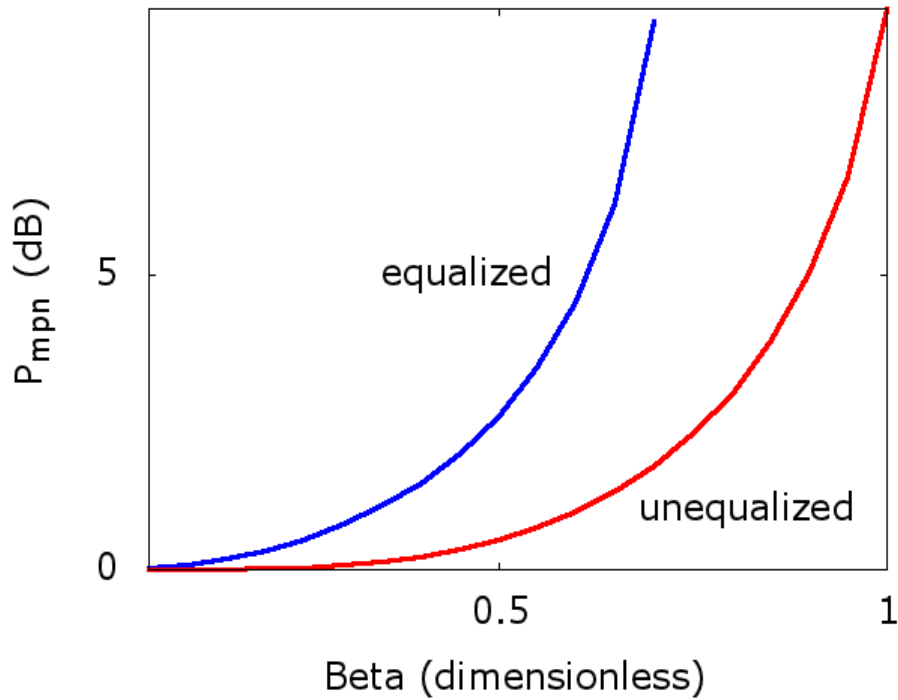| Parameter	Value	Units
B	28.05	GBd
L	100	meters
λ_c	850	nm
D	108	ps/nm*km
$\Delta\lambda$	0.5	nm
β	0.476	dimensionless
k_{oma}	0.3	dimensionless
σ_{mpn}	0.091	dimensionless
Q_0	7.03	dimensionless
S	1.9	dimensionless
P_{mpn}	1.14	dB

Figure 4.25 - Comparison of MPN power penalty for unequalized and equalized links.

4.7 Forward Error Correction (FEC) in link budget analysis

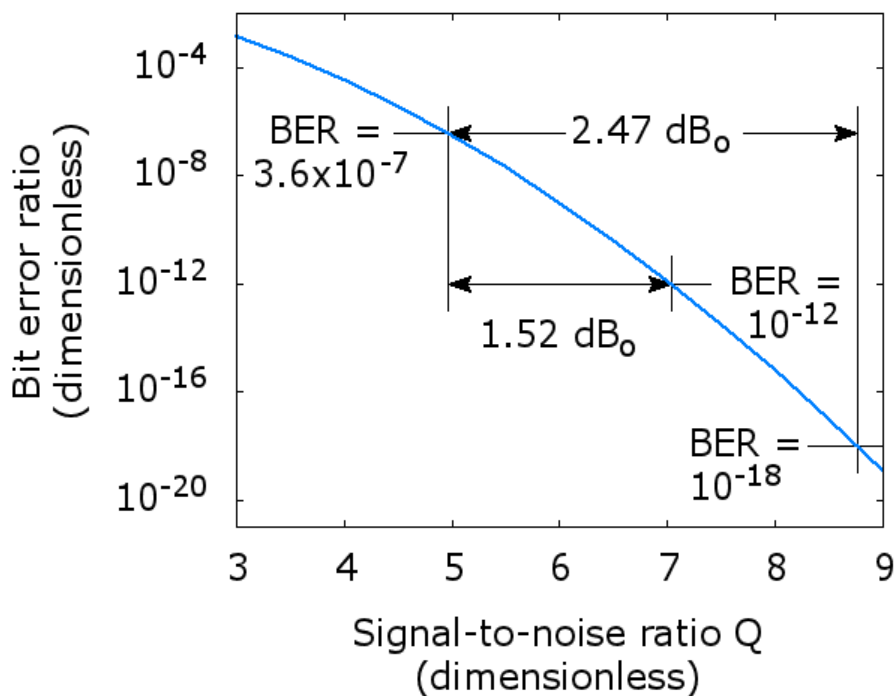Forward error correction (FEC) offers a technique for reducing noise impairment. Data are queued into

Figure 4.26 - Example of forward error correction (FEC) coding gain

blocks at the host and encoded with redundant patterns. The encoded blocks are decoded at the far host. Because of the redundant data patterns, modest errors in transmission can be identified and corrected.

Coding performance is typically analyzed by an additive white Gaussian noise model, leading to a dimensionless signal-to-noise ratio measure Q. Bit error ratio (BER) and Q are related by Equation 4.41, with results as shown in Figure 4.26. FEC performance is expressed in terms of coding gain in dB, the improvement in signal-to-noise ratio Q.

Table 4.7 - Sample forward error correction (FEC) performance

Parameter	Value
FEC selection	RS(528,514)
Transcoding selection	G(1024)
Random coding gain	2.89 dB_O
Burst coding gain	2.47 dB_O
Nominal Fibre Channel error goal	BER = 10^{-12} $Q = 7.03$
Corrected error goal with FEC	BER = 10^{-18} $Q = 8.76$
Uncorrected error performance	BER = 3.6×10^{-7} $Q = 4.96$

Consider one particular FEC selection under consideration for 32GFC links, shown in Table 4.7 with expected performance as diagramed in Figure 4.26. The FEC code selection is RS(528,514); RS stands for Reed-Solomon, a major class of forward error correction code. This class of code has very low overhead, meaning the increase in signaling rate needed to accomodate the redundant code. This overhead can be made transparent to the user by means of transcoding. Instead of using a 64b/66b encoding specified for 16GFC, a more efficient coding (G(1024) is selected.

Traditional Fibre Channel practice has been to design for 10^{-12} BER as the limit of acceptable performance. However at a symbol rate of 28.05 GBd, this corresponds to an error a minute which would be considered unacceptable. For FEC system design, we therefore propose a design goal of 10^{-18} BER with FEC, corresponding to an error every year. This corresponds to a error corrected Q of 8.76.

Coding gain for RS(528,514) is 2.89 dB_O for random errors and 2.47 dB_O for error bursts. Let us assume the more conservative number. A coding gain of 2.47 dB_O on a Q of 8.76 implies an uncorrected Q of 4.95, which corresponds to an uncorrected BER of 3.6×10^{-7}. Compared with nominal Fibre Channel practice, this represents a relaxation of the Q parameter by 1.52 dB_O, as seen in Figure 4.26.

This relaxation of Q affects link budget as given by Equation 4.62 for RIN power penalty and by Equation 4.109 for MPN power penalty. This change can be easily implemented in the spreadsheet model by substituting Q = 4.95 in place of Q = 7.03 in the appropriate cell.

The relaxation of uncorrected bit error target also has an additional advantage for link budgeting. The receiver sensitivity is defined to achieve a given BER target. If this BER target is relaxed, then an improved receiver sensitivity applies; for the example shown in Figure 4.26, this improvement is 1.5 dBo.

01
02
03
04
05
06
07
08
09
10
11
12
13
14
15
16
17
18
19
20
21
22
23
24
25
26
27
28
29
30
31
32
33
34
35
36
37
38
39
40
41
42
43
44
45
46
47
48
49
50
51
52
53
54
55
56

01
02
03
04
05
06
07
08
09
10
11
12
13
14
15
16
17
18
19
20
21
22
23
24
25
26
27
28
29
30
31
32
33
34
35
36
37
38
39
40
41
42
43
44
45
46
47
48
49
50
51
52
53
54
55
56

01
02
03
04
05
06
07
08
09
10
11
12
13
14
15
16
17
18
19
20
21
22
23
24
25
26
27
28
29
30
31
32
33
34
35
36
37
38
39
40
41
42
43
44
45
46
47
48
49
50
51
52
53
54
55
56

01
02
03
04
05
06
07
08
09
10
11
12
13
14
15
16
17
18
19
20
21
22
23
24
25
26
27
28
29
30
31
32
33
34
35
36
37
38
39
40
41
42
43
44
45
46
47
48
49
50
51
52
53
54
55
56

5 Transmitted output waveform signal characteristics for 3200-DF-EA-S variants

5.1 Introduction

The transmit device includes programmable equalization to compensate for frequency-dependent loss of the channel and facilitate data recovery at the receiver. The functional model for the transmit equalizer is the three tap transversal filter shown in figure 5.1. The state of the equalizer and hence the transmitted output waveform may be manipulated via the Transmitter Training process defined in FC-FS-3 clause 9 or an unspecified management interface. The transmit function responds to a set of commands issued by the link partner's receive function and conveyed by a back-channel communications path. This command set includes instructions to

a) increment coefficient c(n),

b) decrement coefficient c(n),

c) hold coefficient c(n) at its current value, or

d) set the coefficients to a pre-defined value "preset" or "initialize".

In response, the transmit device relays status information to the link partner's receive function. The status messages indicate that

a) the requested update to coefficient c(n) has completed,

b) coefficient c(n) is at its minimum value,

c) coefficient c(n) is at its maximum value, or

d) coefficient c(n) is ready for the next update request.

The following process is defined for the verification of transmit equalizer performance.

1) The transmitter under test is "preset" such that $c(-1)$ and $c(1)$ are zero and $c(0)$ is its maximum value.

2) Capture at least one complete cycle of the test pattern PRBS9 at test point B (as defined in FC-MSQS reference [2]) per 5.5.

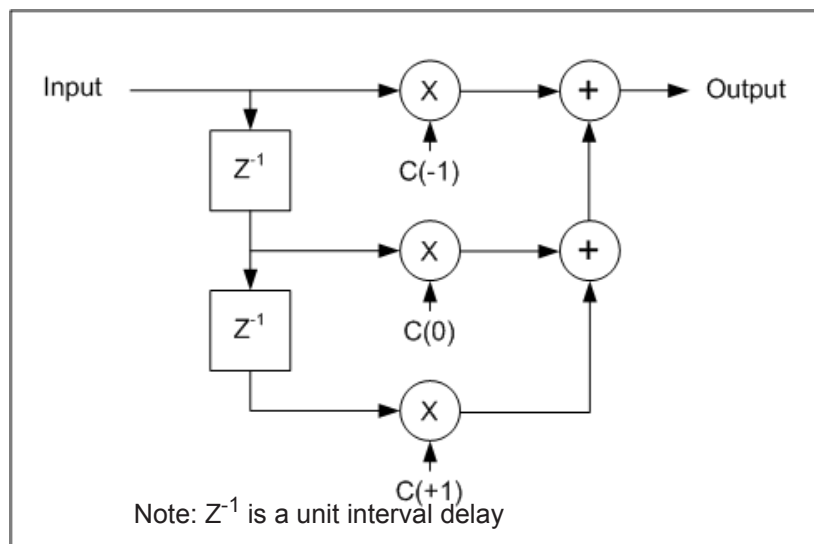3) Compute the linear fit to the captured waveform per 5.6.

Note: Z^{-1} is a unit interval delay

Figure 5.1 - Transmit device equalizer function model

4) Define t_x to be the time where the rising edge of the linear fit pulse, p, from step 3 crosses 50% of its peak amplitude.

5) Sample the linear fit pulse, p, at symbol-spaced intervals relative to the time $t_0 = t_x + 0.5$ UI, interpolating as necessary to yield the sampled pulse p_i.

6) Use p_i to compute the vector of coefficients, w, of a N_w-tap symbol-spaced transversal filter that equalizes for the transfer function from the transmit function to test point B per 5.7.

The parameters of the pulse fit and equalizing filter are given in FC-PI-6, reference [5].

The differential output voltage at test point B in the steady state, v_f, is estimated by

$$v_f = \frac{1}{M} \sum_{k=1}^{MN_p} p(k) \tag{5.1}$$

where, p is the linear fit pulse from step 3 and M is the number of samples per symbol as defined in 5.5. The peak value of the linear fit pulse from step 3, p_{max}, shall satisfy the requirements of FC-PI-6, reference [5]. The RMS value of the error between the linear fit and measured waveform from step 3, σ_e, shall satisfy the requirements of FC-PI-6, reference [5].

For each configuration of the transmit equalizer:

7) Configure the transmitter under test as required by the test.

8) Capture at least one complete cycle of the test pattern PRBS9 at test point B per 5.5.

9) Compute the linear fit to the captured waveform per 5.6.

10) Define t_x to be the time where the rising edge of the linear fit pulse, p, from step 9 crosses 50% of its peak amplitude.

11) Sample the linear fit pulse, p, at symbol-spaced intervals relative to the time $t_0 = t_x + 0.5$ UI, interpolating as necessary to yield the sampled pulse p_i.

12) Equalize the sampled pulse p_i using the coefficient vector, w, computed in step 6 per 5.7 to yield the equalized pulse q_i.

The RMS value of the error between the linear fit and measured waveform from step 9, σ_e, shall satisfy the requirements of FC-PI-6, reference [5].

The normalized amplitude of coefficient $c(-1)$ is the value of q_i at time $t_0 + (D_p - 1)$ UI. The normalized amplitude of coefficient $c(0)$ is the value of q_i at time $t_0 + D_p$ UI. The normalized amplitude of coefficient $c(1)$ is the value of q_i at time $t_0 + (D_p + 1)$ UI.

5.2 Coefficient step size

The magnitude of the change in the normalized amplitude of coefficient $c(n)$, Δ_c, shall satisfy the requirements of FC-PI-6, reference [5]. A request to "increment" a coefficient shall result in positive change in that coefficient value while a request to "decrement" a coefficient shall result in a negative change in the coefficient value.

The change in the normalized amplitude of the coefficient is defined to be the difference in the value measured prior to the assertion of the "increment" or "decrement" request (e.g. the coefficient update request for all coefficients is "hold") and the value upon the assertion of a coefficient status report of "update complete" for that coefficient.

5.3 Coefficient range

When sufficient "increment" or "decrement" requests have been received for a given coefficient, the coefficient will reach a lower or upper bound based on the coefficient range or restrictions placed on the minimum steady state differential output voltage or the maximum peak-to-peak differential output voltage.

With $c(-1)$ set to zero and both $c(0)$ and $c(1)$ having received sufficient "decrement" requests so that they are at their respective minimum values, the ratio $R_{pst} = (c(0) - c(1))/(c(0) + c(1))$ shall satisfy the requirements of FC-PI-6, reference [5].

With $c(1)$ set to zero and both $c(-1)$ and $c(0)$ having received sufficient "decrement" requests so that they are at their respective minimum values, the ratio $R_{pre} = (c(0) - c(-1))/(c(0) + c(-1))$ shall satisfy the requirements of FC-PI-6, reference [5].

Note that a coefficient may be set to zero by first asserting a coefficient "preset" request and then manipulating the other coefficients as required by the test.

In addition transmitter shall not implement an update request that would cause the sum of the magnitudes of the normalized coefficients, S_c, to exceed the maximum value given in FC-PI-6, reference [5].

5.4 Coefficient initialization

When the transmit device is directed to "initialize", the coefficients of the transmit equalizer shall be set to values given in FC-PI-6, reference [5].

These requirements apply upon the assertion a coefficient status report of "update complete" for all coefficients.

5.5 Waveform acquisition

The transmitter under test repetitively transmits the specified test pattern. The waveform shall be captured with an effective sample rate that is M times the signaling rate of the transmitter under test. The value of M shall be an integer not less than 7. Averaging multiple waveform captures is recommended.

The captured waveform shall represent an integer number of repetitions of the test pattern totaling N bits. Hence the length of the captured waveform should be MN samples. The waveform should be aligned such that the first M samples of waveform correspond to the first bit of the test pattern, the second M samples to the second bit, and so on.

5.6 Linear fit to the waveform measured at test point B

Given the captured waveform $y(k)$ and corresponding aligned symbols $x(n)$ derived from the procedure defined in 5.5, define the M-by-N waveform matrix Y as shown below.

$$Y = \begin{bmatrix} y(1) & y(M+1) & \ldots & y(M(N-1)+1) \\ y(2) & y(M+2) & \ldots & y(M(N-1)+2) \\ \ldots & \ldots & \ldots & \ldots \\ y(M) & y(2M) & \ldots & y(MN) \end{bmatrix} \qquad (5.2)$$

Rotate the symbols vector x by the specified pulse delay D_p to yield x_r.

$$x_r = \begin{bmatrix} x(D_p+1) & x(D_p+2) & \ldots & x(N) & x(1) & \ldots & x(D_p) \end{bmatrix} \qquad (5.3)$$

Define the matrix X to be an N-by-N matrix derived from x_r as shown here.

$$X = \begin{bmatrix} x_r(1) & x_r(2) & \cdots & x_r(N) \\ x_r(N) & x_r(1) & \cdots & x_r(N-1) \\ \cdots & \cdots & \cdots & \cdots \\ x_r(2) & x_r(3) & \cdots & x_r(1) \end{bmatrix} \tag{5.4}$$

Define the matrix X_1 to be the first N_p rows of X concatenated with a row vector of 1's of length N. The M-by-$(N_p + 1)$ coefficient matrix, P, corresponding to the linear fit is then defined by:

$$P = YX_1^T (X_1 X_1^T)^{-1} \tag{5.5}$$

The superscript "T" denotes the matrix transpose operator.

$$E = PX_1 - Y = \begin{bmatrix} e(1) & e(M+1) & \cdots & e(M(N-1)+1) \\ e(1) & e(M+2) & \cdots & e(M(N-1)+2) \\ \cdots & \cdots & \cdots & \cdots \\ e(M) & e(2M) & \cdots & e(MN) \end{bmatrix} \tag{5.6}$$

The error waveform, $e(k)$, is then read column-wise from the elements of E. Define P_1 to be a matrix consisting of the first N_p columns of the matrix P as shown below.

$$P_1 = \begin{bmatrix} P(1) & P(M+1) & \cdots & P(M(N_p-1)+1) \\ P(2) & P(M+2) & \cdots & P(M(N_p-2)+2) \\ \cdots & \cdots & \cdots & \cdots \\ P(M) & P(2M) & \cdots & P(MN_p) \end{bmatrix} \tag{5.7}$$

The linear fit pulse response, $p(k)$, is then read column-wise from the elements of P_1.

5.7 Removal of the transfer function between the transmit function and test point B

Rotate sampled pulse response P_i by the specified equalizer delay D_w to yield P_r.

$$P_r = \begin{bmatrix} P_i(D_w+1) & P_i(D_w+2) & \cdots & P_i(N_p) & P_i(1) & \cdots & P_i(D_w) \end{bmatrix} \tag{5.8}$$

Define the matrix P_2 to be an N_p-by-N_p matrix derived from P_r.

$$P_2 = \begin{bmatrix} P_r(1) & P_r(N_p) & \dots & P_r(2) \\ P_r(2) & P_r(1) & \dots & P_r(3) \\ \dots & \dots & \dots & \dots \\ P_r(N_p) & P_r(N_p - 1) & \dots & P_r(1) \end{bmatrix}$$
(5.9)

Define the matrix P_3 to be the first N_w columns of P_2. Define a unit pulse column vector x_p of length N_p. The value of element $x_p(D_p + 1)$ is 1 and all other elements have a value of 0. The vector of filter coefficients w that equalizes p_i is then defined by:

$$w = (P_3^T P_3)^{-1} P_3^T x_p$$
(5.10)

Given the column vector of equalizer coefficients, w, the equalized pulse response q_i is determined by:

$$q_i = P_3 w$$
(5.11)

01
02
03
04
05
06
07
08
09
10
11
12
13
14
15
16
17
18
19
20
21
22
23
24
25
26
27
28
29
30
31
32
33
34
35
36
37
38
39
40
41
42
43
44
45
46
47
48
49
50
51
52
53
54
55
56

01
02
03
04
05
06
07
08
09
10
11
12
13
14
15
16
17
18
19
20
21
22
23
24
25
26
27
28
29
30
31
32
33
34
35
36
37
38
39
40
41
42
43
44
45
46
47
48
49
50
51
52
53
54
55
56

6 Compliance test accuracy

6.1 Introduction

When defining compliance test requirements, it is necessary to consider whether multiple laboratories and multiple vendors obtain the same measurements using nominally the same test prescriptions.

The first topic concerns the phase lock loop (PLL) specified by FC-MSQS [2] to extract the jitter timing reference from a data stream under test. A PLL conforming to Clause 6.10 of FC-MJSQ [3] is referred to as a "Golden" PLL.

6.2 Golden PLL

Clock recovery is an essential part of many signal measurements, for which either a timing reference is not available, or the properties of the timing reference must correlate well at lower frequencies with the signal to be characterized. For example, many jitter measurements ignore low-frequency jitter and drift because they do not contribute to bit errors in transmission systems. Clock recoveries can be realized based on phase-locked loops in hardware or in software algorithms applied after the signals have been digitized. The specific properties of the clock recovery affect how instruments such as oscilloscopes and bit error ratio testers "see" jitter, hence potentially affecting measurement results.

The basic block diagram of a clock recovery unit is shown in Figure 6.1. A phase detector compares the edges of an incoming data signal with a clock from a voltage controlled oscillator (VCO). The phase detector creates an error signal that is proportional to the phase difference between the two signals. An error amplifier then causes the VCO to run faster or slower until the edges at the phase detector's inputs on average arrive at the same time.

Many standards refer to a "Golden PLL" type of clock recovery. Mathematically a "Golden PLL" is a Type 1 First Order PLL (see definitions of PLL type and order in Clause 6.3; see also Derickson and Müller [13]). Because the phase detector, error amplifier, and VCO of the "Golden PLL" have infinite bandwidth (and no integrating elements in the error amplifier), such a clock recovery can only be approximated in software. Mathematically the open loop gain of a "Golden PLL" can be described as

$$A(s) = \frac{\omega_1}{s} = \frac{2\pi f_1}{s} \tag{6.1}$$
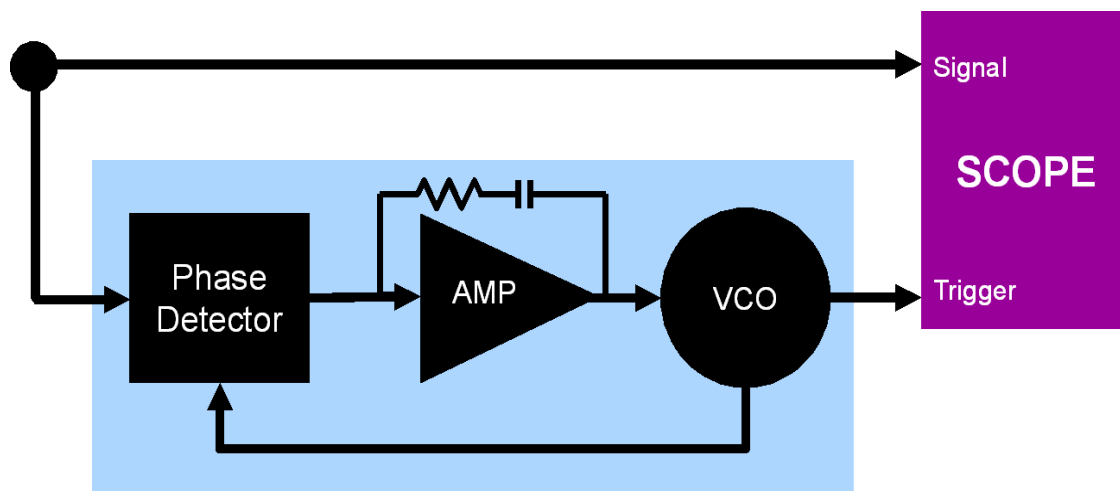
in which

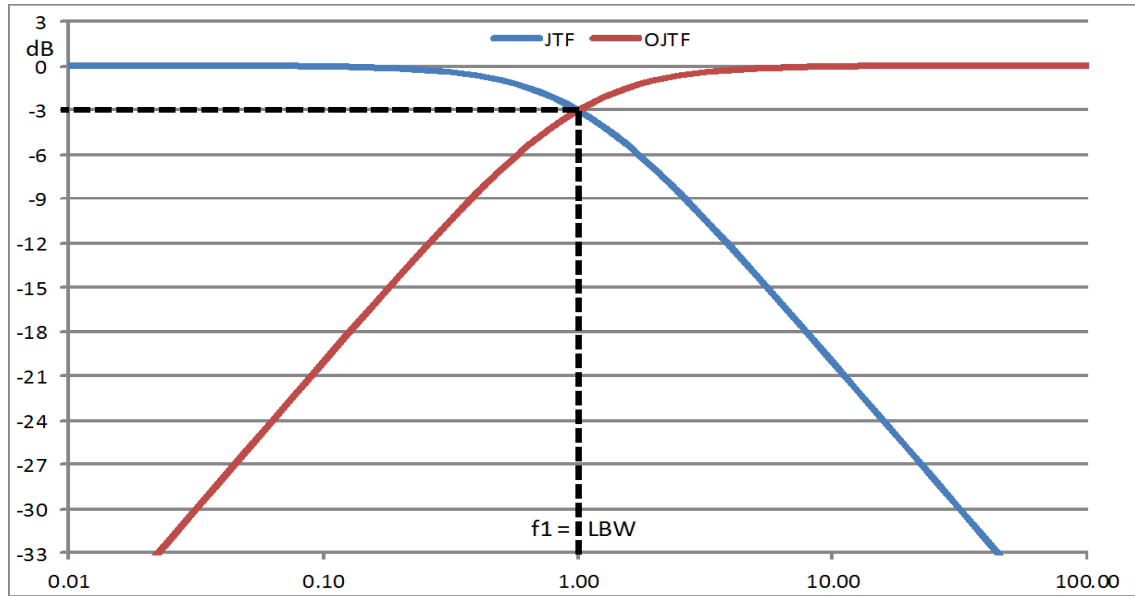**Figure 6.1 - Block diagram of a typical clock recovery unit.**

Figure 6.2 - Example of a first order phase lock loop.

$$\omega_1 = g \cdot Kpd \cdot Kvco \qquad (6.2)$$

In Equation 6.2, *g* is the gain of the error amplifier, *Kpd* is the conversion factor of the phase detector, and *Kvco* is the conversion factor of the voltage controlled oscillator.

Practical hardware clock recoveries deploy a low-pass filter in the phase detector in order to smoothen the pulses created by a non-linear or digital phase comparator, and the error amplifier uses an integrating element in order to track more effectively jitter and wander at low frequencies. Hence the open loop gain is a Type 2 Third Order PLL:
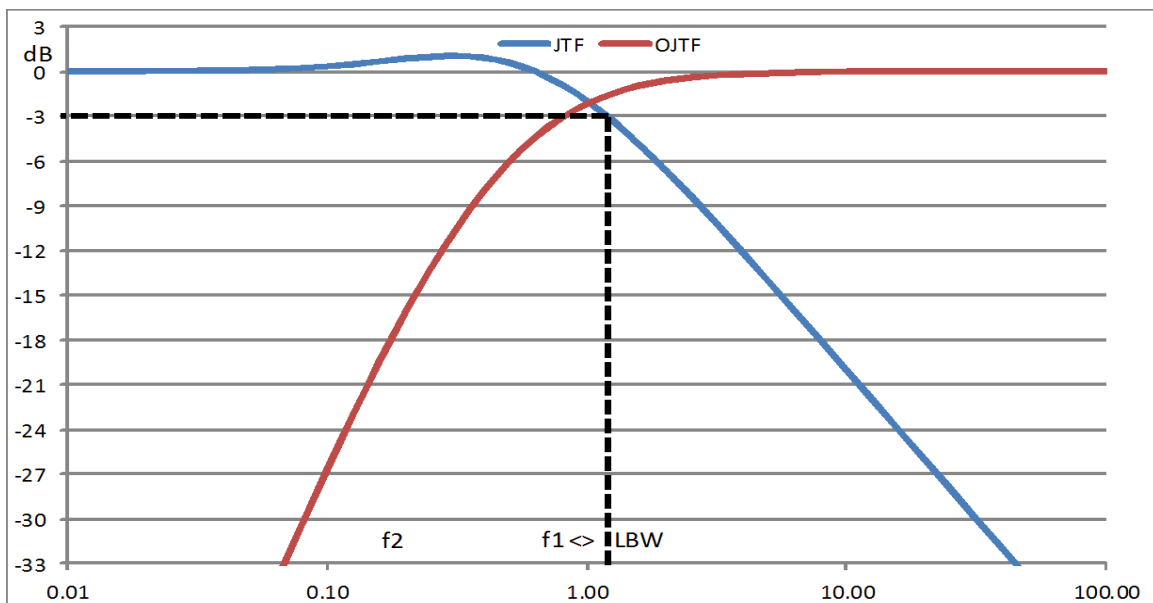

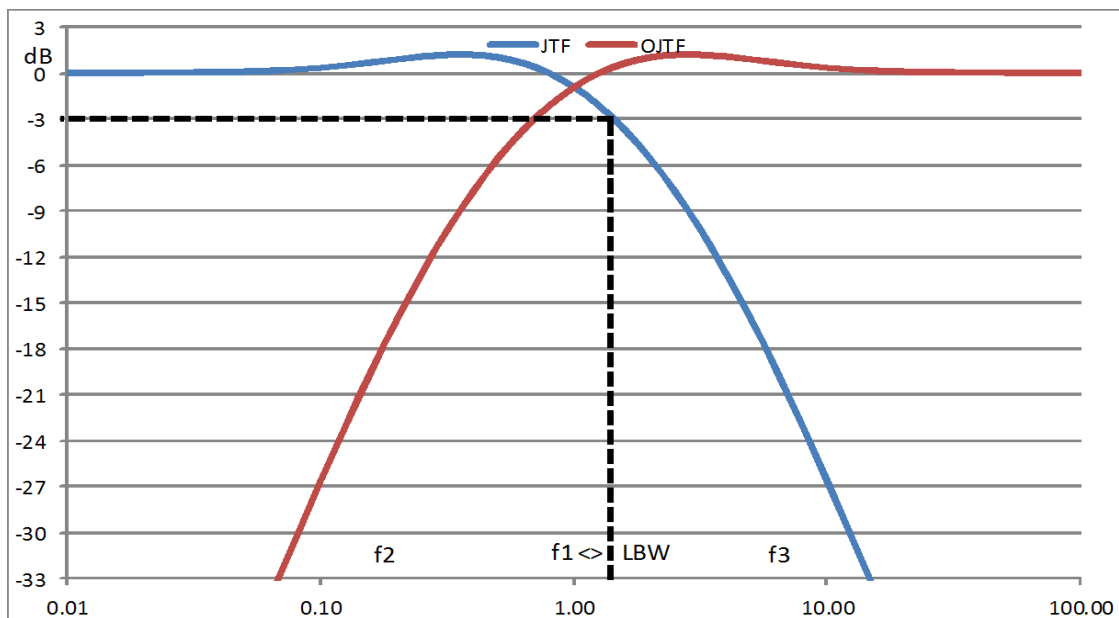**Figure 6.3 - Example of a second order phase lock loop (f2 = 0.2*f1).**

Figure 6.4 - Example of a third order phase lock loop (f2 = 0.2*f1; f3 = 5*f1).

$$A(s) \; = \; \frac{\omega_1}{s} \cdot \langle 1 + \frac{\omega_3}{s} \rangle \cdot \left(\frac{1}{1 + \frac{\omega_2}{s}} \right) \qquad (6.3)$$

In Equation 6.3, ω_2 is the bandwidth of the phase detector and ω_3 is the integrator bandwidth of the error detector.

Ignoring intrinsic noise, the output jitter of a PLL equals its input jitter times its Jitter Transfer Function:

$$J_{out}(s) \; = \; J_{in}(s) \cdot JTF(s) \qquad (6.4)$$

JTF itself is a function of the PLL's open loop gain:

$$JTF(s) \; = \; \frac{A(s)}{1 + A(s)} \qquad (6.5)$$

Many instruments use the recovered clock as the time reference to measure signals. Consequently the jitter observed is the difference between the jitter of the signal and the jitter put out by the clock recovery:

$$J_{measured} = J_{signal} - J_{trigger} = J_{signal} - JTF \cdot J_{signal} = J_{signal} \cdot (1 - JTF) \qquad (6.6)$$

In other words, jitter measured by the instrument has been filtered by the Observed Jitter Transfer Function (OJTF), defined as

$$OJTF \; = \; 1 - JTF \; = \; 1 - \frac{A(s)}{1 + A(s)} \qquad (6.7)$$

Due to cables, the path of the signal through the clock recovery to the trigger input of the oscilloscope often has more delay than the direct path (i.e., the signal to the oscilloscope input). The delta τ between the two paths further affects the OJTF, potentially resulting in significantly higher OJTF peaking:

$$OJTF = 1 - JTF \cdot \exp(-j\omega t) = 1 - \frac{A(s)}{1 + A(s)} \cdot \exp(-j\omega t) \tag{6.8}$$

in which τ is the path delay.

Figure 6.2, Figure 6.3, and Figure 6.4 compare the JTF and OJTF propertis of different clock recoveries. Figure 6.2 shows a Type 1 First Order PLL, similar to a first-order low-pass (JTF) or high-pass (OJTF). Figure 6.3 illustrates a Type 2 Second Order PLL showing gain in the JTF, which in turn affects the OJTF. The loop bandwidth of the JTF is higher than the 3-dB bandwidth of the OJTF, and no longer sits at frequency f_1.

Figure 6.4 represents a Type 2 Third Order PLL showing gain in both the JTF and OJTF. Again, the 3-dB bandwidth of the OJTF differs significantly from frequency f_1 and the loop bandwidth.

At sufficiently high frequencies all three OJTFs transfer jitter unmodified. Jitter in the transition region, however, gets differently amplified or attenuated. The amount of gain/loss depends on the time constants and corner frequencies of the hardware PLL and can vary between models and brands as well as due to manufacturing tolerances. Consequently measurements requiring the highest accuracy must "normalize" the OJTF to the desired function through mathematical transformations:

$$J(s) = J_{measured}(s) \cdot \frac{OJTF_{desired}(s)}{OJTF_{hardware}(s)} \tag{6.9}$$

The desired OJTF can be based on a Type 1 First Order "Golden PLL" or on any other type and order, so long as its JTF is sufficiently specified.

6.3 Definitions

6.3.1 PLL Type

PLL Type refers to the number of integrators in the PLL loop. If a PLL is realized as a closed loop circuit involving a phase detector, an error amplifier, a voltage controlled frequency oscillator, and potentially a frequency divider / multiplier, then the minimum PLL type is 1: the phase at the phase detector's reference input is proportional to the integral of frequency out of the voltage controlled oscillator or frequency multiplier / divider. If in addition the error amplifier involves both proportional and integrating elements then the PLL type is 2. Many oscillators require a second integrator because at very low frequencies the phase noise of the oscillator exeeds the PLL's ability to track it.

6.3.2 PLL Order

PLL Order refers to the polynomial order in the closed loop equation. A first-order PLL is often referred to as a "Golden PLL" and can only be realized in software and approximated with hardware. Hardware PLLs that involve three or more building blocks (phase detector, error amplifier, and voltage controlled oscillator) are at least third order PLLs because each building block has a finite bandwidth, hence contributing at least one polynomial term in the closed-loop equation.

6.3.3 Jitter Transfer Function (JTF)

Jitter Transfer Function (JTF) is the vector ratio of output jitter $J_{out}(s)$ divided by the input jitter $J_{in}(s)$ in

the frequency domain. It can be calculated from the open loop gain *A(s)*:

$$JTF = \frac{A(s)}{1 + A(s)} \qquad (6.10)$$

A plot of JTF versus frequency resembles a low-pass filter function: unity gain at DC or very low frequencies and high suppression at very high frequencies. Because hardware PLLs are of third or higher order, there is at least one frequency in the transition region where the gain is greater than one. This point is often referred to as PLL peaking.

6.3.4 Observed Jitter Transfer Function (OJTF)

Observed Jitter Transfer Function (OJTF) is the difference between the input jitter $J_{in}(s)$ and the output jitter $J_{out}(s)$. OJTF can be expressed as

$$OJTF = 1 - JTF = 1 - \frac{A(s)}{1 + A(s)} = \frac{1}{1 + A(s)} \qquad (6.11)$$

A plot of OJTF versus frequency resembles a high-pass filter function, with unity gain at high frequencies and high suppression at very low frequencies. Consequently test instruments such as oscilloscopes that observe a signal while being tiggered / timed by a clock recovery PLL will measure only the high frequency content of the signal's jitter.

6.3.5 Loop Bandwidth (LBW)

Loop Bandwidth (LBW) is defined as the 3 dB bandwidth of the jitter transfer function (JTF). It equals the observed jitter transfer function (OJTF) only for first order PLLs. Otherwise the JTF and OJTF bandwidths can differ significantly. The LBW based on JTF can be mathematically transformed into the LBW of the OJTF and vice versa.

Note that there is disagreement in standards in the definition of JTF and OJTF. Fibre Channel defines these terms as shown in the equations above. Because of this disagreement in definitions, different types or brands of test instruments implement LBW based on different definitions resulting in different PLL behavior, and subsequently unexpected measurement results. For example, a measurement may require clock recovery with 10 MHz loop bandwidth based on the JTF and LBW definitions given above. An instrument using these definitions will need to be set to "10 MHz" while a different instrument using different JTF, OJTF, and hence LBW definitions, might require a "4.9 MHz" entry in order to give comparable performance.

6.3.6 PLL Peaking

PLL Peaking is used to describe the behavior of a higher order PLL. It is defined as the highest gain in the jitter transfer function (JTF).

01
02
03
04
05
06
07
08
09
10
11
12
13
14
15
16
17
18
19
20
21
22
23
24
25
26
27
28
29
30
31
32
33
34
35
36
37
38
39
40
41
42
43
44
45
46
47
48
49
50
51
52
53
54
55
56

01
02
03
04
05
06
07
08
09
10
11
12
13
14
15
16
17
18
19
20
21
22
23
24
25
26
27
28
29
30
31
32
33
34
35
36
37
38
39
40
41
42
43
44
45
46
47
48
49
50
51
52
53
54
55
56